ISMETT Istituto di Ricovero e Cura a Carattere Scientifico

Fondazione Ri.MED

KING'S College LONDON

UNIVERSITÀ DEGLI STUDI DI PALERMO

Dottorato di Ricerca in Medicina Molecolare e Biotecnologie XXXII

Dipartimento di Fisica e Chimica

S.S.D. FIS/07 BIO/11

UNDERSTANDING THE RELATIONSHIP BETWEEN NORMAL FUNCTION AND ABERRANT AGGREGATION: THE CASE OF ATAXIN-3

IL DOTTORE

Anna Fricano

IL COORDINATORE

Prof. Massimo Midiri

TUTOR UNIVERSITARIO

Prof.ssa Valeria Vetri

TUTOR AZIENDALE

Dott.ssa Caterina Alfano

TUTOR UNIVERSITÀ ESTERA

Prof.ssa Annalisa Pastore

CICLO XXXII

ANNO CONSEGUIMENTO TITOLO 2020

UNIONE EUROPEA
Fondo Sociale Europeo

Ministero dell'Università e della Ricerca

PON RICERCA E INNOVAZIONE

CONTENTS

INTRODUCTION

The present work was funded by “PON research and innovation Industrial PhD program” on a project titled “*Understanding the relationship between normal function and aberrant aggregation: the case of Ataxin-3*”. The main focus of the project is to investigate molecular mechanisms involved in Spinocerebellar Ataxia type 3 (SCA3), a neurodegenerative pathology belonging to the group of polyglutamine (polyQ) neurodegenerative diseases which are caused by the expansion of the polyQ tract in the corresponding proteins. The expanded proteins are typically found to accumulate in intra-nuclear aggregates which are involved in neurodegeneration. Although a large number of studies have approached to the pathogenesis of these diseases, many important questions still remain open and suitable therapies are not developed yet. In particular, the aberrant aggregation of Ataxin-3 (Atx3) constitutes the fundamental basis of the SCA3 disease and the search of suitable molecules able to inhibit its supramolecular assembly is believed to be an efficient therapeutic strategy for this pathology.

Atx3 is a ubiquitin hydrolase involved in the protein degradation system in cell, able to bind and cleave specific polyubiquitin chains, and it was chosen as a model for this study as it is the smallest protein involved in polyQ pathologies. In this work the hypothesis that the interaction of Atx3 with polyubiquitin chains may exert a protective role against aggregation has been investigated, based on the idea that the natural binders involved in the physiological function of the target proteins may stabilise their native structure. If this is verified it will constitute a concrete basis to develop therapeutic molecules, such as mimetic-peptides derived from Ubiquitin (Ub) able to modulate the aberrant aggregation process of Atx3.

Due to the complexity of the system in analysis and of the Atx3 aggregation process, a multiplexed experimental approach was developed, based on molecular biology methods and spectroscopic techniques, that allows observing different aspects of the phenomenon under investigation both in-vitro and in cellular environment.

1 State of the Art

1.1 Protein aggregation

Proteins are essential elements for the life of organisms, and their extraordinary diversity and functional versatility is determined by the large number of conformations they can acquire[1]. The process by which a polypeptide chain reaches its unique and active three-dimensional conformation is called “Protein folding” which is among the most important and complex reaction in biology[2][3]. After being produced by ribosomes, proteins must fold to their functional native state and in most of the cases undergo folding and unfolding (at least partial) during their lifetime[4].

Classically the description of folding is based on the idea that all the information needed for a protein to reach the correct three-dimensional conformation is contained in the amino acid sequence. Based on this idea, the stability of a protein and the protein folding pathways are generally described by means of a funnel shaped free energy landscape[5]. The shape of the energy landscape surface depends on the amino acid sequence of the protein and on the interactions with the environment[3]. Each point on the surface describes all the accessible conformations that a polypeptide chain can adopt going through many independent pathways involving intermediate states that lead to the protein native state, which represents the minimum of the folding funnel. The failure of protein folding may lead to misfolded conformations, and as a consequence non-native contact may be formed. The incorrectly folded molecules may then access intra-molecular contacts and interact with other molecules leading to the formation of disordered or highly ordered aggregates[6]. The path leading to aggregation is considered as an alternative route, acting in competition with the folding process, and it may depends on several factors including amino acid sequence, temperature and solution conditions such as pH and ionic strength[7]. In this context, the energy landscape can be extended to a multi-protein system where both inter-molecular and intra-molecular contacts are considered (Fig. 1.1). The resulting supramolecular aggregates present different structures and morphologies ranging from amorphous structures to highly organized amyloids. Amorphous aggregates are mostly made up of disordered polypeptides chains, without defined shape or structure[8]; oligomers are small globular aggregates (less than 50 nm) formed by a low number of partially unfolded units (usually less than 50)[9]; amyloid fibrils, now recognised as the most stable state that a polypeptide chain can adopt[10], are elongated ordered protein aggregates characterised by a highly organized hydrogen-bonded structure, independent on the protein they are made of, which gives

them a unique kinetic stability[11]. In particular, they are stabilized by a common core cross-β-sheet structure in which β-sheets run parallel to the fibril axis[6][12].

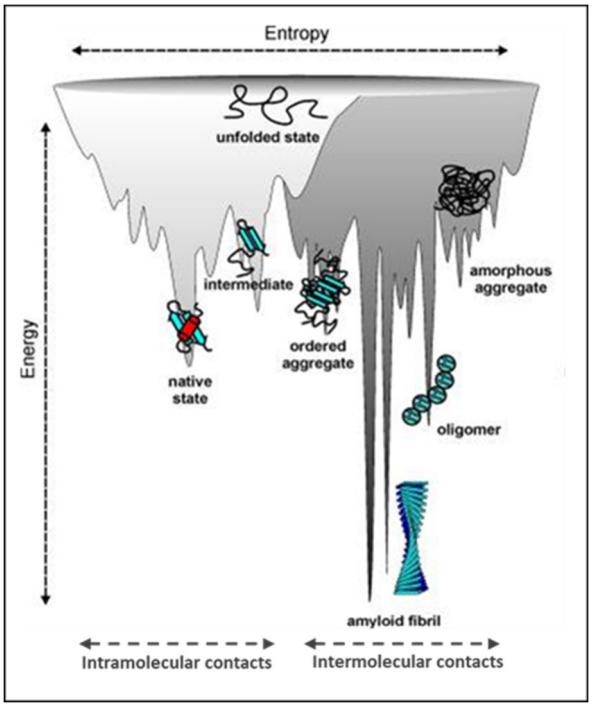

Figure 1.1: Energy landscape for folding and aggregation pathways of a polypeptide chain in a multiprotein energy surface. Figure adapted from [7]. Local minima represent the ensembles of unfolded and intermediate states. A deep minimum is assigned to the native state, while the thermodynamically most stable structure of the protein is in the amyloid fibril.

Although recent findings have lighted on that amyloid fibrils may have functional roles[13], they are of great interest as their formation has been implicated in the aetiology of a large variety of human diseases, including neurodegenerative disorders such as polyglutamine diseases (polyQ), Alzheimer's disease and Parkinson's disease. The understanding of the processes that lead to the formation of amyloid fibrils is, therefore, of crucial importance to identify possible therapeutic strategy of intervention.

Protein association processes are intrinsically complex phenomena which may implicate multiple interconnected mechanisms, such as protein conformational changes and inter-molecular bonds formation involving single residues, specific regions or the whole molecule, nucleation mechanisms, solution-demixing, and growth of aggregates. All these mechanisms are interconnected in different rates and their occurrence and extension is regulated by external conditions[14][15].

In this respect, aggregation processes involve protein molecules both on a microscopic scale as single proteins undergo structural and conformational changes, and on a macroscopic scale

since a large number of molecules are involved in inter-molecular bonding and collective interactions[15]. The driving forces for aggregation are the dominant interactions that regulate protein folding: the hydrophobic interactions contribute to the inter-molecular association of the intermediate structures, while polar interactions essentially contribute to the inter-molecular hydrogen bonds substantiating the cross-β-structure that constitutes amyloid fibrils[16].

Several studies indicate the possibility of the existence of general physical principles that govern protein aggregation and supramolecular structure formation, and several models for amyloids formation have been proposed[17]. Amyloid formation mainly occurs through nucleation and growth mechanisms, including primary and secondary nucleation pathways[18][19][20]. Other mechanisms include initial micelle formation[21], conformational conversion[22][23] and filament–filament association[24]. Protein aggregation through non-nucleated process have been also observed[25][26][15][27]. Although non exhaustive, a schematic representation of the protein self-assembly into different species is reported in Fig. 1.2.

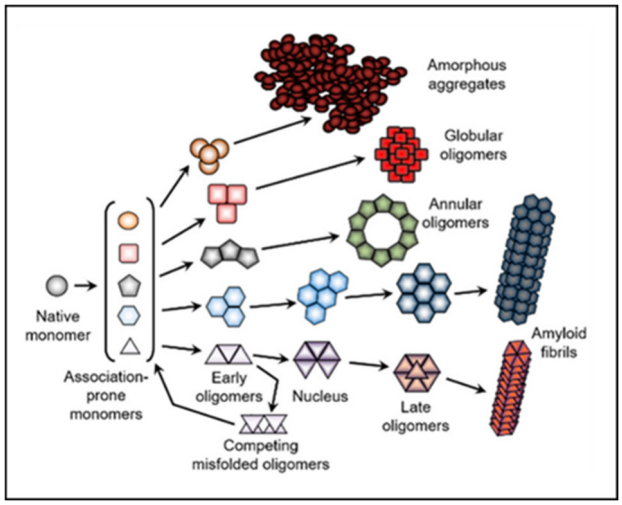

Figure 1.2: Schematic representation of protein aggregation pathways. Figure adapted from [28]. All aggregation pathways are generated through the formation of multiple association-prone monomeric forms. The aggregation reaction may generate amorphous aggregates, different soluble oligomers with diverse morphologies, and morphologically-divergent amyloid fibrils.

1.2 Neurodegenerative diseases

Neurodegenerative diseases are pathologies of the central nervous system involving dysfunction or progressive death of neurons cells in specific brain regions. These group of incurable diseases include Alzheimer's disease, Parkinson's disease, amyotrophic lateral sclerosis, frontotemporal dementia, prion diseases, and polyQ diseases such as, Huntington's disease and spinocerebellar ataxias. Generally, the symptoms for these pathologies include cognitive

deficits, loss of memory, motor impairments and psychological and behavioural disorders with severe progression[29][30]. Although these diseases are different for transmission, clinical and progression, they share common features, such as old age-onset and the accumulation of aggregated proteins in the brain[31]. Coherently with the last evidence, it has been extensively demonstrated that protein aggregation processes are implied in these pathologies and may induce cellular toxicity[32][33][34][35]. A growing consensus exists in considering a continuum of aggregates species formed during supramolecular assembly, rather than a single uniform species as main toxicity effector[36]. Evidences have emerged suggesting that these species share both common structural features and the ability to permeabilise cell membranes, potentially initiating multiple processes leading to cell impairment and death critical in the onset and progression of disease[37][38]. In particular, both fibrils and oligomers formed during the aggregation pathways have been found to induce toxicity, but notwithstanding the large number of studies the role of toxic species and the equilibria between oligomers and fibrils remains to be clarified, both in terms of assembly of oligomers into fibrils and potential dissolution of fibrils into oligomers. Many controversial results exist in literature and no clear conclusions can be drawn due to the great variety and heterogeneity of different experimentally observed states.

In this context, the investigation of the origin of high impact neurodegenerative disorders cannot be separated from an accurate description of the inter- and intra-molecular interactions involved in the formation of amyloid aggregates. This is of fundamental importance because the increased understanding of the factors that control supramolecular assembly, resulting species and their toxicity, can allow the development of new therapeutic strategies.

1.3 Polyglutamine disease

PolyQ disorders are dominant late-onset genetic neurodegenerative disorders accompanied by progressive death of neuronal cells in distinct regions of the brain, with consequent neurological symptoms such as cognitive impairment and motor disorder, depending on the affected brain regions[39][40]. Even if each polyQ disease has a specific symptomatology, and present neuronal cells damage in specific brain regions, the neurotoxicity of all these diseases always correlates with the expansion of poly-CAG repeats in the gene encoding for the causative protein of the pathology, which as consequence will contains a long consecutive glutamine (Q) tract in its sequence[41]. Furthermore, the length of the expansion correlates with the age of onset of the disease and with the severity of the symptoms[42][43].

Nine neurodegenerative disorders belong to polyQ diseases family: Spinocerebellar Ataxia type 1, 2, 3, 6, 7 and 17 (SCAs), Huntington's disease (HD), Dentatorubral Pallidoluysian Atrophy (DRPLA), and Spinal Bulbar Muscular Atrophy X-linked type 1 (SMAX1/SBMA). These pathologies are dominantly inherited disorders, except for SBMA which is an X-linked disorder. A list of the nine pathologies belonging to polyQ diseases is reported in Table 1.1, together with relative causative proteins, and the position of the polyQ tract in each protein. The proteins involved in the aetiology of these diseases, differ in size, cellular localization and biological function, but they have in common an expansion of their polyQ trait, suggesting that the expansion of this trait has an important role in the pathogenetic mechanism of the disease, although the details of the molecular mechanism are not yet well understood and are largely debated[39]. Toxic effects may be directly caused by aberrant supramolecular assemblies formed by the causative proteins, or may be an indirect effect of these assemblies due to their ability in sequestering functional proteins hindering their physiological function[31]. Moreover, the increased tendency to aggregate of causative proteins may alter their binding to biological partners and thus leading to pathology[44].

PolyQ disease	Protein	Expansion	Protein architecture
Huntington's disease (HD)	Huntingtin	36-100	
dentatorubral pallidoluysian atrophy (DRPLA)	Atrophin	49-88	
spinal bulbar muscular atrophy X-linked type 1 (SMAX1/SBMA)	Androgen receptor	38-65	
spinocerebellar ataxias 1 (SCA1)	Ataxin-1	39-83	
spinocerebellar ataxias 2 (SCA2)	Ataxin-2	33-77	
spinocerebellar ataxias 3 (SCA3)	Ataxin-3	55-84	
spinocerebellar ataxias 6 (SCA6)	A2A- voltage dependent calcium channel	21-33	
spinocerebellar ataxias 7 (SCA7)	Ataxin-7	34-306	
spinocerebellar ataxias 17 (SCA17)	TATA box binding protein	47-55	

Table 1.1: PolyQ diseases and related causative proteins. The range of polyQ expansions found for each pathology is also indicated. Highlighted in yellow, the region that contains the polyQ tract for each protein. Table adapted from [45].

Several studies have shown that proteins containing expanded polyQ tract may undergo conformational changes leading to β-sheet rich structure in the monomeric state, which assembles into oligomers and insoluble aggregates with amyloid fibrillar structures, potentially leading to accumulation as intracellular inclusions[46]. Among others, two models explaining polyQ

aggregation mechanisms received larger consensus in the scientific community: one is the nucleation-elongation model, where a monomer is in rapid equilibrium between un unfolded state and a thermodynamically unfavourable β-structured state. This acts as a nucleus and works as a template to add other monomers, forming an elongated β-structure fibrils[47]. The other model is the association-conformational conversion model, that consists in the association of soluble oligomers, driven by hydrophobic interactions between disordered monomers, followed by further conformational rearrangements resulting in insoluble fibrils[41][48]. Both models consider the reactivity of the only polyQ trait, and are based on the idea that long polyQ tracts are highly reactive and readily undergo to misfolding and aggregation, resulting in an assembly of its host protein into insoluble aggregates with β-sheet rich amyloid fibrillar structures. However, it was demonstrated that polyQ flanking domains can modulate the aggregation process. The result is a two stages aggregation process, where conformational changes and early oligomerization are mediated by the polyQ-flanking domain, while the formation of SDS-insoluble fibrils, is polyQ-dependent[49][50][51]. Moreover, flaking polyQ domains play a crucial role in the formation of intermediaries species during aggregation, that are considered more toxic than insoluble aggregates in nuclear inclusions[52][53]. The scenario is further complicated by several studies reporting that proteolytic cleavage of polyQ proteins is required for inclusion formation in the brain[54][55][56].

In this intricate scenario, aggregation mechanisms of proteins implied in polyQ pathologies and how they are involved in neurodegeneration is not fully understood yet. The experimental conditions of related studies are critical in modulating observed aggregation pathways, newly formed oligomeric intermediates, and toxic effects. Since the aggregation process is thought to be a crucial event in the common pathogenic cascade of the polyQ diseases, finding strategies to suppress or delay it is of utmost importance for the development of therapies to cure patients affected by these diseases. Many approaches have been proposed based on small chemical molecules or peptides which inhibit the aggregation process by specifically binding to the expanded polyQ tract or specifically targeting the causative protein, but none of them has been successful so far[57].

In this thesis, aggregation mechanisms of Ataxin-3 (Atx3) and possible strategies for inhibiting its supramolecular assembly were investigated. Atx3 is responsible of Spinocerebellar Ataxia type 3 (SCA3), the most common among ataxias, and it is the smallest causative protein within polyQ diseases family[58]. Atx3 represents a good model for studying different aspects of polyQ diseases as its small size and its modular structure, containing a globular domain and an intrinsically disordered flexible tail, may allow studies on selected features of the aggregation

process. For instance, it is possible to highlight the role of different regions in modulating aggregation, thus giving information on possible strategies to stabilise the native state.

1.4 Spinocerebellar Ataxia type 3

SCA3, also known as Machado–Joseph disease (MJD), is the most common inherited spinocerebellar ataxia belonging to the group of polyQ neurodegenerative diseases. This disease presents the common pathogenic characteristics of polyQ diseases and is caused by Atx3, a protein encoded by a gene mapped in the 14q32.1 chromosome region[59]. The number of glutamines in the normal and expanded polyQ tract of Atx3 ranges between 12-50 and 55-84, respectively[60][61].

Clinical manifestations of SCA3 include cerebellar ataxia, progressive external ophthalmoplegia, dysarthria, dysphagia, pyramidal signs, dystonia, rigidity, and distal muscle atrophies[59]. The first identification of SCA3 occurred in four families of Azorean ancestry and described as four distinct pathologies, that subsequently were recognized as variations of the same disorder defined as Machado-Joseph disease[62][63][64][65][66]. Type 1 begins early in life, before age 20, and it is characterized by prominent pyramidal signs (rigidity and spasticity) and extrapyramidal features (bradykinesia and dystonia) as well as ataxia[63][67]. Type 2, the most common type, has an intermediate age onset (20–50 years) with cerebellar ataxia, progressive external ophthalmoplegia and pyramidal signs[68]. Type 3 has a later onset (40–75 years) and it is characterized by peripheral signs such as motor neuronopathy and muscle atrophy together with ataxia[69]. Type 4, the rarest type, is characterized by parkinsonism associated with other core clinical features[65][70]. More recently, a type 5 was proposed for rare cases presenting pure spastic paraplegia[71].

Currently, SCA3 disease still remains incurable. Therapeutic approaches have been investigated to inhibit Atx3 protein expression, using antisense oligonucleotides mRNA or duplex RNA able to slowing down the progression of the disease[72]. The length of the polyQ tracts certainly affects the success of this approach, in fact the longer polyQ tracts are able to form hairpin structures that could interfere with the success of gene therapy[73]. Other therapeutic approaches involve the use of molecular chaperones targeting expanded Atx3 to suppress its misfolding[74][75], or the induction of expanded Atx3 autophagy to reduce its deleterious effects[76], or the transcriptional deregulation of Atx3 gene[77]. The approach considered in this thesis, is based on the hypothesis that peptide-mimetics compounds derived from Atx3 natural interactors, may be able to interact with Atx3 and modulate its aggregation propensity.

1.5 Ataxin-3 structure and function

Atx3 is a de-ubiquitinating enzyme (DUB) ubiquitously expressed in human tissues, and belonging to the family of cysteine proteases. It is a multidomain protein and its structure consists of an N-terminal catalytic domain called Josephin domain (Jos, amino acid region 1-182), and a C-terminal region that consists of the polyQ tract and 2 or 3 Ubiquitin interactive motifs (UIMs) (Fig. 1.3)[78]. The Josephin domain also contains two nuclear exporting signal (NES) motifs, necessary to efficiently retain Atx3 in the cytoplasm, while a nuclear localization sequence (NLS) is situated at the C-terminal tail of full-length Atx3 before the polyQ region, and allows Atx3 to act also as a transcriptional regulation player. NLS most likely allows translocation to the nucleus also of C-terminal fragments generated by cleavage of expanded Atx3, which lead to the formation of intranuclear aggregates[79].

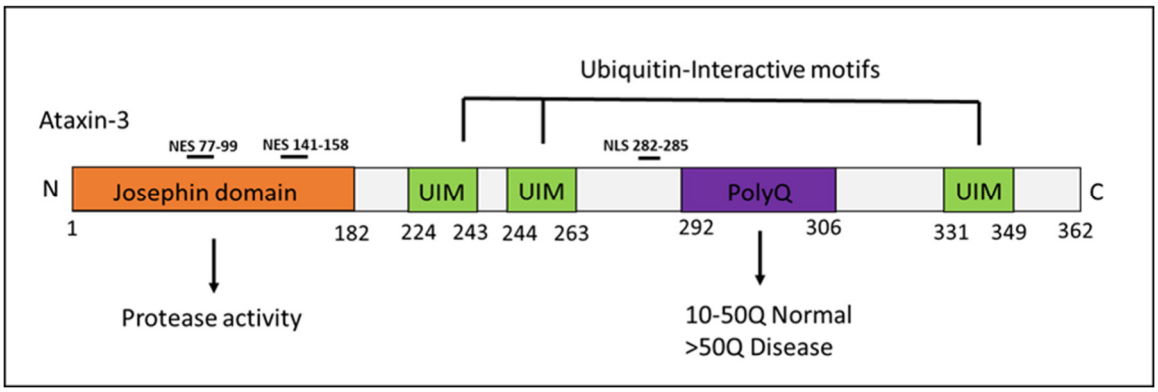

Figure. 1.3: Schematic representation of domains organization of Atx3 protein. Atx3 has a molecular weight of about 42KDa. The healthy isoform, generally contains a range of 8-50 glutamine residues, while the pathological isoforms contain a range of 55-84 glutamine residues[60].

Atx3, as DUB enzyme, mainly recognizes K48- and K63-linked polyubiquitin chains (polyUb), and cleaves them thanks to the catalytic triad formed by Cystein 14, Histidine 119 and Asparagine 134 residues[50][80][81][82][83]. The catalytic triad is flanked and supported by two Ubiquitin-binding sites within the Josephin domain, Site 1 and Site 2. Site 1 is close to the catalytic site, and it is important for polyUb cleavage activity since it binds a Ubiquitin (Ub) moiety and helps its positioning into the catalytic site[50]. Site 2 is responsible for ubiquitin-chain linkage preference, and interacts with N-terminal domain of the Ubiquitin-like domain of HHR23B, a protein involved in the ubiquitin proteasome pathway as well as Atx3[50][82]. The NMR solution structure of the Josephin domain is reported in Figure 1.4, with highlighted the catalytic triad (Cys 14, His119 and Asn 134), Site 1 (Ile77, Leu91, Trp120, and Phe163), and Site 2 (Tyr27, Phe28, and Trp87)[82].

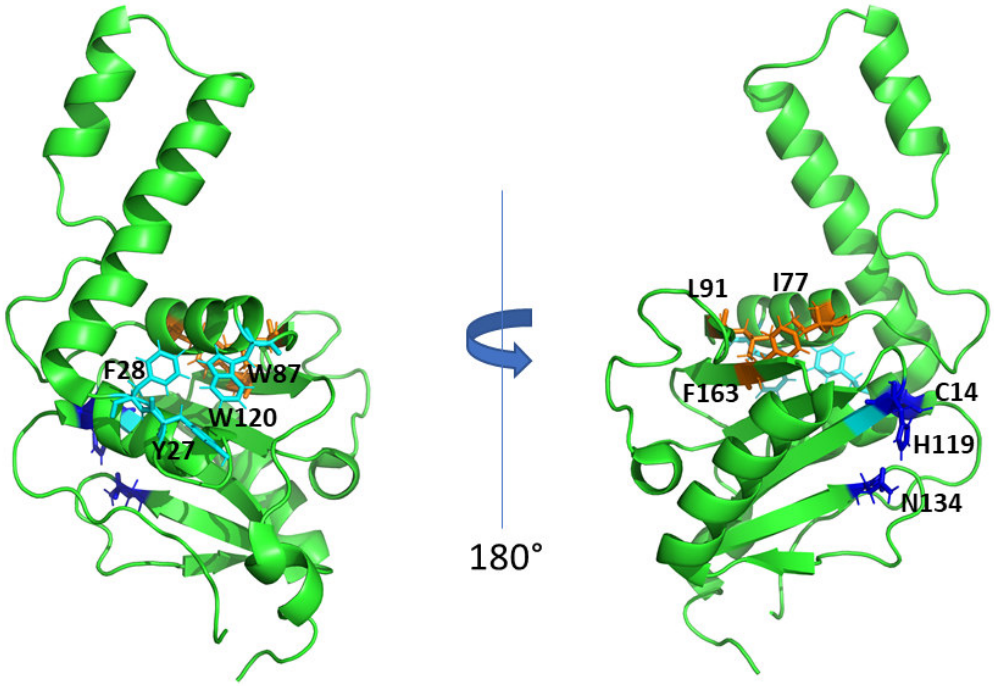

Figure 1.4: NMR solution structure of Josephin domain (PDB ID: 1yzb)[50]. The left and rigth structures are related by a rotation of 180° around a vertical axis. Josephin shows a predominant α-helical fold that is typical of cysteine proteases. The catalytic triad is highlighted in blue, while the residues of Site 1 and Site 2 are highlighted in orange and in cyan, respectively.

The presence of different Ub binding sites in Atx3 sequence, and its ability to bind and cleave polyubiquitinated proteins, demonstrates that the principal function of Atx3 in cell deals with the cellular protein quality control system, in particular, with the ubiquitin proteasome system (UPS)[80]. Indeed, it was shown that where Atx3 expression is suppressed or altered in animal models, an accumulation of polyubiquitinated proteins occurs[84][85]. Moreover, several evidences show that Atx3 interacts with proteins belonging to the UPS system, such as p97/valosin-containing protein (VCP)[86][87][88], and several E3 Ubiquitin ligases[89].

Atx3, specifically binds and cleaves K48-linked, K63-linked and mixed K48-, K63-linked polyUb chains attached to target proteins as post-translational modification (PTM)[50][90]. K48-linked poly-ubiquitination PTM affects predominantly proteins for proteasomal degradation, whereas K63-linked poly-ubiquitination PTM seems to regulate protein function, subcellular localization and protein–protein interactions[91].

Although, the main biological role of Atx3 correlates with the regulation of protein degradation, it has also a role in transcriptional regulation. Indeed, Atx3 binds DNA and interacts with transcription regulators, such as cAMP-response element binding (CREB)- binding protein (CREBBP), inhibiting the CREB-mediated transcription pathway[92]. Moreover, Atx3

modulates transcription by interacting with several transcription factors, such as the Forkhead box O4 peptide (FOXO4), Wilm's tumor protein 1 (WT1), and the TATA box protein (TBP) belonging to the Transcription factor II D complex (TFIID)[93]. Atx3 also promotes the deacetylation of histones, by its binding to specific chromatin regions of the metalloproteinase-2 (MMP2) gene promoter, and recruiting the histone deacetylase 3 (HDAC3) and the nuclear receptor co-repressor 1 (NCOR1) to these regions[93].

1.6 Ataxin-3 aggregation

Atx3 shows an intrinsic propensity to aggregate in vitro under native conditions[51]. Both wild type Atx3 and expanded Atx3, and also the isolated Josephin domain, show tendency to aggregation and are able to form amyloid-like fibrils[94][95][96][97]. The first accredited model for Atx3 aggregation process consisted in a nucleation-dependent process (Fig. 1.5). In this model, the first step involves the self-association of Josephin domain, able to form SDS-soluble aggregates[94]. This step does not involve the polyQ tract, and the kinetics of aggregation is characterized by a nucleation-dependent process[95][98]. The second step involves the polyQ tract, responsible for a faster aggregation kinetics and for the formation of SDS-insoluble fibrils[95]. Further evidences highlighted that self-cleavage propensity of Atx3 may cause seeds formation favouring aggregation processes[99]. More recently, it has been found that not only the Josephin domain, but also the partially disordered region between Josephin domain and polyQ trait (182–291) plays a key role in the aggregation process and in developing the disease[100].

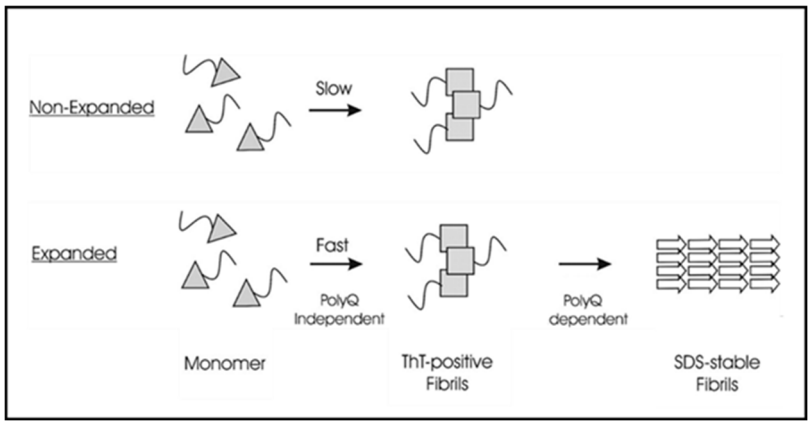

Figure 1.5: Two-step model of Atx3 aggregation. The first step of Atx3 self-assembly, independent on polyQ tract, is triggered by the Josephin domain. The resulting oligomers and small protofibrils are sensitive to SDS. The second step, dependent on the polyQ expansion, leads to the formation of mature and SDS-resistant Atx3 fibrils. Figure adapted from [94].

Although the expansion of the polyQ remains to be considered among the main causes of the onset of polyQ-related degenerative diseases, it is now well recognized that protein context greatly influences polyQ protein aggregation. Misfolding of polyQ flanking domains seems to have a key role in Atx3 aggregation process, promoting fragmentation and formation of oligomeric species, considered more toxic than the mature fibrils[101][102]. These observations suggest that new therapeutic approaches may be generated by targeting flanking domains rather than targeting the polyQ region.

The experimental design of this thesis work, was directed at analysing aggregation process of Atx3 using recombinant proteins and spectroscopic techniques. This was mainly aimed at investigating the possibility of modulating supramolecular assembly using Atx3 physiological binding partners, such as ubiquitin chains and Ub-derived peptide-mimetics compounds. Atx3 and Ub stability were then investigated in order to evaluate the hypothesis that the interaction between polyUb and Atx3 may have effects on Atx3 stability and/or interferes with the aggregation process. Selected models of Atx3 were engineered in order to compare aggregation processes of non-expanded Atx3, expanded Atx3, and Josephin domain in specific conditions. Atx3 proteins were mutated to obtain the substitution of the cysteine residue in position 14 with an alanine residue (C14A). This mutation inactivates the protein catalytic site, and as a consequence reduces self-cleavage activity of Atx3[99]. This was intended to isolate "seeding" which may trigger heterogeneous aggregation mechanisms. Furthermore, the point mutation C14A, introduced also in Josephin, inhibits the catalytic activity against polyUb chains giving the possibility to study the interaction. The conformational stability of non-expanded and expanded Atx3 was studied in vitro, revealing no differences in supramolecular assembly at different polyQ length. These results were also confirmed in in-cell studies. These experiments were performed to establish suitable conditions to analyse the effects of polyUb on the selected aggregation processes. The effects of natural binders of Atx3 on its aggregation propensity was previously analysed using isolated Josephin domain and mUb, and resulted in a decrease of Atx3 aggregation propensity and in a slowdown of the aggregation kinetics[103]. Based on this evidence, and on the fact that Atx3 presents a higher affinity for polyUb chains than for mUb, the synthesis of triUb chains was performed and its effect on the Josephin domain aggregation process was evaluated. The results clearly indicated that aggregation process is successfully reduced, confirming that the design of Ub-derived peptide-mimetics compounds can be a good therapeutic strategy.

2 Material and Methods

2.1 Recombinant Proteins Production

Non expanded Ataxin-3 (Atx3-Q14), expanded Ataxin-3 (Atx3-Q54) and Josephin domain (Jos) used in this experimental work have been prepared recombinantly. Recombinant proteins are important tools for studying biological processes and provide important findings in biomedical research. The production of recombinant proteins involves several steps and techniques and allows to have samples with high grade of purity (above 90%) suitable for in vitro studies. The first step generally consists in isolating the DNA sequence encoding for the protein of interest, cDNA, and amplifying it by Polymerase Chain Reaction (PCR). This is a widely used molecular biology technique developed in 1983 by Kary Mullis, which allows exponential enzymatic amplification of small amount of DNA sequences by a series of repeated temperature changes, called thermal cycles[104]. Once the cDNA is isolated and amplified, it is inserted into an expression vector which is a plasmid or a virus used to introduce the cDNA into a host cell, and can command the protein synthesis machinery of the host cell to produce the protein encoded by the cDNA. For this purpose, expression vectors have to provide an inducible promoter activable by a chemical inducer, the origin of replication, the correct translation initiation sequence and a selection marker (generally an antibiotic resistance gene)[105][106]. Furthermore, expression vectors are often modified in order to introduce a nucleotide sequence encoding for a tag or a fused protein upstream or downstream the sequence encoding for the protein of interest. This facilitates the purification or detection of the final protein product and/or enhances recombinant protein productivity[106]. The method of insertion of the cDNA into the vector depends on the chosen cloning strategy, such as restriction enzymes-based cloning, TA-cloning, TOPOTM-cloning, ligation independent cloning (LIC) or cloning via recombination (GatewayTM, CreatorTM)[107][108][109][110][111]. The expression vector containing the cDNA is then transferred, by electroporation or by chemical treatment, into the host cell which can be prokaryotic or eukaryotic. The choice of the host is made to ensure the maximal amount of expression, the proper folding of the product, and to sustain the protein in the intact and functional state[112]. Vector-modified host cells are then cultured in the appropriate culture medium, and protein expression is induced at a specific stage of growth by adding the chemical inducer of the vector promoter. Culturing conditions are quite standard for the chosen host cell, while induction conditions (temperature, time and inducer concentration) are optimized to guarantee the maximum protein production[113]. The recombinant protein is released by the cells to the culture medium or kept inside the cells and recovered by cells lysis, and purified generally

by liquid chromatography methods such as ionic-exchange and/or affinity chromatography. A final step of size exclusion chromatography is also often performed to gain high grade purity protein samples suitable for structural and biophysical studies[112].

2.1.1 Recombinant Atx3-Q14, Atx3-Q54 and Jos

A successful expression strategy consists of the production of proteins with functional and biochemical characteristics corresponding to the biological and native state. The prokaryotic expression system *Escherichia Coli* (*E. coli*), the most widely used[114], resulted suitable for the production of the three recombinant proteins used in this experimental work: Atx3-Q14, Atx3-Q54, and Jos (proteins sequences are reported in Annex I). In particular, *E. Coli* BL21 (DE3) pLysS strain was chosen for reducing background expression of the proteins before induction that might result toxic for the cell[105]. The bacterial expression vectors were all pET (Plasmid for Expression by T7 RNA polymerase)[115] containing the T7 bacteriophage promoter and the gene for the resistance to ampicillin antibiotic. They were provided by Dr C. Alfano from Ri.MED Foundation, and engineered in order to obtain the recombinant proteins fused to a poly-histidine tag (6xHis-tag) which allowed protein purification by Immobilized Metal Affinity Chromatography (IMAC)[116]. To enhance the protein solubility and facilitate the purification, expression vectors for Atx3-Q14 and Atx3-Q54 were also modified in order to generate the recombinant proteins fused with the highly soluble Maltose Binding Protein (MBP)[117]. In all the three vectors, the sequence encoding for the cleavage site of Tobacco Etch Virus (TEV) protease was also inserted downstream the sequencing encoding for the 6xHis-tag[118]. This allowed the enzymatic removal of the MBP region and/or the 6xHis-tag from the purified recombinant products since they might interfere with the biophysical and structural studies[119][120]. Moreover, all constructs had the point mutation C14A in order to inactivate their catalytic sites, avoiding the auto-cleavage propensity of full length Atx3[99], and the cleavage of polyUb chains when biophysical studies were performed on both Jos/polyUb and Atx3/polyUb complexes. Domains organization of the three constructs is reported in Fig. 2.1.

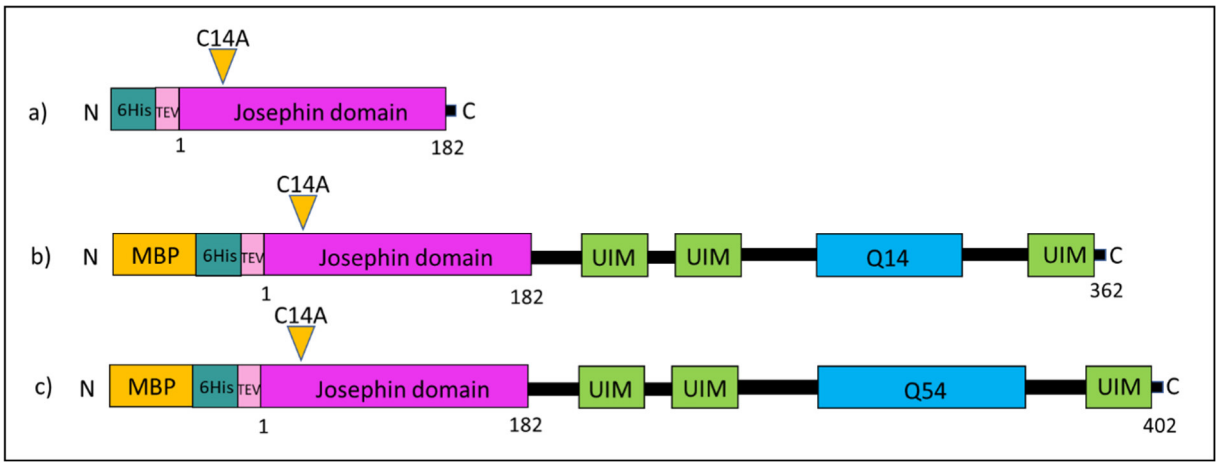

Figure 2.1: a) Domains organization of recombinant Jos: N-terminal 6xHis-tag (dark green), the site recognized by TEV protease (pink) and Jos catalytic domain (violet); **b)** Domains organization of Atx3-Q14: Maltose binding protein (MBP) (orange), 6xHis-tag (dark green), the site recognized by TEV protease (pink), Jos domain (violet), 3 Ubiquitin interactive motifs (UIM) (green) and polyQ tract with Q14 (light blue); **c)** Domains organization of Atx3-Q54: MBP (orange), 6xHis-tag (dark green), the site recognized by TEV protease (pink), Jos domain (violet), 3 UIMs (green) and polyQ tract with Q54 (light blue). Point mutation C14A, which inactivates the catalytic proprieties of all the three constructs, is also indicated.

In details, for the production of each of the three constructs, competent *E. Coli* BL21 (DE3) pLysS cells were transformed with plasmids using the standard heat shock protocol[121]. Transformed cells were then cultured in Luria Bertani medium (LB) supplemented with 50 µg/ml of ampicillin, at 37°C until the culture reached an optical density at 600nm of 0.6. Proteins expression was then induced by adding Isopropil-β-D-1-tiogalattopiranoside (IPTG) which allows the expression of the T7 RNA polymerase by binding the protein responsible for the repression of its transcription (Lac operon repressor protein)[122]. IPTG was used at a final concentration of 0.5mM, and expression was carried out for 4 hours at 37°C under shaking. Harvested cells were resuspended in 20 mM Tris-HCl, 300 mM NaCl, 5% Glycerol, 1mM DTT, 5mM $MgCl_2$, pH 7.2, supplemented with 0.5mg/ml Lysozyme, 10µg/ml DNase I, and Complete EDTA-free protease inhibitor cocktail, then lysed by sonication. Recombinant proteins were purified from the soluble fractions of the cell lysates by IMAC using ready-to-use HisTrap FF crude column pre-packed with Nickel-Sepharose resin. His-tagged proteins were retained by the column, thanks to the histidine residues that readily coordinate the Nickel ions immobilized on the column resin. Proteins elution was performed fluxing through the column 20 mM Tris-HCl, 300 mM NaCl, 500 mM imidazole, 5% Glycerol, 1mM DTT, pH 7.2 since imidazole competes with the His-tag for binding to the Nickel-charged resin. Before elution, 20 column volumes (CV) of 20 mM Tris-HCl, 1M NaCl, 5% Glycerol, 1mM DTT, pH 7.2 were passed through the column to wash out unspecific-bounded components. Eluted fractions were

collected and analysed by denaturing Sodium Dodecyl Sulphate – Poly-Acrylamide Gel Electrophoresis (SDS-PAGE). Fractions containing the target protein were then pooled together and digested with TEV protease (TEVp) to remove the N-terminal tag. Digestion was performed while dialyzing the protein/TEVp mix in 20 mM Tris-HCl, 300 mM NaCl, 5% Glycerol, 1mM DTT, pH 7.2. TEVp:Protein 1:2 and 1:6 molar ratio were used for Atx3 isoforms and Jos, respectively. Digested proteins were then separated from undigested protein, tags, and TEVp by IMAC using again a ready-to-use HisTrap FF crude column pre-packed with Nickel-Sepharose resin. Digested proteins were recovered from the flow through fraction as they lost the His-tag, and were subjected to a final step of Size Exclusion Chromatography (SEC)[123] using a Hi-Load 26/600 Superdex 75 pg GE Helthcare column equilibrated with 20mM Na-phosphate, 1mM TCEP, pH 6.5. SEC is widely used to separate proteins and polymers in solution by their size thanks to the size heterogeneity of the porous beads composing the column resin. Smaller solutes have access to more pores and are then retained for a longer period of time compared to larger solutes. In the present experimental work, the use of SEC as final purification step allowed the removal of both protein aggregates and degradation products resulting in high grade purity proteins samples suitable for the biophysical studies later performed.
In Figg. 2.2, 2.3 and 2.4 are reported the chromatography profiles and the SDS-PAGE results of Atx3-Q14, Atx3-Q54 and Jos, respectively.

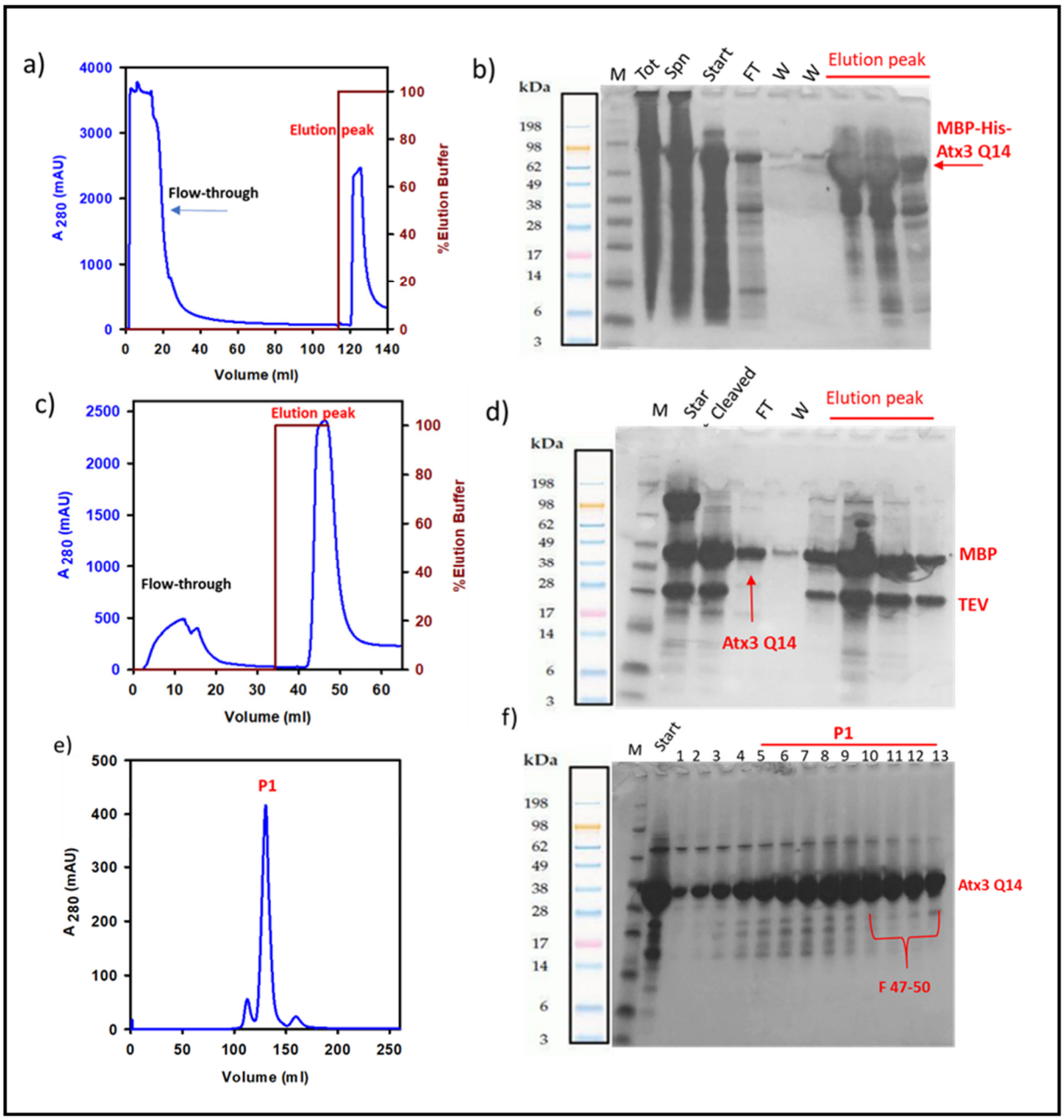

Figure 2.2: Purification of Atx3-Q14: **a)** affinity chromatography profile of the first IMAC step performed on His-tagged protein. Left axis in blue indicate absorbance at 280nm, while right axis in dark red indicate % elution buffer. **b)** SDS-PAGE analysis related to **a)** fractions. **c)** affinity chromatography profile of the second IMAC step performed after His-tag removal. Left axis in blue indicate absorbance at 280nm, while right axis in dark red indicate % elution buffer, and **d)** SDS-PAGE analysis related to **c)** fractions. **e)** SEC profile and **f)** SDS-PAGE analysis performed on cleaved Atx3-Q14 as final purification step. Lanes 10-13 correspond to the purest fractions of peak P1 in SEC profile (F47-50) and have been used for aggregation kinetic experiments.

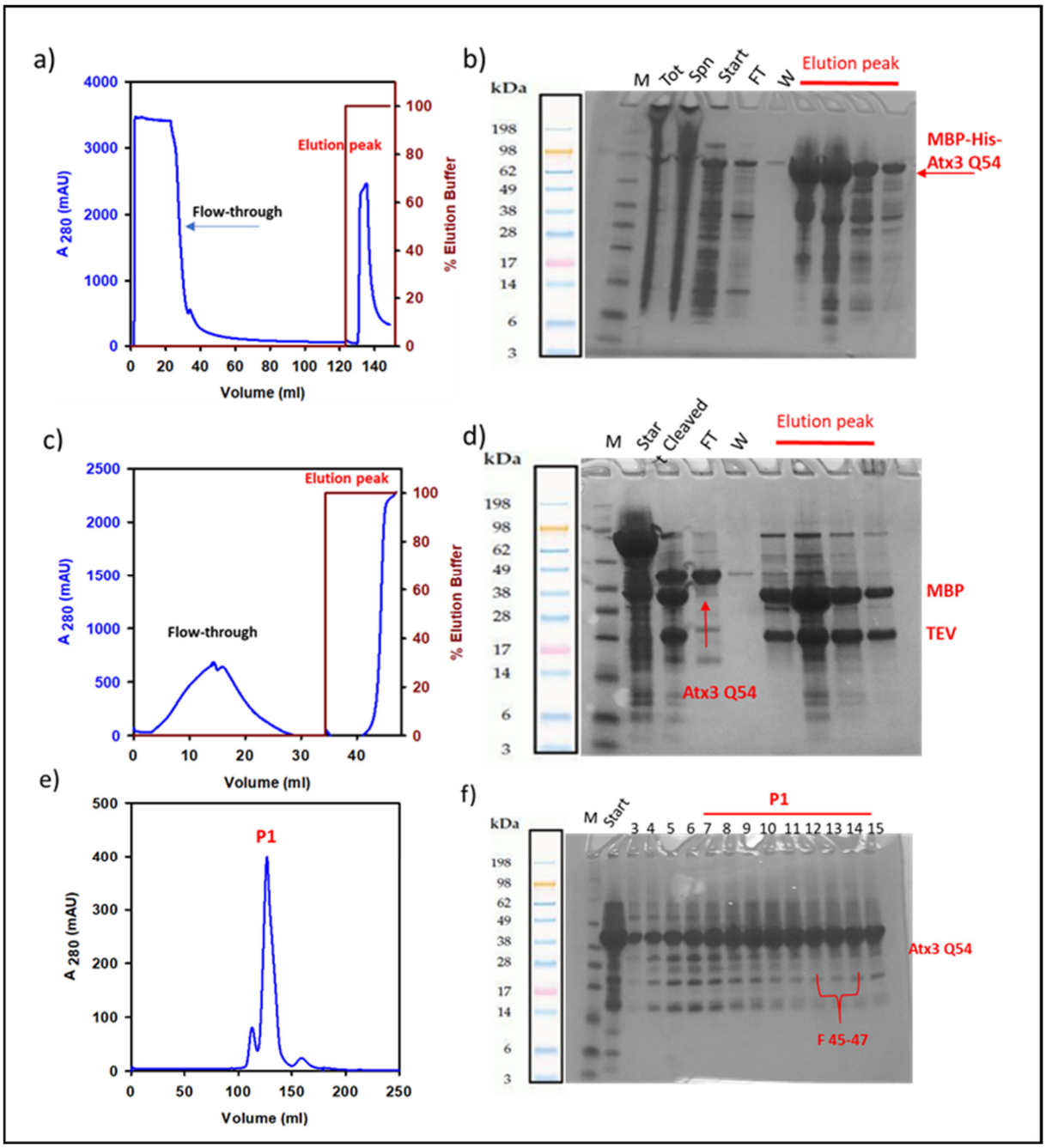

Figure 2.3: Purification of Atx3-Q54: **a)** affinity chromatography profile of the first IMAC step performed on His-tagged protein. Left axis in blue indicate absorbance at 280nm, while right axis in dark red indicate % elution buffer. **b)** SDS-PAGE analysis related to **a)** fractions. **c)** affinity chromatography profile of the second IMAC step performed after His-tag removal. Left axis in blue indicate absorbance at 280nm, while right axis in dark red indicate % elution buffer and **d)** SDS-PAGE analysis related to **c)** fractions. **e)** SEC profile and **f)** SDS-PAGE analysis performed on cleaved Atx3-Q54 as final purification step. Lanes 12-14 correspond to the purest fractions of peak P1 in SEC profile (F45-47) and have been used for aggregation kinetic experiments.

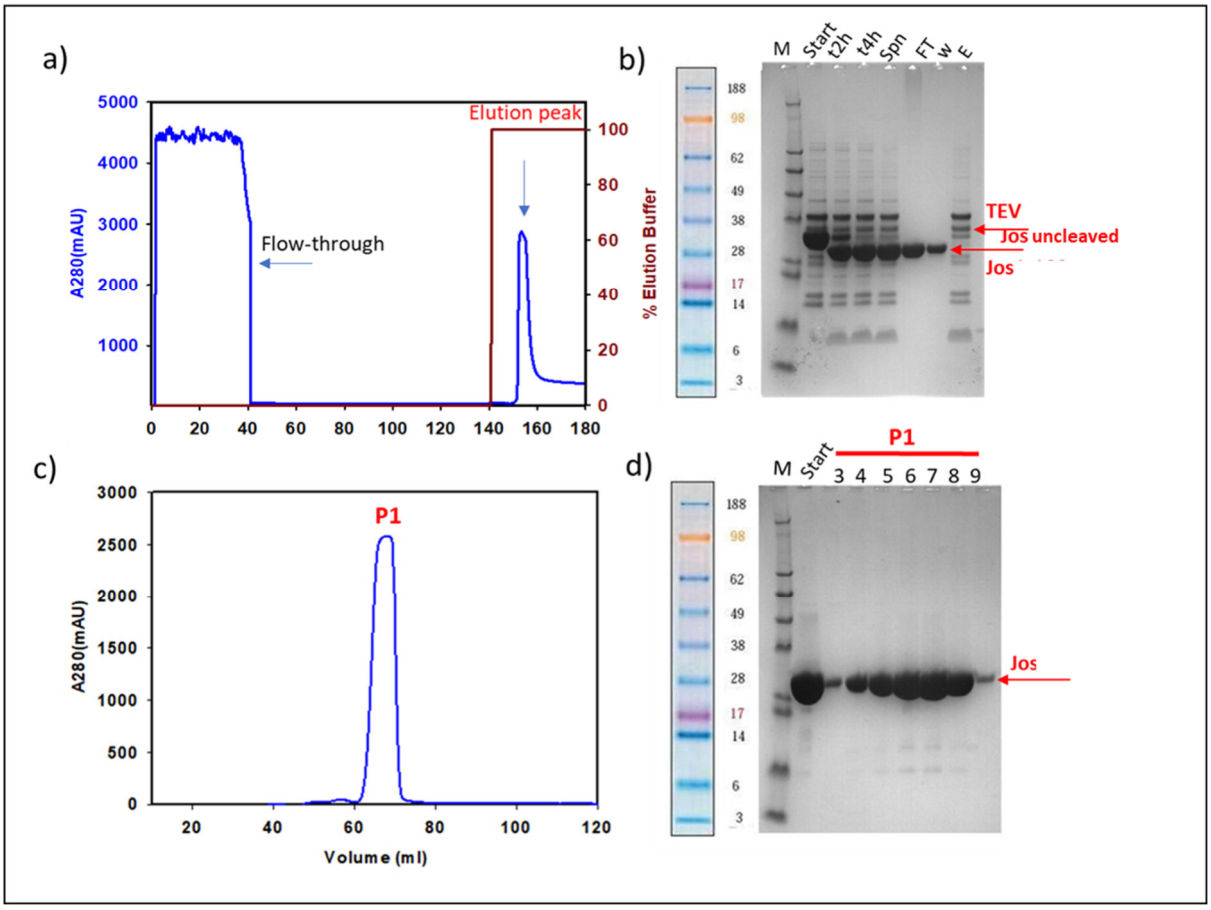

Figure 2.4: Purification of Jos domain: **a)** affinity chromatography profile of the first IMAC step performed on His-tagged protein. Left axis in blue indicate absorbance at 280nm, while right axis in dark red indicate % elution buffer. **b)** SDS-PAGE analysis of affinity chromatography step performed after His-tag removal. **c)** SEC profile and **d)** SDS-PAGE analysis performed on cleaved Jos as a final step. All SEC fractions resulted high-grade pure and where all used for aggregation kinetic experiments.

2.2 Ubiquitin samples

As discussed in chapter 1, polyUb chains are natural partners of Atx3. In particular, Atx3 has a high affinity for K48-linked and K63-linked polyUb chains[82][90]. In this experimental work we produced K48-linked polyUb chains by enzymatic reaction, and investigated the effect of these chains on the aggregation process of Josephin domain. Free mono-Ub (mUb) samples were also used to investigate the general aggregation features of ubiquitin samples.

2.2.1 mono-Ubiquitin samples preparation

mUb samples were freshly prepared in solution just before each measurement. Protein powder was purchase from Sigma Aldrich, and dissolved in 20 mM sodium phosphate buffer, pH 6.5 at different concentrations (0.5, 0.7 and 1.8 mg/ml) then filtered through 0.20 µm filters. Protein

concentration was spectrophotometrically determined using a molar extinction coefficient of 1254 $dm^3mol^{-1}cm^{-1}$ at 280 nm [124].

2.2.2 Enzymatic production of K48-linked tri-Ubiquitin samples

The production of polyUb chains by enzymatic reaction was first developed by Pickart's group, who prepared K48-linked di- and tetra-Ub chains for crystallographic studies starting from wild-type Ub[125]. Since then, the method was further optimized by several research groups to obtain multi milligram quantities of material required for biophysical and/or structural studies (reviewed in [126]). The formation of polyUb chains occurs through linkage between the lysine residue of one Ub monomer and the C-terminal glycine residue of another Ub monomer. The method is based on the formation in one reaction of Ub chains of different lengths, using the ubiquitin-activating enzyme (E1), and a specific ubiquitin-conjugating enzyme (E2). In detail, first, the C-terminal Gly residue of Ub is activated in an ATP-dependent process by E1, with the formation of ubiquitin adenylate, releasing PPi, then Ub binds a Cys residue of E1 forming a thiol-ester linkage, releasing AMP. In the second step, activated Ub is next transferred to an active Cys residue of E2 (Cdc34), that directly transfers Ub to a lysine 48 of successive Ub in order to obtain K48-linked polyUb chains, where ubiquitins are linked by an isopeptide bond between side chain of Lys 48 and the carboxyl group of Gly 76[127].

In this experimental work we produced K48-linked triUb chains using the enzymatic reaction described above. Components used to prepare K48-linked triUb samples are reported in Table 2.1. Reagents were mixed together and incubated at room temperature for 2 hours. Reaction was then stopped by adding Dithiothreitol (DTT) at a final concentration of 50mM, and the mix was incubated on ice for 30 mins to release all E1- and E2-linked ubiquitin molecules. The mixture was then diluted 1:15 with 50 mM Sodium Acetate, pH 4.5 and loaded onto a 1ml pre-packed cationic exchange chromatography Hitrap SP column. A linear gradient of 240 column volumes (CV) of 50 mM Sodium Acetate, 0.5 M NaCl, pH 4.5 was performed to separate the polyUb of different length. In Fig. 2.5 the SP chromatography profile of polyUb mix purification and the respective SDS-PAGE are reported.

Component	Final concentration
E1	2µM
Cdc34	40µM
Wilde type mUb (from Sigma)	800µM
$MgCl_2$/ATP	10mM
DTT	0.5mM
10x reaction buffer	1x
H_2O	

Table 2.1: Components and concentrations used for enzymatic reaction for K48-linked triUb production.

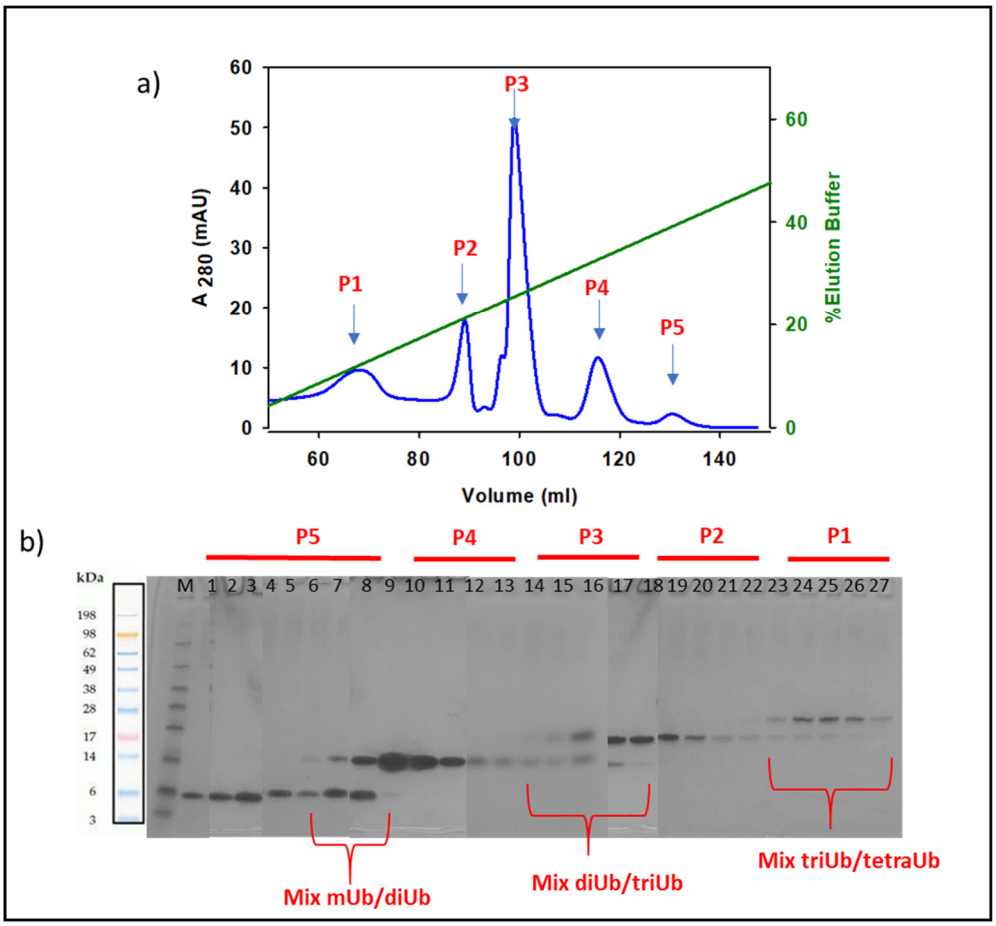

Figure 2.5: Purification of polyUb chains mixture: **a)** SP chromatography profile. Left axis in black absorbance at 280nm and red axis in green, % of elution buffer. **b)** SDS-PAGE of SP column fractions: Lane 1-9, corresponding to peak P5, reveal the presence in the peak of both isolated mUb and a mix of mUb and diUb; Lane 10-13, corresponding to peak P4, reveal the presence in the peak of isolated diUb; Lane 14-18, corresponding to peak P3, reveal the presence in the peak of a mix of diUb and triUb; Lane 19-23, corresponding to peak P2, reveal the presence in the peak of isolated tri-Ub; Lane 24-27, corresponding to peak P1, reveal the presence in the peak of a mix of triUb and tetraUb.

In order to increase the yield of the preparation, and at the same time to obtain a final sample free of any aggregate, fractions from SP column containing a mix of diUb and triUb and those containing only triUb, were pooled together and further purified by SEC using HiLoad 16/600 Superdex 75 pg GE Healthcare column, previously equilibrated in 20mM Na phosphate buffer with 1mM TCEP, pH 6.5. As shown in Fig 2.6, K48-linked triUb eluted as a well isolated peak and resulted in a high-grade purity sample suitable for biophysical studies.

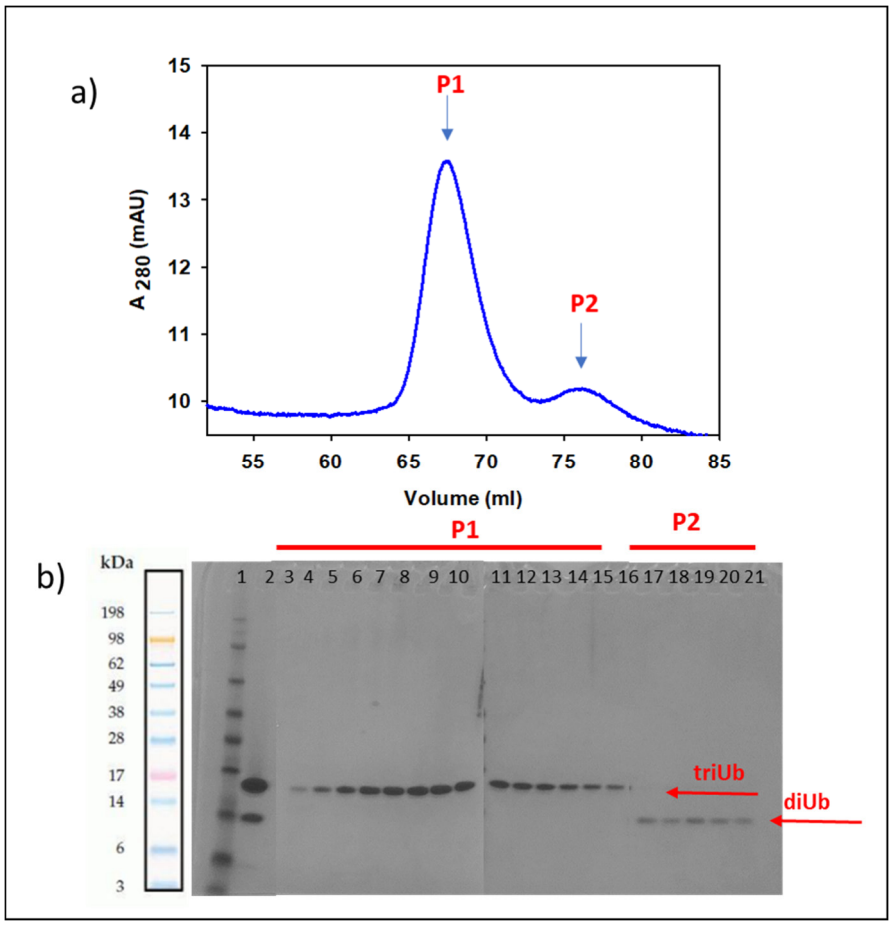

Figure 2.6: Final purification step of diUb and triUb mix: **a)** SEC profile, **b)** SDS-PAGE of SEC fractions. Lane 1: marker; Lane 2: start; Lanes 3-16: fractions corresponding to peak P1, which reveal the presence of isolated triUb; Lane 17-21: fractions corresponding to peak P2, which reveal the presence of isolated diUb.

2.3 Preparation of reference proteins

In order to perform comparison measurements to evaluate the effect of UV exposure observed for Ub, two amyloidogenic proteins, Human Insulin and Aβ(1-40) peptide, were used.

The samples were freshly prepared before each measurement. Human Insulin powder (Sigma-Aldrich) and Aβ(1-40)peptide (prepared as described in[128]), were dissolved in 20mM sodium phosphate buffer, pH 6.5. Protein concentration of Human insulin and Aβ(1-40) peptide were

estimated by means of absorbance measurements using a molar extinction of 1.067 cm^{-1} $(mg/ml)^{-1}$ at 276 nm[129], and of 1390 M^{-1} cm^{-1} at 276nm[130], respectively.
Moreover, in order to obtain aggregates, 0.2 mg/ml Human insulin in 20 mM sodium phosphate buffer, pH 6.5, was incubated at 60°C stirring at 500 rpm for 24 hours, and 0.2 μM Aβ(1–40) in 20 mM sodium phosphate buffer, pH 6.5, was incubated at 37°C with stirring at 500 rpm for 24 hours.

2.4 Preparation of Jos/K48-linked triUb complex

In order to study the effect of polyUb chains on the aggregation process of Atx3, Jos/K48-linked triUb complex was prepared. Freshly purified recombinant Jos was incubated with purified K48-linked triUb, in a 1:1 molar ratio at room temperature for about 1 hour. The mixture was then separated by SEC, using a HiLoad 10/300 GL Increase 200 pg GE Helthcare column previously equilibrated in 20mM sodium phosphate buffer with 1mM TCEP, pH 6.5. As shown in Fig.2.7 a), the complex was eluted as an isolated peak and resulted in a high-grade purity sample.

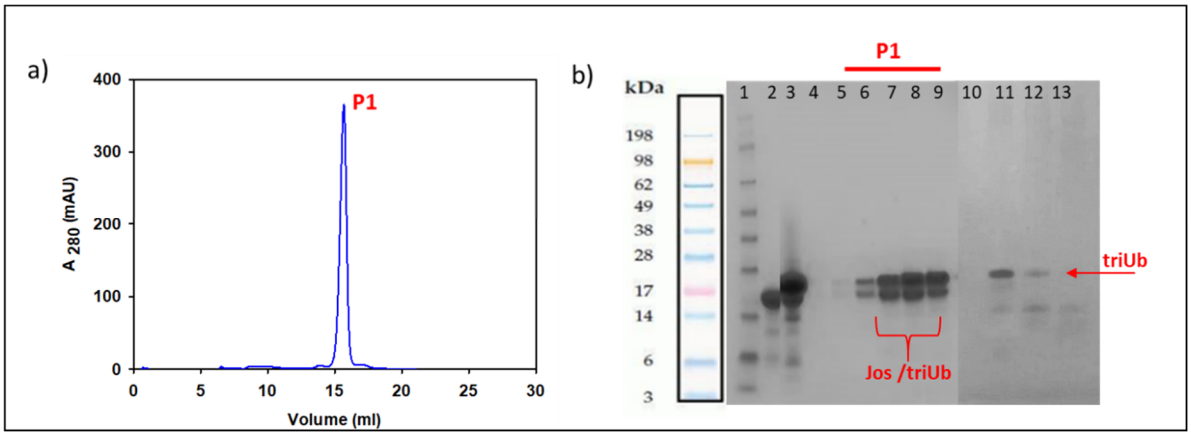

Figure 2.7: Purification of Jos/K48-linked triUb complex: **a)** SEC profile; **b)** SDS-PAGE analysis of SEC fractions. The complex comes out of the column earlier as an isolated peak, while unbounded triUb elutes later.

2.5 Spectroscopic Techniques

In order to understand the molecular mechanisms underlying the supramolecular assembly of Atx3, and hopefully to find a strategy to prevent or interfere with them, thermal aggregation was induced in different Atx3 variants and kinetic measurements were performed and analysed. In particular, aggregation of Atx3-Q14 and Atx3-Q54 variants, free Jos and Jos/K48-linked triUb complex, were investigated. Aggregation was induced by high temperature (50°C) and

supramolecular assembly was analysed by multiple methods in a time resolved fashion to obtain complementary information on protein secondary structure, hydrophobicity, and protein native state stability[7][18]. The experimental platform was firstly developed and tested on the model protein Ub. Interestingly, the analysis of Ub aggregation kinetics at high temperature revealed that standard measurement methods may induce unwanted modifications in proteins which were identified as UV-light induced oxidation of tyrosine residues. Moreover, the same conformational changes induced by UV exposure were also observed for Human Insulin and Amyloid β(1-40) peptide, that instead Ub are able to form amyloid aggregates but as Ub do not contain Trp residues in their sequences [131][132][133].

Aggregation kinetics were investigated by varying systematically relevant physicochemical parameters, such as pH, protein concentration, temperature and ionic strength, as the comparison between them provide selective information on fundamental interactions regulating supramolecular assembly[134]. In fact, was widely demonstrated that particular conditions could induce or inhibit aggregation processes[135][136].

The multiple methods used in parallel for the investigation, included UV-visible (UV-vis) absorption spectroscopy, which also gives information on the sample turbidity (Rayleigh Scattering), Fluorescence spectroscopy methods, and Circular Dichroism (CD), which gives information on secondary structure changes. The sensitivity of fluorescence methods was exploited using multiple chromophores which allowed selectively the monitoring of specific properties of the samples. In particular, both intrinsic chromophores inherently present in proteins structures and extrinsic dyes, such as Thioflavin T (ThT) and 8-Anilino-1-naphthalenesulfonic acid (ANS), were used. The principle of all methods used are shortly described in the following paragraphs.

2.5.1 UV-visible absorption Spectroscopy

In this work, UV-vis Spectroscopy was mainly used to measure protein concentrations, thanks to the ability of proteins to absorb UV-vis light at 280 nm by the two aromatic residues, tryptophan (Trp) and tyrosine (Tyr), present in their amino acid sequence[137]. UV-vis spectra were recorded from 200 nm to 600 nm in order to verify also the presence of impurities. Furthermore, UV-vis spectra from 300 nm to 600 nm were recorded to measure the concentrations of fluorescent dyes (as ThT and ANS). UV-vis spectroscopy was also used to monitor structural modifications of protein samples[133] and the growth of scattering intensity during kinetics experiments.

2.5.2 Rayleigh Scattering

A method to obtain qualitative information on the time evolution of aggregation processes, is based on the monitoring of the time evolution of Rayleigh peak during fluorescence measurements. Scattering signal can be acquired simultaneously with fluorescence kinetics measurements as it can be quantified monitoring the maximum of the elastic peak of excitation light during fluorescence measurements. This is because in dilute solutions, according to Rayleigh theory, if the particles size is smaller than the wavelength of incident light the scattered intensity from an N spherical non absorbing independent particles of V volume is given from:

$$Is=ANV^2$$

Rayleigh Scattering represents then a good tool for following aggregation/polymerization kinetics especially at low protein concentration[138][139]. The time evolution of the scattering peak growth, in fact, may give information about time scale and lag phase of aggregation processes and highlights the effect that different experimental conditions may have on them[15][140].

2.5.3 Intrinsic Fluorescence

The Trp fluorescence emission changes depend on conformational rearrangements, the environment around this residue, and/or changes in its solvent accessibility during aggregation process[141]. In particular, Trp fluorescence intensity is known to be affected by the polarity of the environment, hydrogen bonding, and non-covalent interactions. During aggregation kinetics, Trp residues may be exposed to the solvent, and as a consequence in most of the cases the fluorescence emission spectrum undergoes a red shift and decreases in fluorescence emission intensity[15][142]. Tyr residues have a lower quantum yield and minor sensitivity to the environment and they are generally used as aggregation marker only when the protein in analysis lack of Trp.

2.5.4 Thioflavin-T Fluorescence measurements

ThT fluorescence was used to detect the growth of amyloid aggregates formation during the aggregation experiments, since its capacity to bind amyloid fibrils. Upon binding to amyloid fibrils ThT fluorescence intensity increases with a maximum at about 480 nm[143] and the emission band is linearly dependent on the amount of aggregates[144]. More detailed information can also be extrapolated from data analysis, such as the presence of fibrils accessible during aggregation[20]. A large number of studies were performed to understand mechanisms behind ThT fluorescence specificity, and the more diffused model attributes the increase in ThT

fluorescence emission intensity to the rotational immobilization of the central C-C bond in ThT molecule upon binding to amyloid fibrils[145].

In this work, ThT fluorescence measurements were used to analyse the process of amyloid aggregates formation by Atx3-Q14 and Atx3-Q54 variants, and also by Jos alone and in complex with K48-linked triUb chains. Importantly, when using ThT dye it is mandatory to do control measurements to assess that supramolecular assembly is not affected by the presence of the molecule. In fact, it was demonstrated that ThT may trigger amyloid aggregation[128], and also chemical changes of the dye may occur due to solution conditions and hinder reliable detection[146]. In order to verify that the use of ThT did not affect the aggregation process, measurements were performed both *in-situ* and *ex-situ* ruling out a significant effect of the presence of the dye.

2.5.5 8-Anilinonaphthalene-1-sulfonic acid fluorescence measurements

ANS is a hydrophobic dye, widely used to obtain information on the conformational changes of hydrophobic regions of proteins, in their native states and during aggregation[147][148][149]. Moreover, detailed analysis of ANS fluorescence is a simple and efficient method to identify molten globule intermediate states of proteins. ANS, in fact, shows stronger affinity to molten globule-like intermediates than to native or unfolded states. This affinity depends on the absence of rigid packing of hydrophobic clusters in these kind of states[150].

ANS is weakly fluorescent in aqueous environment but its fluorescence emission increases with a concurrent blue-shift in its emission maximum from ~510 to ~475 nm when located in a hydrophobic environment. Therefore, in the simpler cases, an increase in ANS fluorescence intensity accompanied by a blue-shift in the emission is observed upon oligomerization and fibrils formation[151].

2.5.6 Circular dichroism

In order to evaluate if secondary structure changes occurred during aggregation experiments performed on the proteins under analysis, CD measurements were performed. CD spectroscopy is an absorption spectroscopy method, in the UV-vis range, which quantifies the differential absorption of circularly polarized light by chiral molecule. In this respect, CD technique can be applied to proteins structural studies[152]. In particular, CD spectra can be assigned to distinct structural features of proteins and give information on their secondary structure composition (%α-helix, β-sheet, turns, etc.), and on conformational changes occurring during aggregation processes[153][154].

Different structures show characteristic CD spectra (Fig. 2.10). In particular, α-helical proteins are characterised by two negative peaks centred at about 220 nm and 208 nm and a positive contribution at 193 nm[155]. Proteins with well-defined antiparallel β-pleated sheets present a large peak centred at 218 nm and positive bands at 195 nm, while disordered proteins have very low ellipticity above 210 nm and negative bands near 195 nm[156].

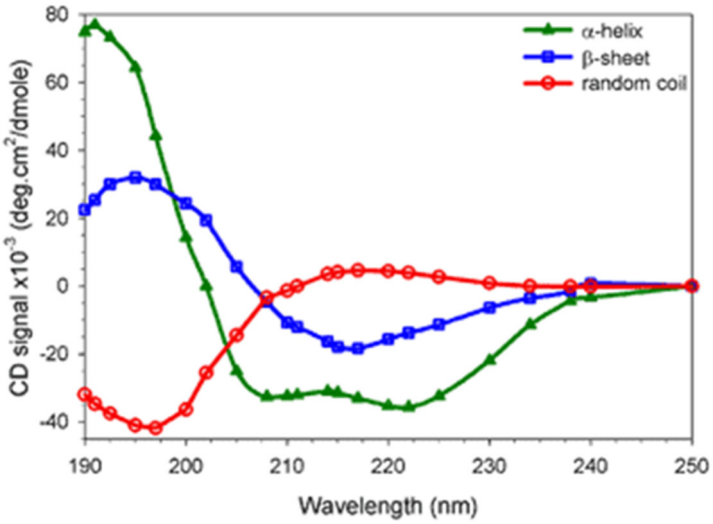

Figure 2.10: Typical CD spectra of proteins: in red CD spectrum of a protein with α-helical secondary structure; in green with random coil, and in blue with β-sheet. Figure adapted from [157].

2.5.7 Fluorescence Lifetime Imaging Microscopy

Fluorescence lifetime imaging microscopy (FLIM) is a technique that allows mapping at pixel resolution of the fluorescence decay of fluorescent molecules, thus revealing details about the structure and dynamics of macromolecules together with spatial information at submicrometric resolution[158]. The analysis of fluorescence decay gives information on the lifetime of fluorescent molecules (the average time in which the molecule remains in the excited state before returning to the ground state), which is specific of each fluorophore and highly dependent on the molecular environment. Importantly, fluorescence lifetime measurements do not depend on concentration of the molecule, potential presence of high scattering (which is common in aggregated samples), and unlike intensity measurements it is not affected by instrumental details. A simple approach to analyse FLIM data is the phasor approach. The phasor approach gives information instantaneous and is not based on fitting, which would require the definition of a model or calculation, but it is a simple approach to analyse data and fluorescence imaging[159]. In phasor analysis, every pixel of the image is transformed to a point in the phasor plot: the coordinates g and s (sine and cosine transforms, respectively) of each point in the phasor plot

are calculated from the fluorescence-intensity decay in the corresponding pixel in the FLIM image[159]. In this way, every possible lifetime is mapped in the phasor plot. All possible single exponential lifetimes lie on the "universal circle," defined as the semicircle going from point (0, 0) to point (1, 0), with radius 1/2. Point (1, 0) corresponds to $\tau = 0$, and point (0, 0) to $\tau = \infty$. As consequence, longer lifetimes are mapped near the origin of the axes and shorter lifetimes are mapped on the circumference toward the bottom right intersection with the x axis. In the phasor coordinates the single lifetime components add directly because the phasor follows the vector algebra. The clouds of points representing the fluorescence lifetime distribution over the two images are selected using a coloured circles in the phasor plot, so that the corresponding pixels are mapped back with selected colour to the image pixels[160].

In this work, FLIM was used to analyse the fluorescence signal resulting from UV-induced oxidation of three different proteins, Ub, Human Insulin and Aβ(1-40) peptide. Importantly, the use of FLIM experiments gave the possibility of highlight a substantial overlap between the signal due to the autofluorescence of tyrosine oxidation products, and the signal referred in literature as "Amyloid intrinsic fluorescence".

2.6 Experimental procedures

2.6.1 Aggregation kinetic measurements of Atx3 variants, Jos and Ub

The aggregation kinetics measurements of all samples were performed using similar methods. Ub aggregation process was induced incubating the sample at 60 °C under continuous excitation at 275 nm wavelength. The protein was placed in a 1 cm path quartz cuvette and spectra were recorded at 0.5 nm wavelength intervals, with excitation and emission bandwidth of 5 nm, scan-speed of 100 nm/min, and integration time of 1 s. Ub was exposed at different exposition times for the duration of spectrum acquisition: every 6 minutes or every 30 minutes. Ub sample aggregation was also induced at high temperature (60°C) or using stirring (500 rpm) under continuous irradiation. For each sample, emission spectra at 25°C, before and after kinetics, were measured to monitor significant variations of the emission band profile. Intrinsic fluorescence emission spectra for Ub analysis, were acquired in the range 270–700 nm with excitation at 275 nm. Simultaneously, Rayleigh scattering was also measured as the maximum of the elastic peaks of excitation light at 275 nm.

Atx3-Q14 and Atx3-Q54 aggregations were induced incubating the proteins at 50°C. In order to evaluate the role of external factors, such as pH and salt concentrations, kinetic measurements were performed at two different pH values (6.5 and 7.4), and in absence and in presence of salt (150mM NaCl). All samples were placed in a 1 cm path quartz cuvette, and spectra were

recorded at 0.5 nm wavelength intervals, with excitation and emission bandwidth of 2.5 and 5 nm, respectively, scan-speed of 100 nm/min and integration time of 1 s. ThT fluorescence emission and ANS fluorescence emission were acquired to study the aggregates formation as a function of the incubation time of the sample at 50°C. ThT emission spectra were acquired in the range 435–700 nm with excitation at 440 nm, while for the ANS assay, the spectra were acquired in the range 375–700 nm with excitation at 380 every 30 minutes.
Kinetics measured of both free Jos and Jos/K48-linked triUb complex were performed incubating samples again at 50°C, but at a single condition of pH (6.5) and in absence of salt. The experimental parameters were the same used for Atx3 proteins.

2.6.2 UV absorption measurements

For all samples, absorption measurements were carried out before and after each aggregation experiment using a Jasco V-760 Spectrophotometer. Samples were placed in 1 cm path quartz cuvette and absorption spectra were acquired from 200 to 600 nm, using a scan speed of 100 nm/ min, 1 nm bandwidth, data intervals of 0.5 nm and response of 0.96 s.

2.6.3 Thioflavin T measurements

ThT fluorescence was monitored using a Jasco FP-8500 spectrofluorimeter equipped with a Jasco ETC-815 peltier as temperature controller. Both, *in-situ* and *ex-situ* ThT measurements were performed. Regarding the *ex-situ* ThT measurements, the ThT dye was added to the samples immediately before the measurement, while to perform *in-situ* ThT measurements, the samples were incubated with ThT, and ThT fluorescence signal was detected in continuous.
For *in-situ* ThT fluorescence assays of Atx3 variants and Jos, samples were incubated at 50°C without shaking with 25 μM ThT. All samples were placed in a 1 cm path quartz cuvette and spectra were recorded at 0.5 nm wavelength intervals, with excitation bandwidth of 2.5 nm and emission bandwidth of 5 nm, scan-speed of 100 nm/min and integration time of 1 s. During kinetic experiments, after thermal equilibration, ThT emission spectra of Atx3 variants and Jos samples, were obtained under excitation at 440 nm in the range 435–700 nm every 30 minutes. Simultaneously, Rayleigh scattering was also measured as the maximum of the elastic peaks of excitation light at 440 nm. For each sample, emission spectra at 25°C, before and after kinetics, were measured to monitor significant variations of the emission band profile.
For *ex-situ* ThT measurements, Atx3-Q14 and Atx3-Q54 samples were incubated at 50°C in thermal bath for different time points: at 0 minutes; after 30 minutes; after 1 hour; after 2 hours; after 6 hours; after 12 hours; after 24 hours; and after48 hours. After thermal treatments, 25 μM

of ThT (as final concentration) were added to each sample, and ThT measurements were performed at 25°C in quartz fluorescence cuvettes. The excitation wavelength was fixed at 440 nm and the emission intensity was monitored at 480 nm.

2.6.4 ANS Fluorescence measurements

ANS fluorescence emission spectra were recorded using a Jasco FP-8500 equipped with a Jasco ETC-815 Peltier thermostat. Samples were placed in a 1 cm path quartz cuvette, and all emission spectra were recorded at 0.5 nm wavelength intervals with excitation and emission bandwidth of 2.5 nm and 5 nm, respectively, scan-speed of 100 nm/min, and integration time of 1s. Kinetic experiments, after thermal equilibration, were performed under excitation at 380 nm in the range 375–700 nm every 30 minutes. Excitation spectra were measured at 25°C before and after the kinetics to control possible variations of the excitation band profile. Simultaneously, Rayleigh scattering intensity was also measured as the maximum of the elastic peaks of excitation light.

2.6.5 CD measurements

CD measurements in the Far-UV region for Ub samples were performed using a Jasco J-715 spectropolarimeter equipped with a Jasco PCT 348WI temperature controller. Spectra were recorded from 270 to 190 nm at 25°C, before and after thermal treatments, using a scan speed of 50 nm/min, a 1 nm bandwidth, and a data pitch of 0.1 nm. Each spectrum is the result of the average of 5 accumulations.
CD measurements of Atx3 variants, were performed at 50°C for about 20 hours, using a Jasco J-1500 spectropolarimeter equipped with a Jasco CTU-100 temperature controller. Each spectrum was recorded every 30 mins, from 270 to 190 nm, using a scan speed of 50 nm/min, a 2 nm bandwidth, and a data pitch of 0.1 nm. Each spectrum is the result of the average of 2 accumulations.

2.6.6 FLIM measurements

FLIM measurements were performed on Ub, Human Insulin and Aβ(1-40) peptide aggregates in the time domain using Leica TCS SP5 inverted microscope with a 63× oil objective (Leica Microsystems), equipped with PicoHarp 300 standalone TCSPC module (Picoquant). 256 × 256 pixels images were acquired at a scanning frequency of 200 Hz under two-photon excitation at 780 nm (Spectra-Physics Mai-Tai Ti:Sa ultra-fast laser). FLIM data were processed using the SimFCS software developed at the Laboratory of Fluorescence Dynamics, University

of California at Irvine. FLIM calibration was performed by measuring the known lifetime of the fluorescein that is a single exponential of 4.0 ns.

2.7 In-cell studies

To study Atx3 aggregation process in a physiological system, and if the interaction with polyUb chains can modulate it, an in-cell model was set up. For this purpose, cDNA for Atx3-Q14, Atx3-Q55, and linear M1-linked triUb were engineered and used to transient transfect human cell. Western blot analysis and immunofluorescence assay were performed in order to detect and localize the presence of the recombinant proteins in cell. In the following section, the experimental procedures used for the in-cell studies are described.

2.7.1 Recombinant Atx3-Q14 and Atx3-Q55 for in-cell studies

In order to study the Atx3 aggregation processes in human cells system, sequence of both Atx3 isoforms, Atx3-Q14 and Atx3-Q55, were cloned into plasmids for mammalian expression. The Doxycycline-inducible vector pTet-ONE (Clonetech) was chosen in order to control and regulate the exogenous proteins expression during time. Human Embryonic Kidney 293 cells (HEK293) were used as host cells.

In order to distinguish the endogenous from the exogenous proteins, all the DNAs sequences were engineered adding a Myc tag at N-terminal (Fig. 2.11). To do this, two PCR reactions were performed: the first to insert Myc tag, and the second one to generate sticky ends necessary for cloning the constructs into the pTet-ONE vector following a Gibson Assembly cloning strategy[161]. This, also known as Seamless cloning, is a cloning method that permits to insert one or more DNA fragments into a vector without the use of restriction enzymes, thanks to combined action of an exonuclease[107]. The method combines three enzymatic activities in a single reaction: 5′exonuclease, 3′extension activity of a DNA polymerase, and DNA ligase activity.

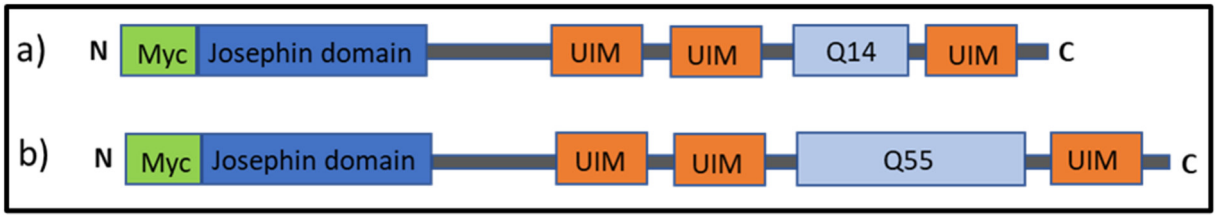

Figure 2.11: Domains organization of Atx3 constructs used for in-cell studies: **a)** Atx3-Q14 construct; **b)** Atx3-Q55 construct. N-terminal Myc tag was added to both constructs to distinguish the endogenous from the exogenous proteins.

The strategies used to design the two couples of primers necessary to perform the two sequential PCR reactions mentioned above are reported in Fig. 2.12. Designed primers were purchased from IDT and are listed in Table 2.2.

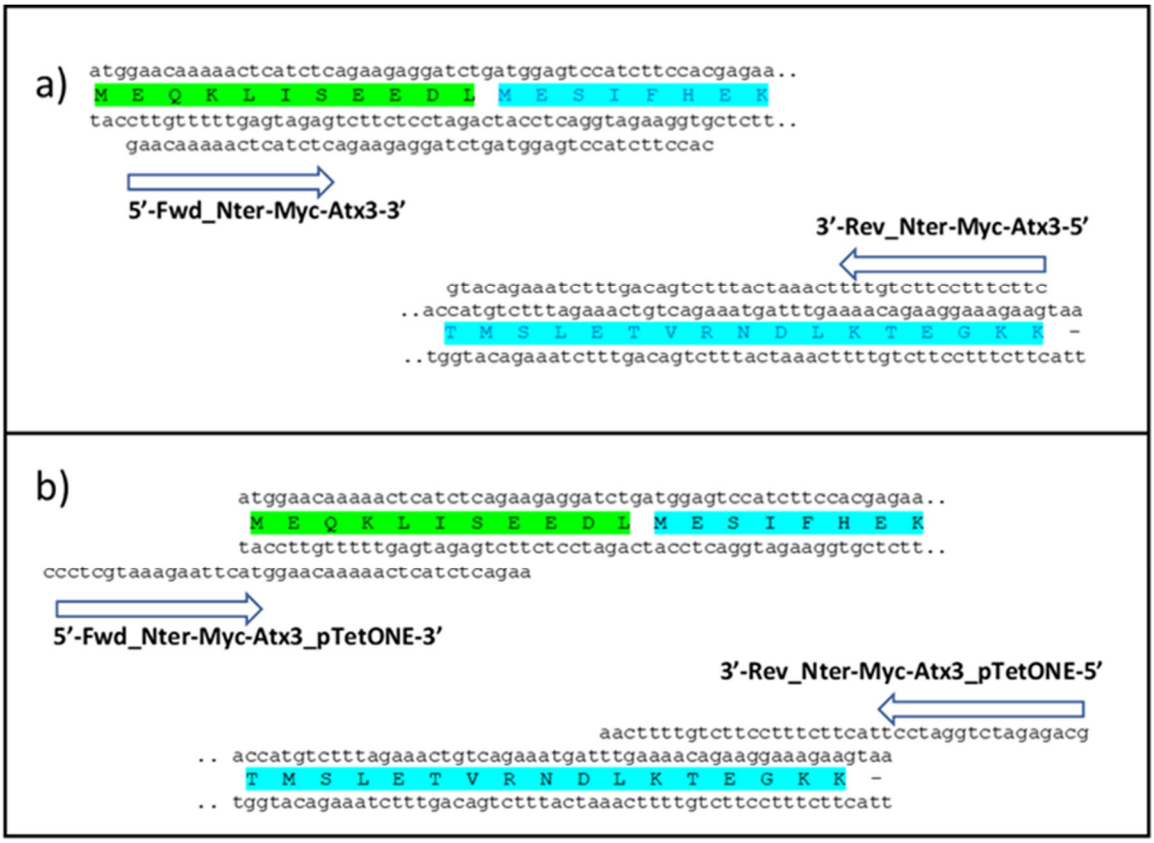

Figure 2.12: Primers design: **a)** alignment of primers used to insert Myc tag in the N-term region of Atx3 sequences. **b)** alignment of primers used to insert sticky ends useful to clone Atx3 sequence into pTet-ONE vector. In both **a)** and **b)**, Myc sequence in green, and Atx3 sequence in cyan.

Primer name	Primer sequence
Fwd_Nter-Myc-Atx3	5'-gaacaaaaactcatctcagaagaggatctgatggagtccatcttccac-3'
Rev_Nter-Myc-Atx3	5'-gaacaaaaactcatctcagaagaggatctgatggagtccatcttccac-3'
Fwd_Nter-Myc-Atx3_pTetONE	5'-ccctcgtaaagaattcatggaacaaaaactcatctcagaa-3'
Rev_Nter-Myc-Atx3_pTetONE	5'- gcagagatctggatccttacttctttccttctgttttcaa-3'

Table 2.2: Primers sequence to insert Myc tag to Atx3 sequence (green), and primers to clone Atx3 into in pTet-ONE vector (red).

The mixtures composition for the two PCR reactions are reported in Tables 2.3 and 2.4, while thermo-cycling conditions, same for the two PCRs, are reported in Table 2.5.

Component	Final Concentration
milliQH_2O	
Q5 Hot Start HF Master Mix	1X
Fwd_Nter-Myc-Atx3 primer	0.5µM
Rev_Nter-Myc-Atx3 primer	0.5µM
Template DNA	1 ng

Table 2.3: Mixture composition of the PCR reaction performed to insert the Myc tag in Atx3 sequence. As templates, Atx3-Q14 and Atx3-Q55 sequences from the pMAL bacterial expression vectors were used.

Component	Final Concentration
milliQH_2O	
Q5 Hot Start HF Master Mix	1X
Fwd_Nter-Myc-Atx3_pTetONE primer	0.5µM
Rev_Nter-Myc-Atx3_pTetONE primer	0.5µM
Template DNA	1 ng

Table 2.4: Mixture composition of the PCR reaction performed to generate sticky end to clone Atx3 sequences into pTet-ONE vector. As templates, Atx3-Q14 and Atx3-Q55 sequences generated for previous PCR (Table 2.2) were used.

Step	Temperature (°C)	Time	No. of Cycle
Initial denaturation	98	30s	1
Denaturation	98	15s	30
Annealing	65	15s	
Extension	72	45s	
Final extension	72	2min	1

Table 2.5: PCR thermal-cycling conditions

After thermal-cycling reactions, the products from the first PCR step were incubated with DpNI enzyme for 30 minutes at 37°C, in order to remove the methylated DNA template, and then analysed by 0.8% agarose gel which confirmed the success of the amplification (Fig. 2.13). Confirmed PCR products were then purified and used as template for the second PCR step. Once confirmed the success also for the second PCR reaction, the resulting products were incubated with empty pTet-ONE vector at 50°C for 30 minutes, following the manufacturing's guidelines.

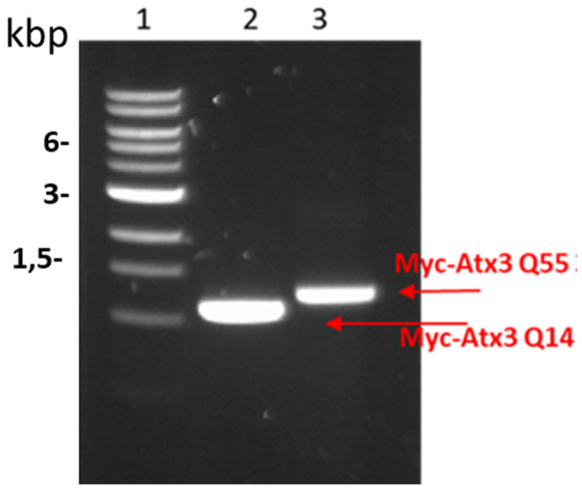

Figure 2.13: Agarose gel analysis of Myc Atx3 PCR products: Lane 1: 1 kb DNA Ladder. Lane 2: PCR product for Myc-Atx3-Q14 amplification. Lane 3: PCR product for Myc-Atx3-Q55. The presence of the bands confirm that the expected amplification has taken place.

Although the huge effort to produce pTet-ONE vectors for Atx3 expression, the system did not allow a high level of protein expression in HEK293 cells. Therefore, the two Atx3 constructs were sub-cloned into another vector for over-expression of proteins in human cells, pCI-Neo vector (Promega). This commercial vector allows over-expression in cells of recombinant proteins continuously thanks to a cytomegalovirus (CMV) promoter. The strategy used to perform

the sub-cloning into pCI-Neo vector was the multisite cloning, the most widely used method based on restriction enzymes[108]. In particular, Myc-tagged_Atx3-Q14 and Myc-tagged_Atx3-Q55 were inserted into pCI-Neo between XhoI and NotI restriction sites (see vector map in Annex II). PCR reaction was performed in order to introduce XhoI and NotI restriction sites in both Atx3 DNA sequences. The primers design strategy is reported in in Fig. 2.14. Designed primers were purchased from IDT and are listed in Table 2.6. PCR components and thermal cycling condition are reported in Tables 2.7 and 2.8, respectively.

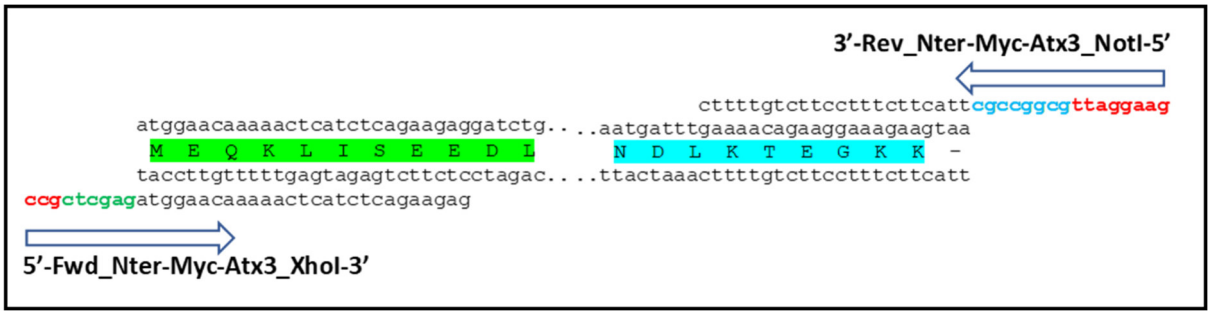

Figure 2.14: Primers design to introduce XhoI and NotI restriction sites in Myc Atx3-Q14 and Myc Atx3-Q55. Highlighted in green the sequence recognized by XhoI enzyme, and in cyan the sequence recognized by NotI enzyme. In both primers the sequence in red indicate the additional base pairs necessary to allow efficient cleavage.

Primer name	Primer sequence
Fwd_Nter-MycAtx3_XhoI	5'-ccgctcgagatggaacaaaaactcatctcagaagag-3'
Rev_ Nter-MycAtx3_NotI	5'-gaaggattgcggccgcttacttctttccttctgttttc3'

Table 2.6: Primers sequences used to insert XhoI and NotI restriction sites in Atx3 sequences. Highlighted in green the sequence recognized by XhoI enzyme, and in cyan the sequence recognized by NotI enzyme. In red the additional base pairs necessary to allow efficient cleavage.

Component	Final Concentration
milliQH_2O	
Q5 Hot Start HF Master Mix	1X
Fwd_ NterMycAtx3_XhoI	0.5µM
Rev_ NterMycAtx3_NotI	0.5µM
Template DNA	1 ng

Table 2.7: Mixture composition of the PCR reaction performed to insert restriction sites in Myc Atx3 sequences. As templates, Myc-tagged Atx3-Q14 and Myc-tagged Atx3-Q55 sequences from the pTet-ONE were used.

Step	Temperature (°C)	Time	No. of Cycle
Initial denaturation	98	30s	1
Denaturation	98	10sec	30
Annealing	65	30sec	
Extension	72	2min 30sec	
Finale extention	72	2min	1

Table 2.8: PCR thermal-cycling program performed to insert restriction sites in Myc Atx3 sequences.

After thermal-cycling reactions, the PCR products were incubated with DpNI enzyme for 30 minutes at 37°C, in order to remove the methylated DNA template, and then analysed by 0.8% agarose gel which confirmed the success of the amplification (Fig. 2.15). Empty pCI-Neo vector and both Atx3 PCR products were then digested with XhoI and NotI restriction enzymes to generate sticky ends. Insertion of the Atx3 sequences into the digested vector was performed thanks to the action of T4 DNA ligase enzyme, which allows the formation of phosphodiester bonds between the 3'-hydroxyl of one DNA terminus with the 5'-phosphoryl of another[108].

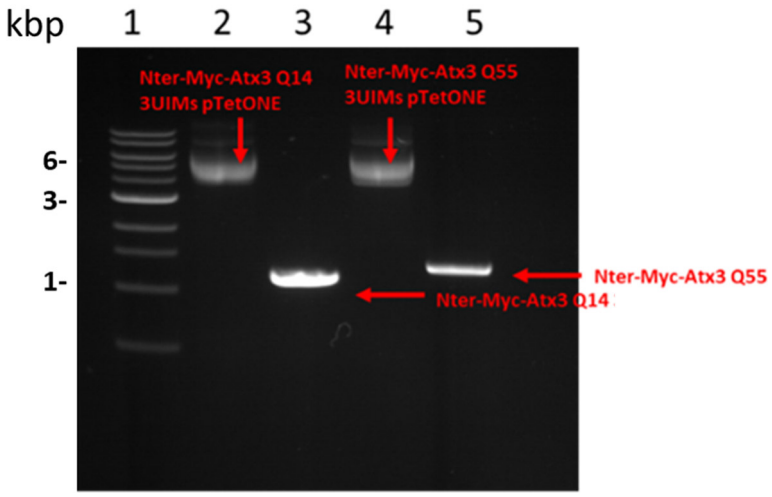

Figure 2.15: Agarose gel analysis of Myc Atx3 PCR products with XhoI and NotI restriction sequences: Lane 1: 1 kb DNA Ladder. Lane 2: Myc-tagged Atx3-Q14 in pTet-ONE plasmid used as template to generate Myc-tagged Atx3-Q14 with XhoI and NotI restriction sites. Lane 3: PCR product for Myc-tagged Atx3-Q14 amplification. Lane 4: Myc-tagged Atx3-Q55 in pTet-ONE plasmid used as template to generate Myc-tagged Atx3-Q55 with XhoI and NotI restriction sites. Lane 5: PCR product for Myc-tagged Atx3-Q55 amplification. The presence of the bands for the two PCR products confirm that the expected amplifications have taken place.

2.7.2 Recombinant M1-linked triUb for in-cell studies

To evaluate the interaction between Atx3 isoforms and polyUb chains in cell, a construct expressing linear M1-linked triUb was engineered and cloned into pCI-Neo vector between XhoI and NotI restriction sites (see vector map in Annex II). A HA tag was inserted at N-terminal region to detect the exogenous protein in cell (Fig. 2.16). DNA sequence was purchase by gBlocks Gene (IDT) already including the HA tag.

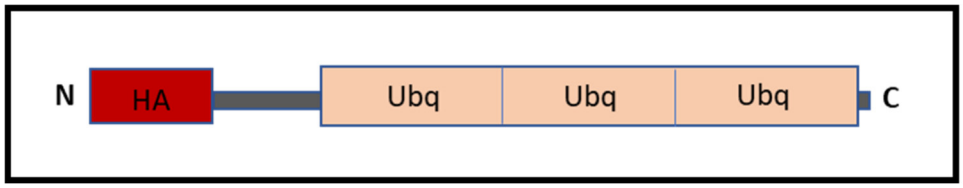

Figure 2.16: Domain organization of linear M1-linked triUb used for in-cell studies. A HA N-terminal tag (red) was added to detect the over-expressed proteins.

PCR reaction was performed in order to introduce XhoI and NotI restriction sites. The primers design strategy is reported in in Fig. 2.17. Designed primers were purchased from IDT and are listed in Table 2.9. PCR components are reported in Tables 2.10, while thermal cycling conditions are the same of those reported in Table 2.8.

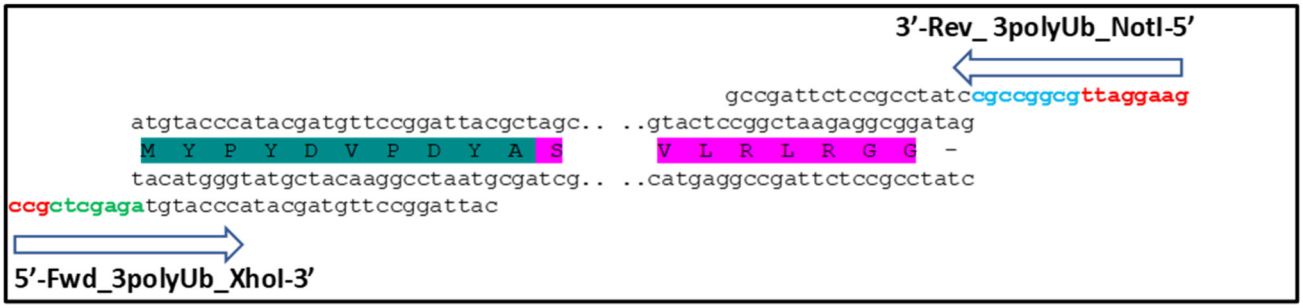

Figure 2.17: Primers design to introduce XhoI and NotI restriction sites in HA-M1-linked triUb construct. Highlighted in green the sequence recognized by XhoI enzyme, and in cyan the sequence recognized by NotI enzyme. In red the additional bp.

Primer name	Primer sequence
Fwd_3polyUb _XhoI	5'-ccgctcgagatgtacccatacgatgttccggattac-3'
Rev_ 3polyUb _NotI	5'-gaaggattgcggccgctatccgcctcttagccg-3'

Table 2.9: Primers sequences used to insert XhoI and NotI restriction sites in HA M1-linked triUb sequence. Highlighted in green the sequence recognized by XhoI enzyme, and in cyan the sequence recognized by NotI enzyme. In red the additional base pairs necessary to allow efficient cleavage.

Component	Final Concentration
milliQH_2O	
Q5 Hot Start HF Master Mix	1X
Fwd_3polyUb _XhoI	0.5µM
Rev_ 3polyUb _NotI	0.5µM
Template DNA HA- M1-linked triub gblock	1 ng

Table2.10: Components and relative concentration for PCR reaction performed to insert restriction sites in HA-tagged M1-linked triUb sequence.

DpNI treatment, XhoI and NotI digestion, and ligation were then performed as already described in the previous paragraph. In Fig. 2.18 the agarose gel of the PCR product is reported.

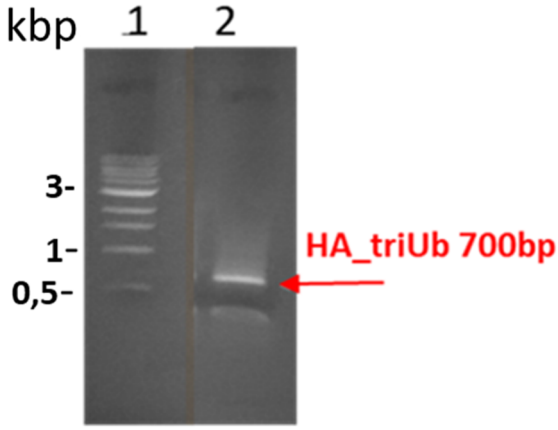

Figure 2.18: Agarose gel analysis of HA M1-linked triUb PCR product with XhoI and NotI restriction sequences: Lane 1: 1 kb DNA Ladder. Lane 2: PCR product for HA M1-linked triUb amplification. The presence of the band in Lane 2 confirms that the expected amplification has taken place.

2.7.3 Transient transfection of Atx-3 variants and M1-linked triUb in HEK293

In order to investigate on the interaction between Atx3 and polyUb chains in human cells, HEK293 cells were transient transfected using Myc-tagged Atx3-Q14, Myc-tagged Atx3-Q55 and HA-tagged M1-linked triUb constructs. HEK293 cells are widely used in cell biology research, because of their reliable growth and propensity for transfection. Cells were cultured in DMEM, high glucose, pyruvate (Gibco), supplemented with 10% heat-inactivated fetal bovine serum FCS (Thermo Fisher), 2 mM GlutaMAX (Gibco), 0.1% MEM no essential amino acids 100X (Gibco). Cells were maintained in humidified 5% CO2/95% air, at 37°C until 24 hours then transfected. Transfection was performed by chemical transfection method, which is based on the use of cationic lipids able to interact with negatively charged DNAs. The resulting lipids/DNA complexes are able to pass through the cell membrane, probably by endocytosis and phagocytosis process, and the exogenous DNA is translated into the protein of interest[162]. In this work, Lipofectamine 3000 Reagent (Invitrogen) was used as chemical transfecting agent following the manufacturing instructions. 2.5 µg of each plasmid was incubated with 5 µl of Lipofectamine, and the complex was then added to HEK293 cells at 70-90% confluence in 6-wells plates. To evaluate the effect of triUb on Atx3 expression and aggregation, co-transfection of the two relative plasmids was performed. Transfected cells were then maintained in humidified 5% CO_2/95% air, at 37°C for 48 h. Cells transfected with green fluorescent protein (GFP) construct were used as control of transfection.

2.7.4 Detection of Ataxin-3 variants and triUb in human cell

To verify the level expression of the proteins of interest, and to test the efficiency of transfection in cells, western blot analysis was performed[163]. Cell lysates containing 15 µg of total proteins were denatured for 5 min at 100°C in Laemmli sample buffer, and subjected to SDS-PAGE analysis, using 12.5% polyacrylamide gels (Life Technologies). The proteins contained in the lysates were separated by size in the gel, and were then transferred from the gel to a Polyvinylidene fluoride (PVDF) membrane (Thermo Fisher) in 1x transfer buffer (0.25M Tris, 1.92M glycine, 20% methanol). Western blotting was carried out using the mini Trans-Blot electrophoretic transfer system (Bio-Rad) for one hour at 100 V. In order to verify the proteins transfer from the gel to the membrane, staining for 5 minutes with Ponceau Red (Sigma-Aldrich) was performed. The membranes were blocked for 1 hour in 1x casein blocking buffer (SIGMA), in order to saturate all non-specific binding sites reducing the background. Membranes were immune-stained over night at 4°C with specific primary antibodies. The primary antibodies used were: rabbit polyclonal anti-Atx3 1H9 clone antibodies (1:500, dilution), rabbit polyclonal anti-Myc antibodies (1:1000, dilution), mouse anti-HA antibodies (1:1000, dilution) and anti-Tom20 antibodies (1:5000, dilution). The primary antibodies are usually coupled with signal-inducing secondary antibodies. For these experiments were used as secondary antibodies, Alexa Fluor 680 goat anti-mouse IgG antibody (1:20000, dilution, red) and Alexa Fluor 488 goat anti-rabbit IgG secondary antibodies (1:20000, dilution, green). Secondary antibodies conjugated with fluorophores were detected by fluorescence detection system Odissey CLx (LI-COR).

2.7.5 Localization of Ataxin-3 variants and triUb in human cell

Immunofluorescence assays were performed to detect and localize over-expressed exogenous proteins in transfected HEK293 cell line. Generally, immunofluorescence assay is used on biological samples to detect proteins in cellular contexts using specific antibodies, giving information on localization of detected proteins in cellular compartments.

Immunofluorescence assays can be direct and indirect. In the first case, a primary antibody conjugated with a fluorophore is used both to capture the protein of interest and for detection. In the second case, a primary antibody is used to capture the protein of interest, and it is then recognized by a secondary antibody conjugated with a fluorophore for detection by fluorescent microscope analysis[164]. In this experimental work, indirect fluorescence assays were performed. After 48 hours from transfection, HEK293 cells were fixed in 4% paraformaldehyde (PFA) pH 7.4, permeabilizated with 1% Triton-X 100. For blocking step, 3% fetal bovine serum

(FCS) in PBS was used. Cells were then immune-stained with the following primary antibodies: rabbit polyclonal anti-Atx3 1H9 clone antibodies (1:100 dilution) to detect both endogenous and exogenous Atx3 proteins; rabbit polyclonal anti-Myc antibodies (1:8000 dilution) was used to detect Atx3 exogenous proteins; mouse anti-HA (1:1000; dilution) was used to detect exogenous triUb. Alexa Fluor 568 goat anti-mouse IgG antibody (red), 1:1000, dilution, and Alexa Fluor 488 goat anti-rabbit IgG secondary antibodies (green), 1:1000, dilution, were used as secondary antibodies. Nuclei were stained with 4′,6-diamidino-2-phenylindole dihydrochloride (DAPI). The cells were visualized using a DM5000B microscope (Leica Microsystems, Wetzlar, Germany).

3 Results

In this section, experimental results obtained in this work will be described. The aim of the project "*Understanding the relationship between normal function and aberrant aggregation: the case of ataxin-3*" (PON industrial PhD program) is to evaluate, in the case of Atx3, if and how the molecular interaction between specific polyUb chains and Atx3 could affect aberrant Atx3 aggregation, and thus pathogenic mechanisms involved in SCA3. As previously reported, Atx3 is a ubiquitin hydrolase, which physiologically binds and cleave specifically, K48-linked polyUb chains [80][90][165]. An ideal experimental approach to reach the project goals would involve the study of the conformational properties and aggregation pathways of individual K48-linked polyUb chains, and then the analyse of these when in interaction with Atx3. Unfortunately, the low quantities of polyUb chains that can be obtained by enzymatic reaction preparation (as explained in chapter 2) discouraged to proceed in the separate analysis of the conformational stability of these molecules. As an alternative route, mUb as a standard model was used as it is the main subunit of polyUb. This allowed the development of a suitable experimental platform and, simultaneously, the analysis of the conformational properties this protein. In section 3.1, the experimental analysis of the thermally induced aggregation processes of mUb, and the analysis of its conformational and structural changes under destabilizing conditions, are reported. Importantly, in this part of the study modifications induced by UV light on Ub were pointed out. In particular, structural changes and oxidation of Tyrosine residues were found to be induced by illumination from the Xenon lamp of the spectrofluorometer during kinetic measurements in aggregation conditions. Target residues were highlighted together with changes in protein structure at molecular level and the appearance of a new fluorescence peak in the visible region characteristic of the oxidation process. Importantly, this peak can be put in relation with the literature regarding the so called "amyloid intrinsic fluorescence signature" which exists in the same range.

In section 3.2, results of experimental studies on aggregation processes of the non-pathological variant Atx3-Q14 and the expanded variant Atx3-Q54 are presented. Different physical-chemical conditions allowed to highlight the role of electrostatic and hydrophobic interactions in the evolution of the process. The model proteins were produced introducing a suitable mutation (C14A) that inactivates the protein catalytic site, and as a consequence reduce both the catalytic activity against polyUb chains and the Atx3 self-cleavage activity. Presented data unambiguously show that both proteins, in the selected experimental conditions, follow the same aggregation pathway, independently on polyQ tract length. In the framework of recent literature, this result can be interpreted taking into account the experimental conditions and clearly highlights

the dominant role of Jos domain and of auto-cleavage mechanisms in pathological aggregation. In-cell experiments in HEK293 cells were also performed, aimed at analysing cellular localization of the selected Atx3 variants and their toxicity when overexpressed. Evidences are presented highlighting that Atx3-Q14 and the expanded variant Atx3-Q55 interact in analogous way with triUb molecules in cellular environment, and that in the presence of triUb self-cleavage events are reduced.

In-vitro and *in-cell* studies encouraged to proceed, *in-vitro*, with the experimental characterization of the interaction between Jos domain and specific triUb chains, which were suitably synthetized by enzymatic reaction. Results indicate that, in line with the hypothesis of the project, native-native interaction with natural binders, in conditions where heterogeneous mechanisms are suppressed, reduce abnormal aggregation and pave the way to further studies on inhibitors derived from natural binders of relevant proteins involved in polyQ pathologies.

3.1 In-vitro analysis of thermal and UV-illumination effects on Ubiquitin

Ub is a small protein, evolutionarily conserved in all eukaryotes, involved in several cellular pathways. The principal biological role of Ub is the involvement in the ubiquitin proteasome system, that regulates proteins degradation in cells. In fact, proteins targeted to degradation are ubiquitinated, thanks to covalent attachment of Ub molecule or polyUb chains before degradation, and this post translational modification permits their recognition by the degradation proteasome system[166].

A multiplexed experimental approach based on spectroscopic techniques, as UV-Visible absorption and, fluorescence spectroscopy, light scattering and circular dichroism, was used to analyse Ub conformational properties under stress conditions as high temperature, stirring and UV- Illumination.

The interest on UV-exposure effect depends on the implication that this exposition could have on proteins structure and functions. Indeed, proteins, for their UV absorption characteristics and their abundance in cells, are primary targets of UV-mediated cellular damages, and the effects of UV-induced oxidation on structure and function and its implications in human pathologies has been widely investigated[167].

Importantly, experimental results have shown that UV-light exposure induces irreversible oxidation processes in Ub structure. In particular, changes attributable to the formation of oxidation products of tyrosine were observed, and in particular the formation of di-tyrosine and DOPA. Structural modifications induced by UV-light exposure were found to modify thermal stability of the protein inducing significant variations in its aggregation pathway.

These results have a specific interest for the present thesis study as they deal with the further analysis of interactions between Atx3 and polyUb chains on aggregation process. Even more importantly, they are of a great interest from a general point as target residues and changes in protein structure at molecular level have been highlighted under UV-stress. Indeed, reported results increase the number of information on the relation between oxidation processes, molecular mechanisms in aggregation, and on the methods to monitor these events also in relation to supramolecular assembly of proteins. Ub was selected as a model system but presented results indicating that analogous results can be obtained also in other system with no tryptophan residues in protein sequence. This gives a general valence to presented findings. Moreover, in view of the fact that considerable evidences link UV-induced oxidative stress to skin cancer, and that ubiquitination process was shown to have a key role in regulating tumor-promoting or tumor suppressing pathways, the present study may also assume specific relevance.

Importantly, the obtained results can also be put in relation with the literature regarding the so called “amyloid intrinsic auto fluorescence signature”, a largely debated topic in the last years[168][169]. The signal due to tyrosine oxidation exists in the same range with analogous feature, so that it may represent a significant hindrance in the specific detection of amyloid intrinsic fluorescence, or it is also possible to infer that the electronic levels that become available when tyrosine is oxidized may be at least one component of the dim blue signal which make fibrils observable in the visible range with standard laser scanning confocal or two photon microscopes. The findings challenge the simple attribution of “amyloid intrinsic auto fluorescence” and point the finger at the need for attention to details of sample preparation, and to control experiments especially with the development of extremely sensitive instrumentation and automated methods.

Figure 3.1a reports the time evolution of emission fluorescence spectra of 0.5 mg/ml Ub incubated at 60°C, for 24 hours. Spectra were acquired every 20 minutes under continuous excitation at 275 nm. The illumination due to the excitation light was kept constant for all the duration of the measurement.

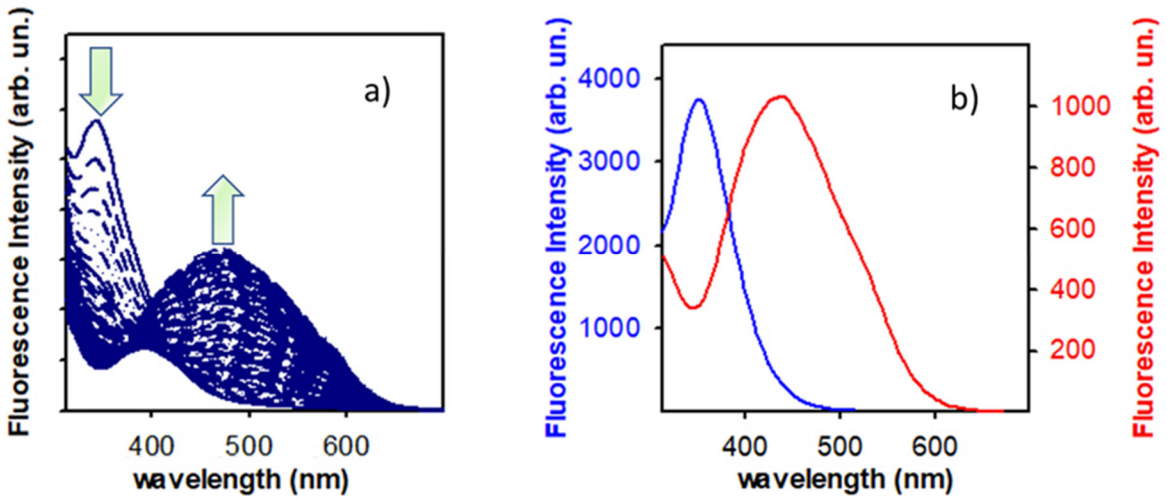

Figure 3.1: a) Time evolution of fluorescence emission spectra of 0.5 mg/ml Ub in 20mM sodium phosphate buffer, pH 6.5, incubated at 60°C for 24h. Fluorescence spectra were acquired every 20 minutes with continuous excitation at λ_{exc}=275 nm. The arrows indicate the changes of the signals as a function of time. **b)** Fluorescence emission spectra measured at room temperature of 0.5 mg/ml Ub in 20mM sodium phosphate buffer, pH 6.5, before (blue line, blue axis) and after (red line, red axis) incubation at 60°C for 24h under continuous UV exposure. Figure modified from [133].

A decrease in fluorescence emission intensity around 350 nm and an increase at 450 nm was observed, as indicated by arrows (Fig. 3.1a). Figure 3.1b reports Ub fluorescence emission spectra measured at room temperature before and after thermal treatment (60°C). Significant spectral modifications are observed. In the time-evolution experiments, before irradiation, Ub showed a maximum peak around 350 nm, typical of native Ub. Under UV irradiation, the peak centred at 350 nm decrease, while a corresponding increase in the blue region of the emission spectrum, with a maximum around 470 nm, was observed. The observed changes were irreversible and did not occur if the sample was not subjected to continuous UV irradiation (data not shown).

Measurements reported in Fig. 3.1a revealed a progressive reduction in fluorescence intensity signal linked to tyrosine while, in parallel the growth of a new peak centred at 470 nm is observed. Data did not show the presence of an isosbestic point, indicating that the observed changes are consequence of multiple phenomena causing the modification of optical properties of the sample.

The main peak at lower wavelength (350nm) is attributable to the emission of the unique tyrosine residue of the protein[124][170][171]; the Tyr residue in position 59 is, indeed, the sole responsible of intrinsic fluorescence of Ub[172].

Although less sensitive to changes in the environment than tryptophan residues[125][173], Tyr residues have often been used to monitor conformational properties and aggregation processes in proteins. Tyr has significantly lower quantum yield than Trp residue and it is used as an intrinsic fluorescent probe only for proteins without Trp residues in their sequence[170][174][173]. In the case of Ub, time resolved fluorescence study in the ps range have suggested that changes in Tyr quantum yield, varying pH, are caused by the interaction with other residues in the surroundings and by the formation of tyrosine-carboxylate hydrogen-bonded complex and tyrosinate[124][175]. Data in the literature suggest that the new band in the blue region, centred at 470 nm can be assigned to oxidation products of tyrosine, such as dityrosine and tyrosinate, as reported in [176][177][178]. In particular, the observed spectral changes can be correlated with the formation of tyrosine oxidation products, involving cyclization and decarboxylation[132][173]. These changes can be related with the oxidation of tyrosine residues resulting in the formation of different products, with optical activity[179][174], such as dityrosine [180][175][171], Dihydroxyphenylalanine (DOPA) and some hydroxycinnamoyls[178]. Di-tyrosine formed by UV irradiation are found to show similar spectral changes as reported in Fig. 3.1.

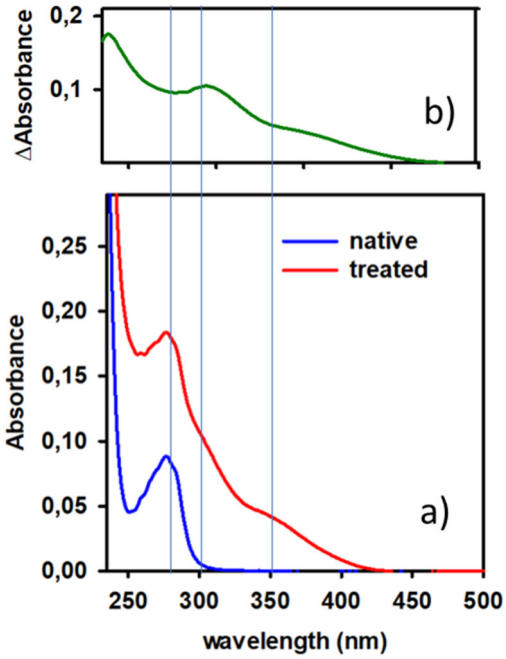

Figure3.2: Ub absorption spectra before and after thermal treatment at 60°C under UV exposure. **a)** Absorption spectra of 0.5 mg/ml Ub sample before (blue line) and after (red line) incubation at 60°C for 24h, under continuous UV-exposure at UV-light at excitation wavelength at λ_{exc}=275 nm. b) Differential Absorption spectrum due to the continuous UV exposure. Blue lines at 280, 300 and 350 nm are guides for eyes. Figure modified from[133].

Figure 3.2a shows Ub absorption spectra before and after thermal incubation at 60°C for 24 hours, under continuous UV exposure in the same conditions as the one in Fig 3.1. In figure 3.2b the difference spectrum between treated and untreated sample is also reported to better highlight the occurrence of two new absorption peaks.

After incubation of Ub at 60°C, an increase of turbidity is clearly observed, attributable to an increased scattering of the solution due to aggregation[177]. Most interestingly, in the absorption spectra reported in Fig. 3.1b, UV exposure caused the growth of two new significant components in the absorption spectrum, one centred at 300 nm and one, more evident in raw data, centred at 350 nm. These observations are in line with the formation of tyrosine oxidation products. In particular, similar modifications in the absorption spectrum are considered, as a marker of di-tyrosine formation and of protein oxidation, responsible for several diseases, which have been associated to aging processes or exposure to UV-light[15][181].

In order to evaluate if the oxidation of Tyr residue is due only by UV irradiation, or depends on other factors that could influence the process, the sample was irradiated under different exposition conditions, such as protein concentration, temperature and agitation of the sample.

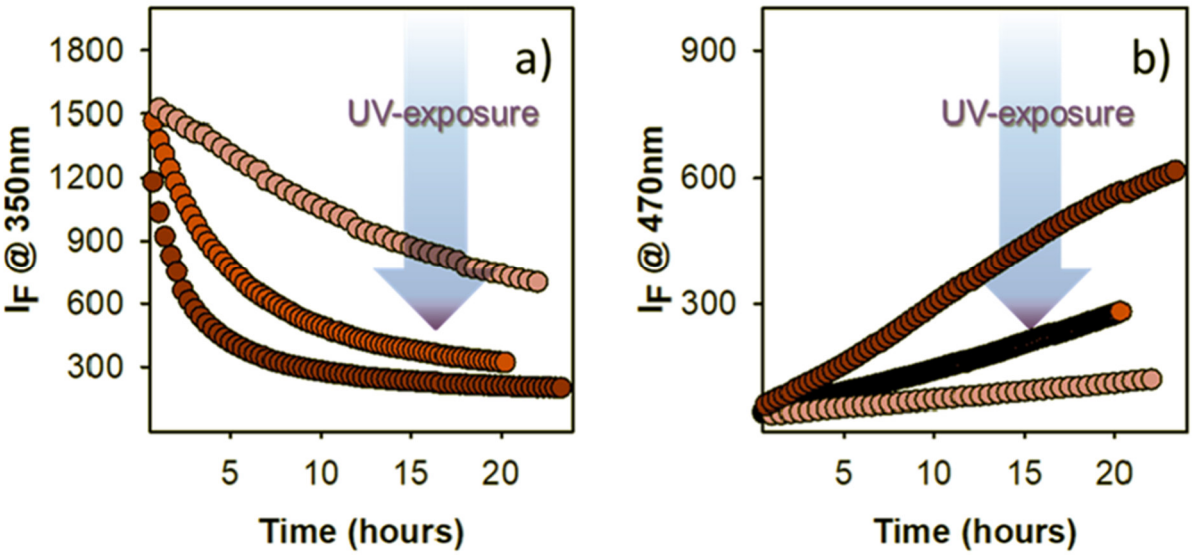

Figure 3.3: Fluorescence emission intensity as a function of time measured at 350 nm **a)** and at 470 nm **b)** for 0.5 mg/ml Ub in 20mM sodium phosphate, pH 6.5, incubated at 60°C for 22 hours; Ub was exposed to UV light (λ_{exc}=275 nm), continues UV-exposure (dark red circles), for 3 minutes (time of spectrum measurement) every 6 minutes (red circles), and for 2 minutes every 30 minutes (pink circles). Figure modified from[133] .

Figure 3.3 reports the kinetics of fluorescence spectral changes for three identical Ub samples, incubated in the same conditions as before, but using three different protocols of irradiation during the fluorescence measurements: continuous irradiation (dark red circles), irradiation

only for the duration of spectrum acquisition every 6 minutes (red circles), and every 30 minutes (pink circles).

Interestingly, exposing Ub for different times of UV radiation, significant changes are observed in the evolution of fluorescence peak signal changes. The samples exposed to UV light for longer times (continuous exposure) show a decrease of fluorescence intensity which reaches a plateau in about 15 hours. Sample with intermediate exposure (every 3 minutes and every 6 minutes) reaches a plateau in 20 hours, while for the sample with the shortest exposure the plateau is not observed even after 36 hours. These results suggest that the effect corresponding to the tyrosine residue oxidation, is caused by UV irradiation.

In order to highlights other possible factors, Ub samples at three different protein concentrations (0.5,0.7 and 1.8 mg/ml) were incubated at 60°C, under continuous exposure to UV-light for 24 hours.

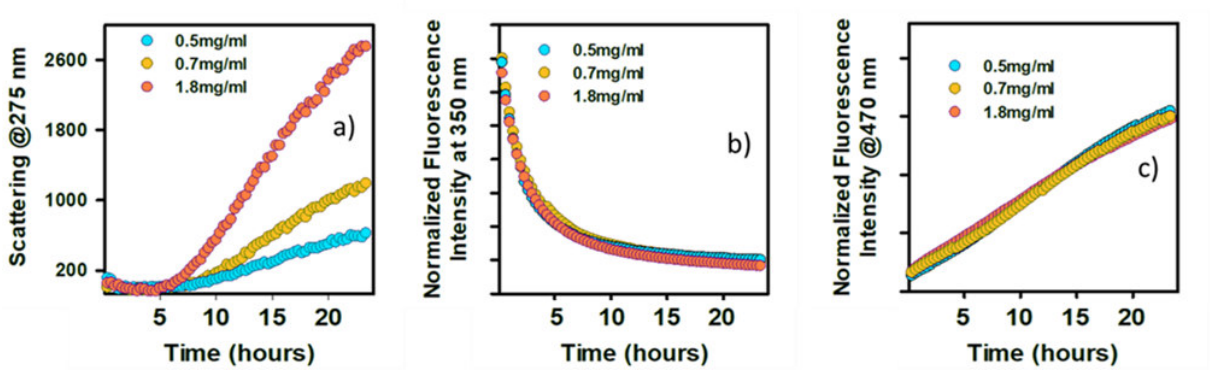

Figure 3.4: **a)** Rayleigh scattering intensity measured at 275 nm as function of time, for three different protein concentrations. **b)** and **c)** Normalized fluorescence emission intensity as a function of time measured respectively at 350 and at 470 nm, at different protein concentrations. Figure modified from[133].

Fig. 3.4 shows the time evolution of Rayleigh scattering (a), and fluorescence intensity measured at 350 nm (b) and at 470 nm (c), respectively. The results in Fig. 3.4a showed that after a short lag-phase lasting about 5 hours, the Rayleigh scattering intensity started to increase as function of time. The observed growth of Rayleigh scattering showed that Ub at 60°C forms aggregates and this aggregation process depended on protein concentration. Although Ub is highly stable[182], presented data indicate that in the presented experimental conditions the protein is able to form aggregates, and that the fluorescence spectral changes, related with Tyr oxidation, are not affected by aggregation extent. Moreover, while Rayleigh scattering, here used as a measure of aggregation in solution, started to increase only after few hours of incubation, fluorescence spectral changes were observed since the very beginning of the kinetics (Fig. 3.4b and c), strongly suggesting that the two processes are independent.

With the aim of evaluating if modification in Ub fluorescence spectra changes may occur also in conditions where aggregation is not observed, we performed analogous experiments at 25°C. Figure 3.5 shows a comparison between data obtained at high temperature 60°C, and at 25°C. Rayleigh scattering measurements clearly indicate that no aggregation occurs at 25°C (Fig. 3.5a), while spectral modifications could still be observed (Fig. 3.5b and c).

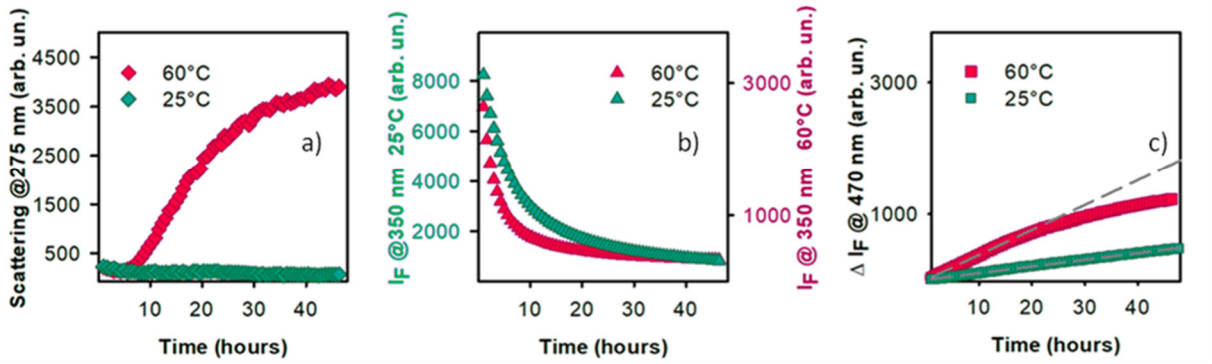

Figure3. 5: Rayleigh scattering intensity at 275 nm as function of time. **a)** Fluorescence emission intensity as a function of time, measured at 350 nm **b)** at 470 nm **c)** for Ub at a concentration of 1.8 mg/ml, incubated at 60°C and at 25°C. In panel **c)**, dashed grey lines are guide to the eye, to highlight the different rates in the increase of the fluorescence intensity measured at 470 nm. Figure modified from[133].

Significant changes in fluorescence peak profile are observed, whose rate depends on temperature. The variations of fluorescence emission intensity at 470 nm are reported in Fig. 3.5c, where dashed grey lines are used as eye guide to highlight the different slopes of the two kinetics and to elicit the change of slope occurring in kinetics at 60°C, which is not observed at 25°C within the experimental observation time. Measures in Fig. 3.5 highlight that the effect of temperature and UV-light cannot be easily disentangled, but the variation of signal attributed to formation of tyrosine oxidation products occurs both in conditions were aggregation occurs (60°C) and in conditions were aggregation is not observed (25°C). Probably, high temperature facilitates the oxidative processes induced in tyrosine by UV-irradiation.

Furthermore, Ub aggregation can be induced also at low temperature by subjecting the sample to stirring (see Fig. 3.6a). The comparison between the fluorescence data observed with or without stirring (Fig. 3.6b and c) again confirms that the aggregation has no effect on the kinetics of the spectral changes occurring in tyrosine fluorescence. For sample under stirring, the monotonic decrease of fluorescence intensity at 350 nm was observed from the initial stage during the lag phase of aggregation. Fluorescent spectra modifications overlapped both in stirring and quiescent conditions.

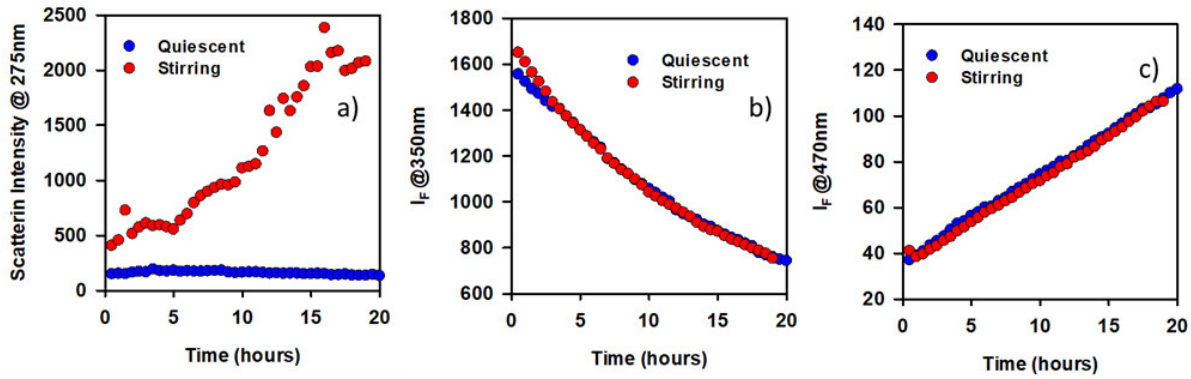

Figure 3.6: Rayleigh scattering intensity at 275 nm **a)** and Fluorescence emission intensity measured at 350 nm **b)**, and at 470 nm **c)** as a function of time. 1.8 mg/ml Ub samples in 20mM sodium phosphate, pH 6.5, for 48h were incubated at 25°C, stirring at 500 rpm (red circles) and in quiescent conditions (blue circles).Figure modified from[133].

In sum, all reported data indicate that UV exposure induces modifications in Ub UV–Visible absorption and in its fluorescence signal that can be ascribed to the formation of tyrosine oxidation products. This process is facilitated by high temperature but occurs both in aggregation conditions and in conditions were massive supramolecular association is not observed.

Results reported above single out modifications induced by UV light in Ub, by UV illumination from the xenon lamp of a spectrofluorometer during kinetic measurements in aggregation conditions. Spectral modifications and, in particular, the growth of a fluorescence peak in the blue region is attributable to tyrosine oxidation and in particular to dityrosine and DOPA.

Ub aggregates formed at high temperature in the presented conditions were found to be not positive to ThT, a worldwide used fluorescent molecule used to selectively stain amyloid aggregates[143][183]. The absence of ThT fluorescence excludes the amyloid nature of the aggregates formed by Ub, as also confirmed by CD spectra and FTIR spectra reported in Fig. 3.7 a) and b), respectively, in which transitions to β-sheet structure was not observed. The above observations rule out any possible contribution in all the above reported measurements of the so called “Amyloid autofluorescence” which lies in the same spectral range[184].

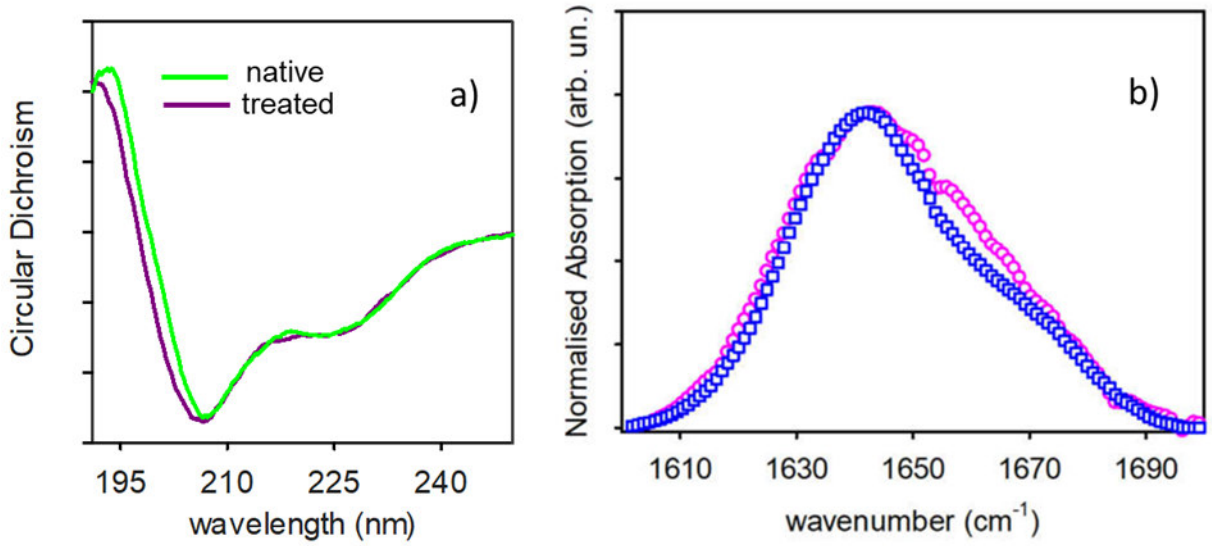

Figure 3.7: **a)** Circular Dichroism spectra of 0.5 mg/ml Ub sample in 20mM sodium phosphate buffer, pH 6.5, before (green line) and after (purple line) incubation at 60°C for 24h. **b)** FTIR spectra in the amide I' region (1575 cm^{-1} – 1710 cm^{-1}) of 1.8 mg/ml Ub sample in 20mM sodium phosphate buffer, pH 6.5, before (blue squares) and after (magenta circles) incubation at 60°C for 72h, under continuous excitation at 275 nm. Spectra are normalized to their maximum. Figure modified from[133].

In Figure 3.8a the contour plot of fluorescence emission intensity in the range 350-700 nm as a function of excitation light in the range 280- 450 nm is reported for Ub sample after incubation at 60°C for 72 hours under continuous UV exposure. In Fig. 3.8b emission profiles for selected excitation wavelengths are shown, and in Fig. 3.8c differential absorption spectrum is reported as a reference. These data show the complex nature of the newly formed species, indeed, the observed fluorescence signal shows at least two components attributable to two energetic levels which correspond to different species. According to the literature, these changes can be attributed to the formation of tyrosine oxidation products such as tyrosinate (emission maximum at 430 nm) and di-tyrosine (maximum peak at 410 nm), which can be formed under our experimental conditions[177][178][185].

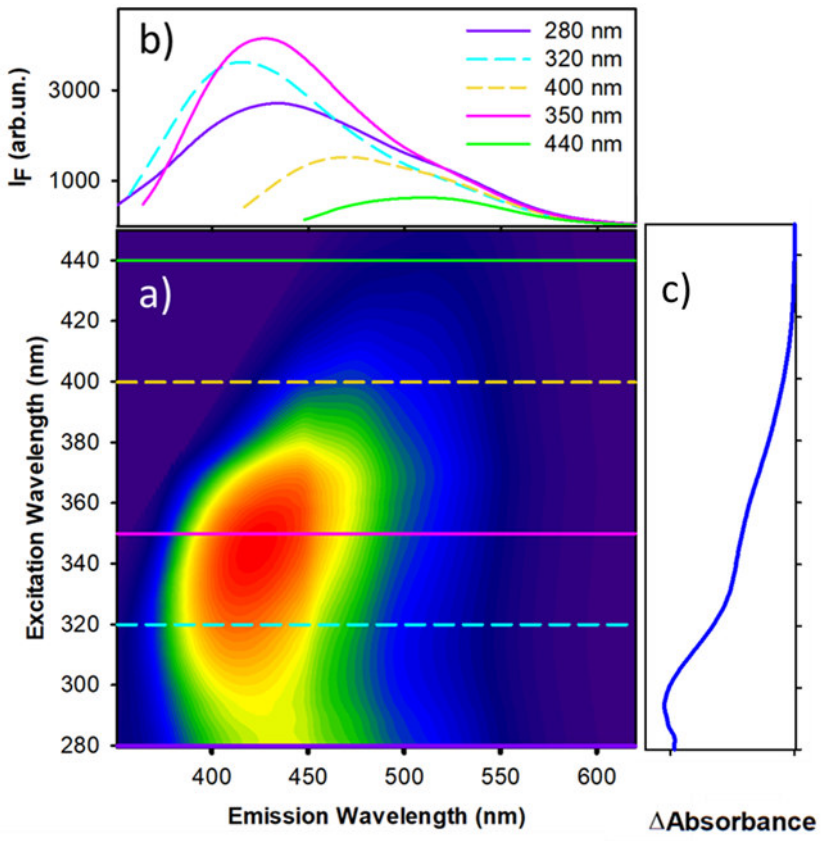

Figure 3.8: 3D fluorescence spectra/contour maps for Ub (1.8 mg/ml), acquired at room temperature after incubation at 60°C for 72 hours, under continuous excitation at 275 nm. **a)** Horizontal lines indicate the excitation wavelengths relative to representative emission spectra, which are reported in panel **b). c)** Differential adsorption spectrum between treated and native sample, showing the variations in absorption profile due to the treatment. Figure modified from [133].

Importantly, this measurement highlights that the blue fluorescence emission peak is observable using excitation wavelengths other than the one typically attributed to tyrosines (<290 nm). In particular, the new fluorescent peak is excited also at higher wavelengths, corresponding to the new absorption peaks in the absorption spectrum reported in Fig. 3.2. Interestingly, we note that the fluorescence signal in the blue range (i.e. above ~450 nm) can be detected and isolated also at excitation wavelengths above 350 nm, i.e. in the same range used in the literature to excite "amyloid autofluorescence peak".

In order to gain further information on this fluorescence signal, fluorescence lifetime measurements were also performed. Fluorescence Lifetime Imaging (FLIM) was used to this aim. Figure 3.9 reports FLIM measurements on 1.8 mg/ml Ub after incubation at 60°C for 72 hours, i.e. in the conditions of data in Fig. 3.8. In this sample the largest spectral changes induced by UV-irradiation are detectable. Representative intensity images of two regions of the sample are shown: one where a uniform distribution of fluorescence is measured linked to the presence of

species with size under instrumental spatial resolution (a), and one where, together with diffuse fluorescence signal, a large micrometric size aggregate was present, characterized by higher intensity (b). Images were acquired under two photon excitations at 780 nm, i.e. at excitation wavelength corresponding to larger intensity of the fluorescence band centred at 430 nm.

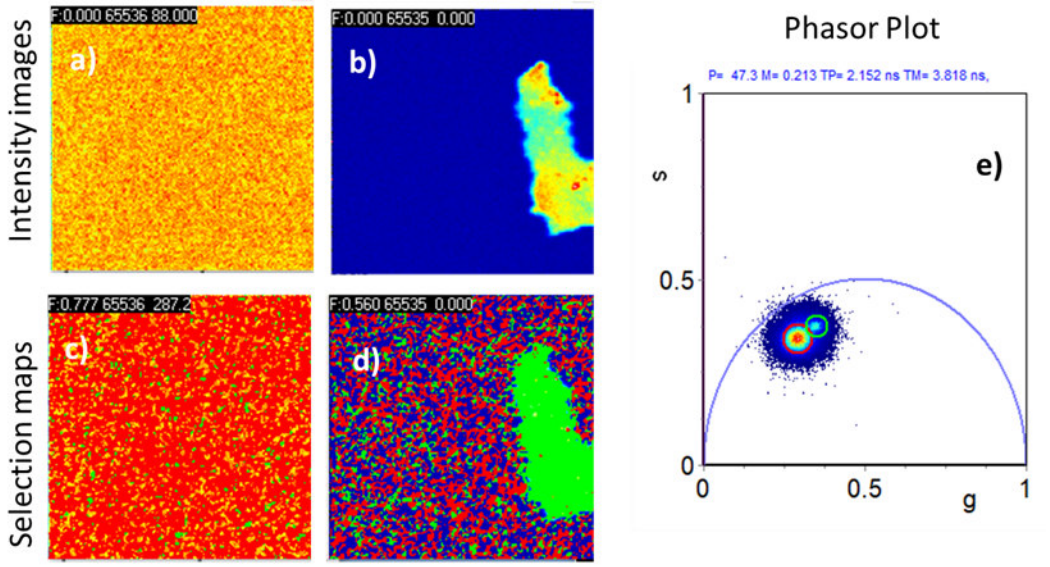

Figure 3.9: Fluorescence intensity images (60µm x 60µm) of 1.8 mg/ml Ub after incubation at 60°C for 72 h, under continuous UV-exposure. Panel **a)** shows a region of the sample with species under resolution and panel **b)** an area with large aggregates. **c)** and **d)** Selection maps of Ub, corresponding to the fluorescence images **a)** and **b)**, respectively. Pixel are coloured depending on their lifetime values. **e)** Phasor plot, showing the distribution of Ub lifetimes after treatment. Red and green cursors select two different lifetime distributions. The size of the images is 60 µm a) and b). Excitation wavelength was λ_{exc}= 780nm; Detection range: 430-700 nm. Figure from [133].

FLIM measurements were analysed by means of the so called phasor approach[159][186]. The corresponding maps and phasor plot are reported in Fig. 3.7c and d and in Fig. 3.7e, respectively. The output of the phasor analysis gives a graphical view of all the measured fluorescence decays at each pixel in the images. In the phasor plot, each point represents the fluorescence lifetime at each image pixel. Single exponential lifetimes are represented as points laying on the so called “universal circle”. Longer lifetimes are found near the origin of the axes, and shorter lifetimes are found on the circumference toward the bottom right intersection with the x axis. The position of the phasor in the universal circle, after system calibration (see paragraph 2.5.7 for details) determines the lifetime values. The fluorescence lifetime distribution over the

two images is represented by the clouds of points that are selected using a coloured circle and the corresponding pixels are mapped back with the selected colour to the image.

These measurements were put in comparison with analogous measurements performed on Insulin and Amyloid β samples, which are worldwide used models for studies on amyloid structures formation. In particular, the experiments were performed on Human Insulin and Aβ(1–40) peptide, since both proteins are able to form amyloid fibrils, and do not present tryptophan residues in their sequence. Furthermore, it was observed that oxidative stress negatively affects neurodegenerative diseases such as Alzheimer's and Parkinson's disease[187], and also is involved in the induction of insulin resistance in Type II diabetes[188], being a link between these pathologies[189][190].

In order to compare the spectral changes observed for Ub, both Insulin and Aβ(1–40) peptide were exposed to UV light excitation at 275 nm. Figure 3.10 reports fluorescence emission spectra and representative 1024x1024 confocal fluorescence microscopy images of aggregated samples stained with ThT. Human Insulin aggregates were obtained by incubating the protein at 60°C in 20mM sodium phosphate buffer at pH 6.5 with stirring at 500 rpm for 24 hours. Sample was kept under continuous UV- illumination at 275 nm during the aggregation process.

Panel a) of Fig. 3.10 reports fluorescence emission spectra at room temperature acquired in the range 280-650nm using λ_{exc}=275 nm before (blue line) and after UV treatment at 60°C (pink line). Panel b) of the same figure reports differential spectra with respect to the first thermalized one of Human Insulin intrinsic fluorescence during the described treatment at 60°C. Representative confocal fluorescence microscopy images reported in panels c-f) clearly show that aggregates are positive to ThT thus confirming the expected amyloid nature of these structures. Importantly, spectral modifications observed in panel a) and b) do not occur if aggregates are produced in the dark and. The spectral modifications observed for this sample are analogous to those observed for Ub samples after exposition to UV light.

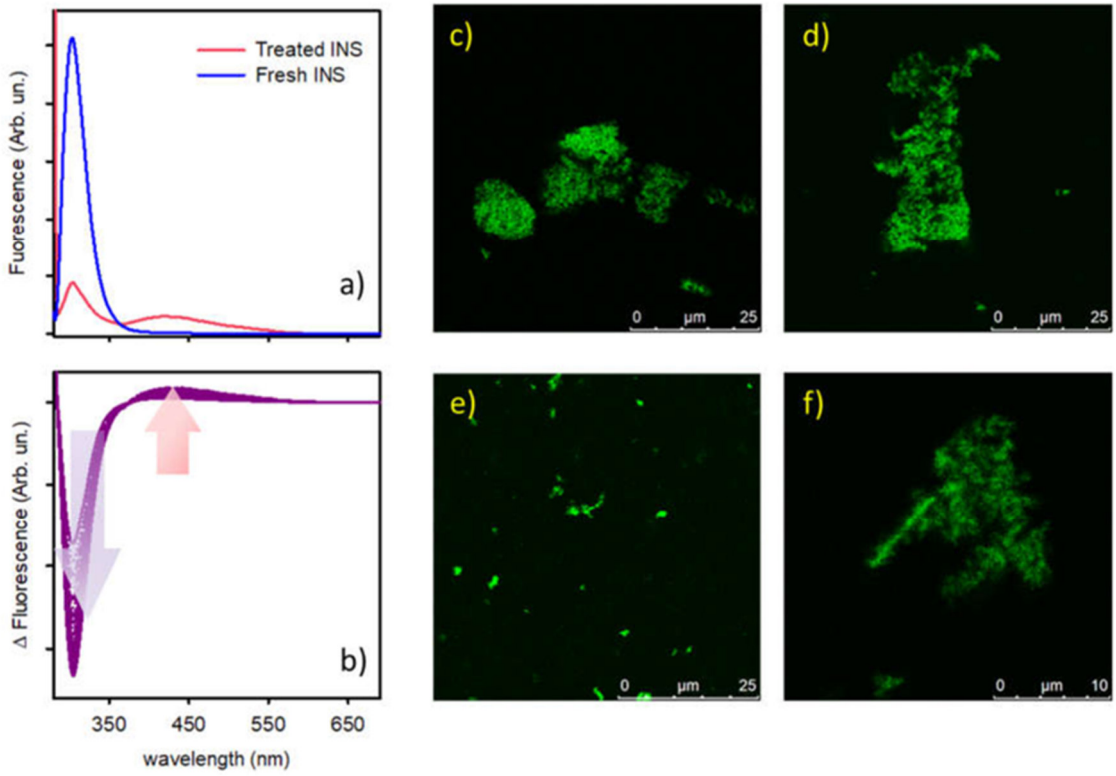

Figure 3.10: 0.2 mg/ml Human Insulin in 20mM sodium phosphate buffer, pH 6.5 was incubated at 60°C with 500 rpm stirring for 24 hours under continuous excitation at 275 nm. **a)** Fluorescence emission spectra acquired in the range 280- 650nm using λ_{exc}=275 nm measured at room temperature before (blue line) and after treatment (pink line). **b)** Differential spectra with respect to the first thermalized one of Insulin intrinsic fluorescence during the described treatment at 60°C. The arrows indicate the changes of the signals as a function of time. **c)-f)** 1024x1024 Representative confocal fluorescence microscopy images of Insulin fibrillar aggregates stained with ThT. Fluorescence signal is excited using a continuous laser line at λ_{exc} =458 nm and acquired in the range 470-650 nm. Figure from[133].

Analogous measurements were performed on Aβ(1–40) peptide and results are reported in Fig. 3.11. Aggregates were obtained by incubating 0.2 µM Aβ(1–40) in 20 mM sodium phosphate buffer, pH 6.5 at 37°C with stirring at 500 rpm for 24 hours. Sample was kept under continuous UV light illumination at 275 nm.

Panel a) of Fig. 3.11 reports fluorescence emission spectra at room temperature acquired in the range 280- 650nm using λ_{exc}=275 nm before (cyan line) and after treatment (pink line). In panel b) differential spectra with respect to the first thermalized one of Aβ(1–40) intrinsic fluorescence during the described treatment at 37°C. Panels c-e) reports 1024x1024 representative confocal fluorescence microscopy images of the aggregated sample. Also in this case, ThT fluorescence indicates that, in the presented conditions, Aβ(1–40) peptide forms amyloid aggregates. In line with measurements on Human Insulin, spectral modifications do not occur if

aggregates are produced in the dark. These results confirm that both proteins that are able to form amyloid aggregates, when exposed to UV light show the similar spectral changes observed for Ub.

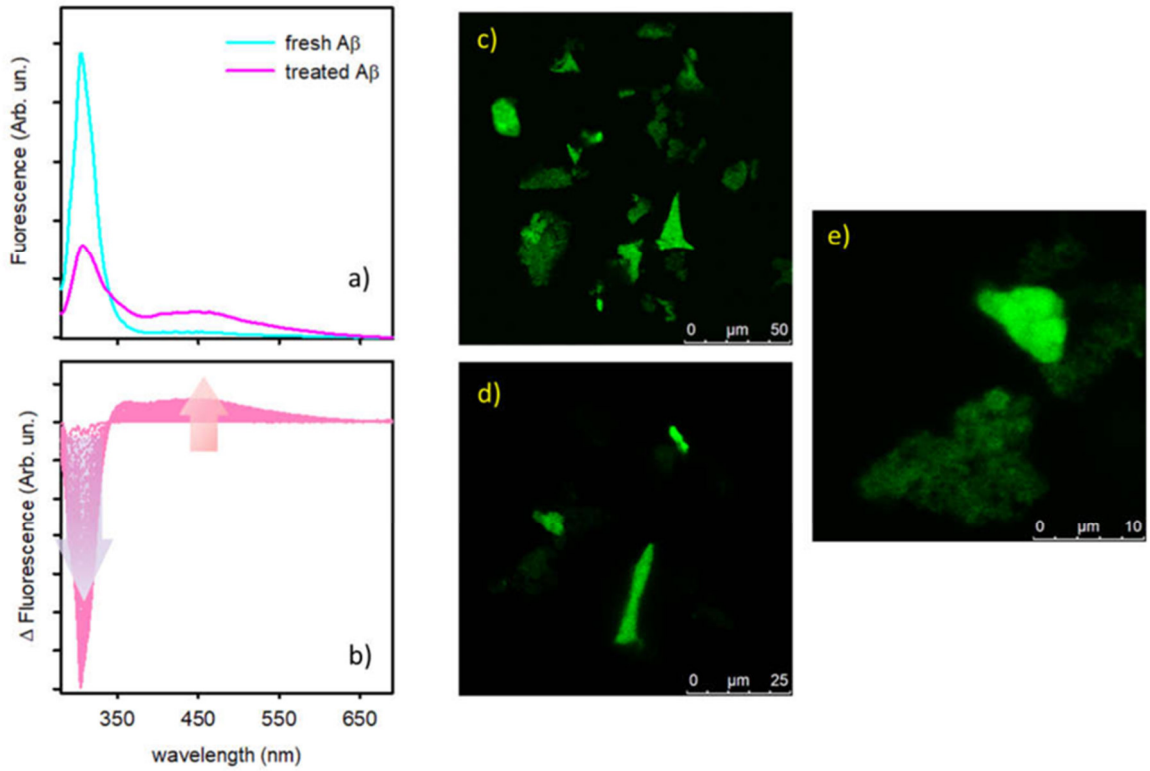

Figure 3.11: 0.2 µM Aβ(1–40) in 20 mM Na phosphate buffer, pH 6.5, was incubated at 37 degrees stirring at 500 rpm for 24 hours under continuous excitation at 275 nm. **a)** Fluorescence emission spectra acquired in the range 280- 650nm using λ_{exc}=275 nm measured at room temperature before (cyan line) and after treatment (pink line). **b)** Differential spectra with respect to the first thermalized one of Aβ intrinsic fluorescence during the described treatment at 37°C. The arrows indicate the changes of the signals as a function of time. **c)-e)** 1024x1024 Representative confocal fluorescence microscopy images of Aβ fibrillar aggregates stained with ThT. Fluorescence signal is excited using a continuous laser line at λ_{exc} =458 nm and acquired in the range 470-650 nm. Figure from[133].

Human Insulin and Aβ (1-40) peptide, after incubation at 60°C and 37 °C, respectively, experienced the same decrease of fluorescence emission around 310 nm and the increase around 450 nm under continuous UV-exposure (λ_{exc}=275 nm). The observed absorption and fluorescence spectra modifications, which can be attributed to the formation of tyrosine oxidation products occur in similar way, both in amyloid and non-amyloid forming samples.

FLIM measures confirmed the presence of newly formed fluorescent species whit analogous properties as the ones reported for Ub. Importantly, an overlap of both steady state and time resolved fluorescence measurements is observed. This is shown in Fig. 3.12 where comparison

between FLIM measurements on Ub, Human Insulin and Aβ (1-40) peptide samples are reported. In the selection maps (Fig. 3.12 d-f) red pixels corresponding to same lifetime in phasor plot (Fig.3.12 g) are picked. Interestingly, all the aggregates reveal an analogous lifetime distribution, strongly suggesting the same origin for the blue autofluorescence signal observed in all samples.

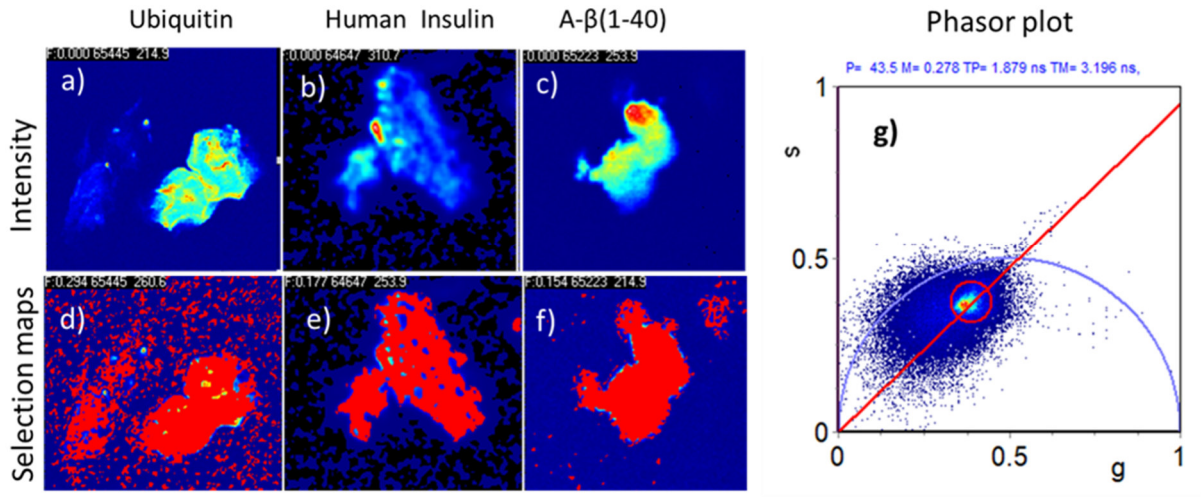

Figure 3.12: Fluorescence intensity images of Ub; **a)** Human Insulin **b)** and Aβ(1-40) **c)**; **d)**, **e)** and **f)**: Selection maps corresponding to the same regions. **g)** Phasor plot representing the distribution of lifetimes in every pixel in the presented images. Red cursor is used to select pixels with the same lifetime. All proteins were incubated under continuous irradiation at λ_{exc}=275 nm. Excitation wavelength was λ_{exc}: 780 nm; Detection range: 430-700 nm. Figure from[133].

The three proteins analysed have as common structural property the lack of tryptophan residues in their sequence, that could quench tyrosine fluorescence protecting tyrosine residues against UV-induced oxidation[191]. As a control, analogous experiments were performed on Bovine Serum albumin (BSA) in sodium phosphate buffer, pH 6.5 at 60°C and no significant spectral modifications were observed (data not shown). All samples after prolonged UV exposure, under two photon excitations at 780 nm, show an intrinsic blue fluorescence in the region 430–700 nm with the same lifetime distribution. In particular, the identical intrinsic fluorescence was revealed as well as in Ub amorphous aggregates, that do not bind ThT, and Insulin and Aβ fibrils which are selectively stained by ThT. In vitro dityrosine formation was previously also observed in α-synuclein samples[181], and in Aβ (1–42) fibrils grown under oxidative stress conditions were observed[192]. Furthermore, a UV-light induced visible fluorescence in the blue range was also observed in Aβ deposits from human brain[193].

As a further control, measurements on polyalanine amyloid fibrils, which do not contain tyrosine, were performed. Aggregates were induced by incubating polyalanine at 60°C for 24h in

20 mM glycine pH 11, under continuous UV- illumination at 275 nm. Confocal fluorescence microscopy images of polyalanine fibrillar aggregates stained with ThT clearly indicated the presence of large ThT-positive aggregates (Fig. 3.13 a-f). Furthermore, the steady state fluorescence measurements measured at λ_{exc} =275 nm and λ_{exc} =350 nm indicated that no fluorescence signal exists in these conditions (Fig. 3.13 g and h).

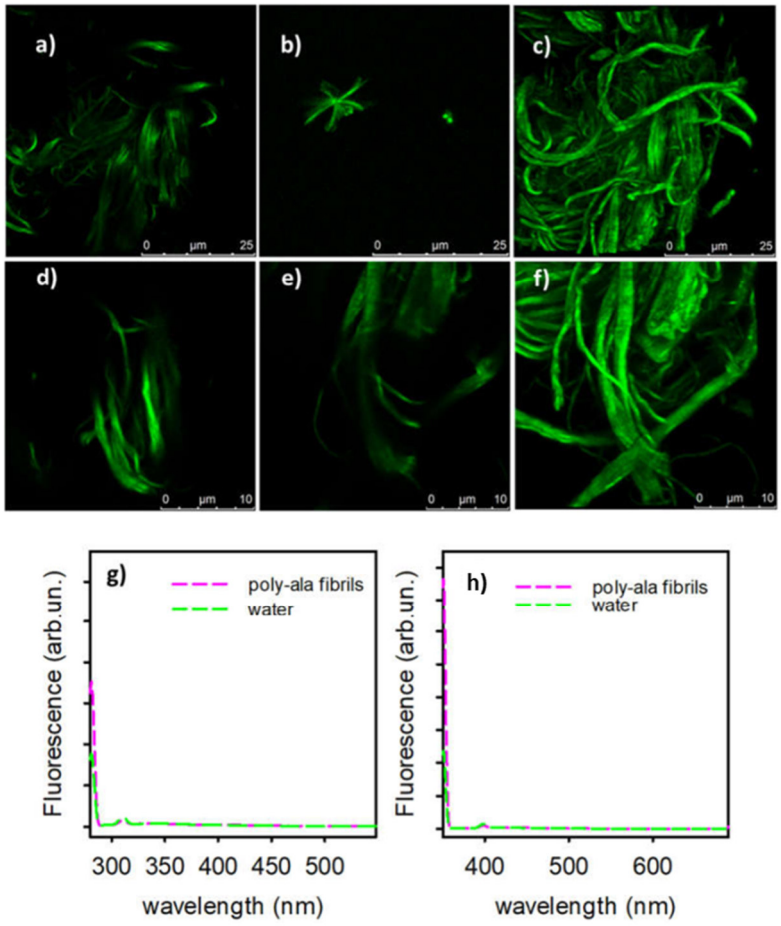

Figure 3.13: Polyalanine 8mg/ml was incubated at 60°C for 24h in buffer glycine 20 mM pH 11 giving rise to amyloid fibrils. Before imaging samples were diluted 1:5 in phosphate buffer pH 5 (to avoid ThT hydroxylation) and then stained with ThT. **a), b) d)** and **e)** 1024x1024 Representative confocal fluorescence microscopy images of polyalanine fibrillar aggregates stained with ThT. **c)** Superimposition of 35 µm z-stack; f) Superimposition of 15 µm z-stack of c. In all images, fluorescence signal is excited using a continuous laser line at λ_{exc} =458 nm and acquired in the range 470-650 nm. **g), h)** Steady state fluorescence measurements of Polyalanine fibrils imaged in **a)-e)** λ_{exc} =275 nm and 350 nm. Figure from[133].

Results described in this section unambiguously show that UV-light induces structural modification in Ub molecule ascribable to Tyr oxidation. These results highlight how simple experimental measurements may induce unsought significant changes in the structure of proteins.

Importantly, the presented measurements also show that, under specific experimental conditions, Ub was also able to form aggregates with non-amyloid nature.

To the aim of the present work, it is also important to underline that the observed modifications occur during standard measurements conditions, and this has been taken into account in planning subsequent experiments. The propensity shown by mUb to UV oxidation is likely to be persistent in polyUb chains and this has to be taken in account both in the production and in the analysis steps. Suitable control measurements based on fluorescence when then set up to exclude samples with oxidative modifications.

Data also presented represent a caveat for studies on the interaction between polyUb chains and Atx3 protein.

3.2 In-vitro Aggregation study of Ataxin-3: the case of Atx3-Q14 and Atx3-Q54

SCA3 belongs to a group of nine polyQ diseases caused by expansion of the polyQ tract of Atx3 protein above a specific repeat length threshold [60][194]. The pathological hallmark of SCA3 is represented by the formation of aggregates in cellular inclusions. These intranuclear aggregates consist of Atx3 proteins aggregates and also proteins involved in proteasome pathway system[65].

As discussed in Chapter 1, although the aggregation processes of Atx3 aggregation was widely investigated [95][195][196][197], the complex pathway of Atx3 self-assembly is not fully elucidated yet. In this work, the study of Atx3 aggregation mechanism is aimed at investigating on the conditions that could modulate the Atx3 aggregation process, and on the role of specific regions of the protein involved in the interaction with its physiological partners, polyUb chains, and how this interaction could modulate the aggregation process.

Atx3 aggregation process was then analysed in order to understand the underlying molecular mechanisms in the pathology. Two Atx3 variants with different polyQ tract length, namely Atx3-Q14 and Atx3-Q54, were selected because, according to the literature, should present different pathological implications. The two Atx3 variants have been expressed in prokaryotic cells, which resulted a suitable system for obtaining folded and active pure proteins to be used in aggregation studies. In particular, the isoforms containing 3UIMs in the C-terminal region were chosen, because these isoforms are those mainly expressed in brain tissue[198][199]. Moreover, both Atx3-Q14 and Atx3-Q54 were produced with the point mutation C14A, that inactivates the catalytic site of Atx3. This allows the reduction of Atx3 autocleavage propensity

as the production of free polyQ fragments may interfere with the aggregation processes analysis inducing heterogeneous nucleation mechanisms[99].

Here, Atx3 protein aggregation mechanisms have been analysed by different techniques such as ThT, ANS fluorescence and CD spectroscopy. These methods aimed at analysing Atx3 aggregation pathway in conditions that may highlight dominant interactions and structural changes involved in supramolecular assembly. This is aimed at assessing a well-defined starting point to evaluate the effect of polyUb chains interaction on Atx3 aggregation.

Surprisingly, the obtained results did not show nucleation-dependent aggregation pathways, and also no significant differences in the aggregation processes of the two Atx3 variants were observed. Probably, in the tested experimental conditions, the use of an expanded Atx3 variant with a border line pathological expansion of polyQ (Q54), and in the absence of self-cleavage, did not allow the appreciation of the contribution of the polyQ tract in the aggregation process. This in turn allowed to analyse common processes that mainly interest the N-terminal region, Jos domain, which obviously is the same in the two proteins.

The aggregation kinetics of Atx3 variants were studied using ThT fluorescence. This being one of the most frequently used methods to monitor amyloid formation. As detailed in the method section, the growth of ThT fluorescence intensity takes in account for the growth of amyloid structures in solutions[143][145]. In the initial stage of these experiments, both *in-situ* and *ex-situ* measurements were performed in order to assess that the dye presence was not affecting aggregation process. Subsequently only *in-situ* measurements were performed, since the two methods gave identical results, and the characteristic times of supramolecular assembly (about two hours) are short enough to exclude artefacts due to ThT hydroxylation[146].

The aggregation processes of Atx3-Q14 and Atx3-Q54 were evaluated incubating the proteins at 50°C. Figg. 3.14 and 3.15 report result of *ex-situ* experiments of both Atx3-Q14 and Atx3-Q54, performed in 20mM sodium phosphate buffer with 1mM TCEP, pH 6.5. Samples were freshly prepared, and then incubated at 50°C in a thermal bath up to 72 hours.

Figure 3.14 reports absorption spectra (a), ThT fluorescence emission spectra (b), and far-UV CD spectra (c) of Atx3-Q14 after incubation at 50°C for different incubation time points. The same measurements were performed for Atx3-Q54 and relative results are reported in Fig. 3.15. For both Atx3 proteins, all spectra were acquired at 25°C after suitable incubation times: after 30 minutes; after 1 hour; after 2 hours; after 6 hours; after 8 hours; after 24 hours; 48 hours; and after 72 hours. All measurements are referred to the one on sample before incubation, indicated as 0 minutes.

As shown in Figg. 3.14a and 3.15a, absorption spectra for both samples appear to be modified. This modification is ascribable to the increase of turbidity signal which takes into account for

the growth of aggregates species in solution. Notably, the observed changes in absorption spectra were closely similar for both Atx3 samples.

These results show that, for both Atx3 proteins, ThT fluorescence intensity and scattering progressively grow as a function of time reaching an apparently constant value after about 24 hours. These observations suggest that, in the presented conditions, both samples undergo aggregation forming amyloid like species with no appreciable differences.

In line with fluorescence results, far-UV CD spectra show similar secondary structures changes for the two Atx3 variants, consisting of a decrease of signal around 220 nm corresponding to an increase in β–sheet content in the proteins (Figg. 3.14c and 3.15c).

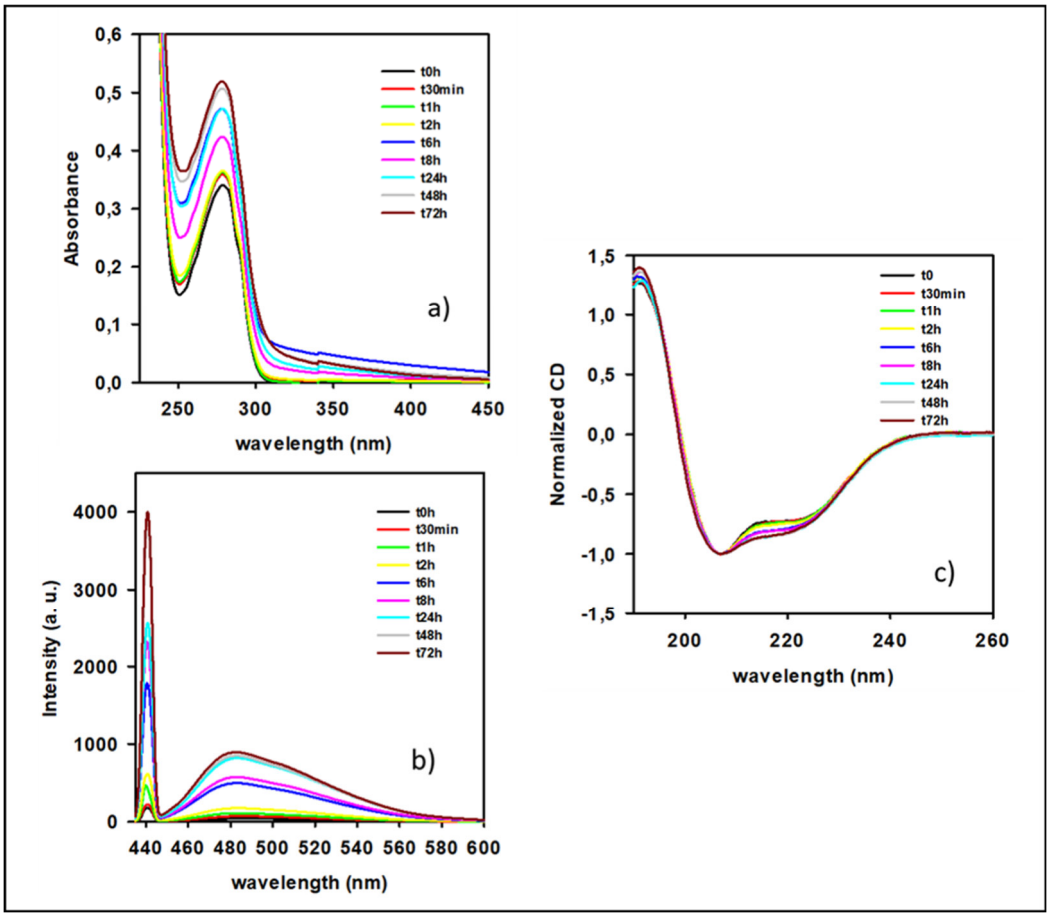

Figure 3.14:*Ex-situ* measurements of 18µM of Atx3-Q14 in 20mm Na phosphate with 1mM TCEP, pH6.5, after incubation at 50°C samples is withdrawn and brought back at 25°C after different times: 30 minutes; 1 hour; 2 hours; 6 hours; 8 hours; 24 hours;48 hours and 72 hours. As a refence the measurements on freshy prepared sample is also reported (t0 min). **a)** UV visible absorption spectra of the samples after different incubation times at 50°C in the range 225-450 nm **b)** ThT fluorescence emission spectra recorded at 25°C 26µM ThT, excitation wavelength was λ_{exc}=440nm detection range 435-600 nm. **c)** normalized far-UV CD spectra, recorded at 25°C in the range 260-190 nm, using a scan speed of 50 nm/min, a 1 nm bandwidth. Each spectrum is the result of the average of 5 accumulations.

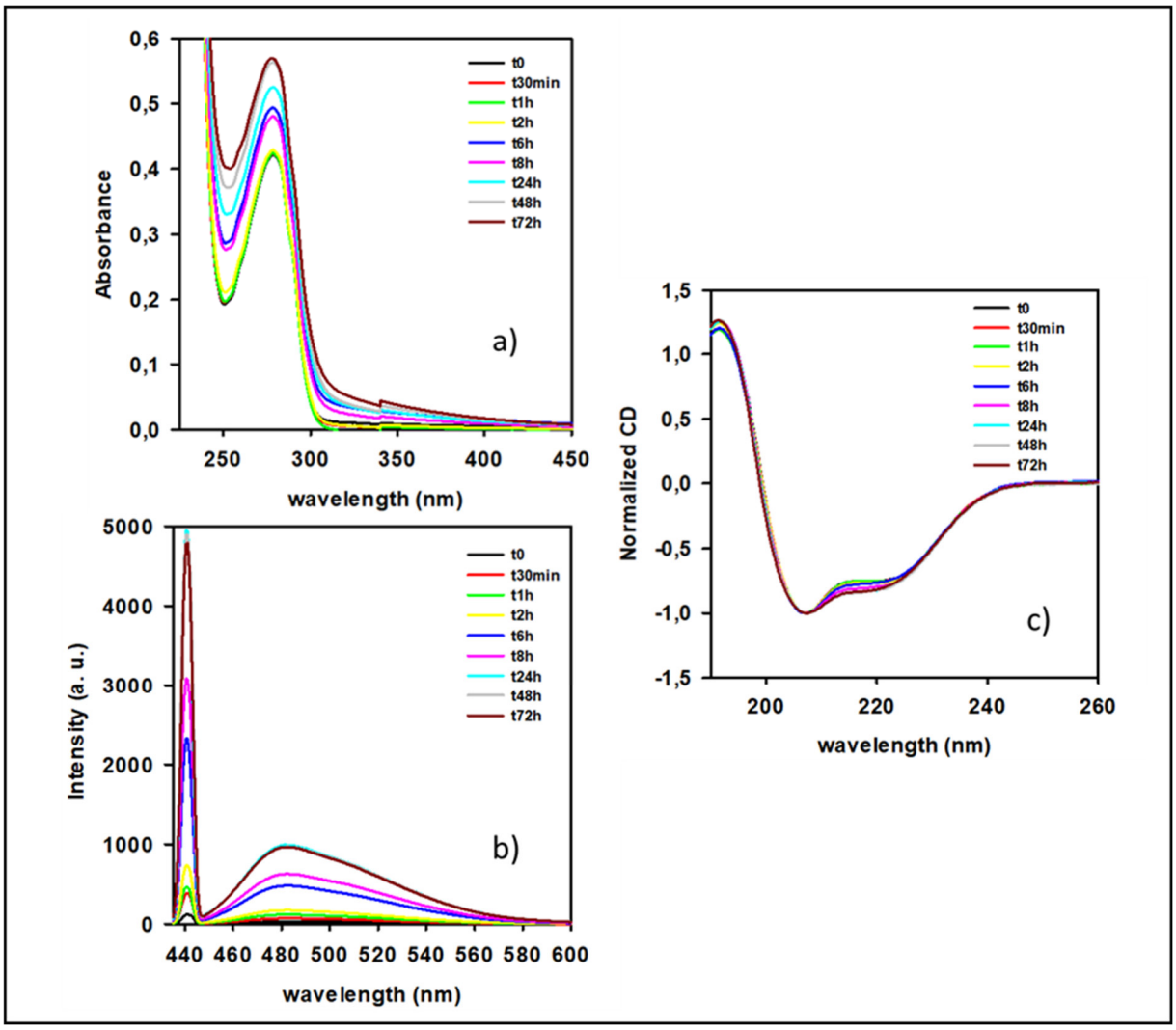

Figure 3.15: *Ex-situ* measurements of 18µM of Atx3- Q54 in 20mm Na phosphate with 1mM TCEP, pH6.5, after incubation at 50°C samples is withdrawn and brought back at 25°C after different times: 30 minutes; 1 hour; 2 hours; 6 hours; 8 hours; 24 hours;48 hours and 72 hours. As a refence the measurements on freshy prepared sample is also reported (t0 min). **a)** UV visible absorption spectra of the samples after different incubation times at 50°C in the range 225-450 nm **b)** ThT fluorescence emission spectra recorded at 25°C using 26µM ThT, excitation wavelength was λ_{exc}=440nm and detection range 435-600 nm. **c)** normalized far-UV CD spectra recorded at 25°C in the range 260-190 nm, using a scan speed of 50 nm/min, a 1 nm bandwidth. Each spectrum is the result of the average of 5 accumulations.

This pivotal screening allowed to highlight that in the selected conditions aggregation sudden occurs and that ThT positive aggregates are formed. The ThT fluorescence and CD measurements were consistent and showed that both Atx3-Q14 and Atx3-Q54 present similar trend. Moreover, the analysis showed high reproducibility of measurements, and although it was observed the formation of amyloid like aggregates, no lag phases or nucleation-dependent aggregation pathways were observed both, *in-situ* and *ex-situ* ThT measurements. These suggest that

probably Atx3 aggregation follow other mechanism involved in amyloid aggregates formation[15][200].

Figure 3.16 reports the comparison of *in-situ* ThT fluorescence emission spectra at 480 nm as function of time of both, Atx3-Q14 and Atx3-Q54, incubated at 50°C for 3 hours. The ThT emission fluorescence increased for both proteins, reaching the plateau phase in about 2 hours. These results confirmed the *ex-situ* ThT measurements, showing that Atx3-Q14 and Atx3-Q54, in 20mM sodium phosphate with 1mM TCEP pH 6.5, were able to form ThT positive aggregates and that the supramolecular assembly kinetics overlap.

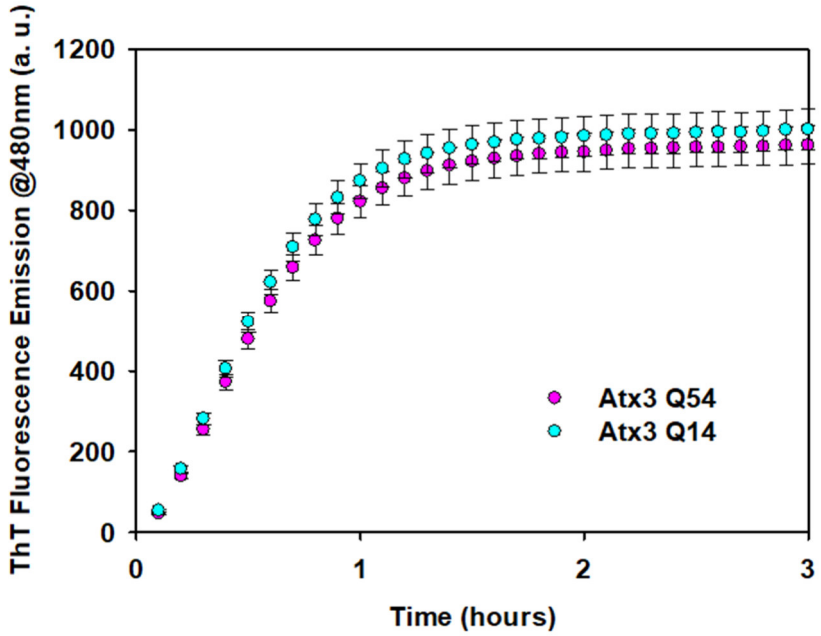

Figure 3.16: Comparison of *in- situ* ThT fluorescence emission intensity measured at 480 nm as a function of time of 18µM of Atx3-Q14 (cyan dots) and 18µM of Atx3-Q54 (pink dots) in 20mM Na phosphate with 1mM TCEP, pH6.5, incubated at 50°C for 3 hours, with 26µM ThT. It was used λ_{exc}=440nm, detection range 435-600nm.

Interestingly, the changes of ThT fluorescence intensity, reaching the plateau after 2 hours, correlate in the range time with the changes observed in ThT *ex-situ* assay reported in Figg. 3.14b and 3.15b.

These results differ from the larger part of results previously reported in literature on Atx3. Indeed, in the present study both proteins undergo aggregation with superimposable kinetics and no significant differences were observed between Atx3-Q14 and the expanded Atx3-Q54. Nucleated mechanisms were observed by Ellisdon and co-workers in *ex-situ* ThT measurements, but, notably, their analysis was performed at 37°C using a higher proteins concentration in a much complex buffer with respect the conditions used in this thesis work, In particular, they used 30 µM proteins samples, in tris-buffered saline (TBS) pH 7.4 containing 10% (v/v)

glycerol, phenylmethylsulfonyl fluoride (2 mM), EDTA (5 mM), and β-mercaptoethanol (15mM)[94][95]. Another work, performed by Chow and co-workers, again showed that expanded Atx3-Q50 forms fibrils faster than non-expanded forms Atx3-Q15 and Atx3-Q28. Again, it is notable that also in this case temperature and buffer conditions were different with respect those used in the present thesis work. They performed *ex-situ* ThT assay using similar protein concentration than the one used here, but incubated samples at 37°C in PBS buffer[197]. More *in-situ* aggregation studies were performed by Scarff and co-workers on Atx3-Q14 and Atx3-Q78 isoforms, incubating at 37 °C for about 48 hours without shaking, in 250 mM ammonium bicarbonate, 1 mM DTT, pH 8.1[201]. Common feature of these studies being lower temperature and higher pH than the one used in the presented experiments. Although, expansion of the polyQ tract has been demonstrated to accelerate Atx3 aggregation, polyQ expansion is also reported not to modify Atx3 stability or folding/unfolding process[197], this suggesting that in present conditions aggregation is modulated by the folded part of the molecule. In line with this hypothesis, several works demonstrated that at least the first phases of aggregation is triggered by Jos domain, while further following phases involve the polyQ tract[95][98][102][202][203].

A possible significant difference between the experimental protocol here performed and the ones that highlighted nucleation mechanisms in Atx3, may consist in the use of an optimized purification protocol designed to produce high purity and fresh protein for each experiment. Furthermore, samples here analysed contain the point mutation C14A, that inactivates the catalytic site, and incubation was performed at higher temperature than physiological. These differences in the experimental procedures, may have allow to highlight non nucleated mechanism common to both variants.

In order to highlight that no difference between the two variants exists at secondary structure level, far-UV CD spectra were acquired at 25°C before and after incubation at 50°C for 20 hours (Fig. 3.17). As can be seen, no significant secondary structure differences between the two Atx3 variants are found comparing in pair spectra before and after thermal treatment.

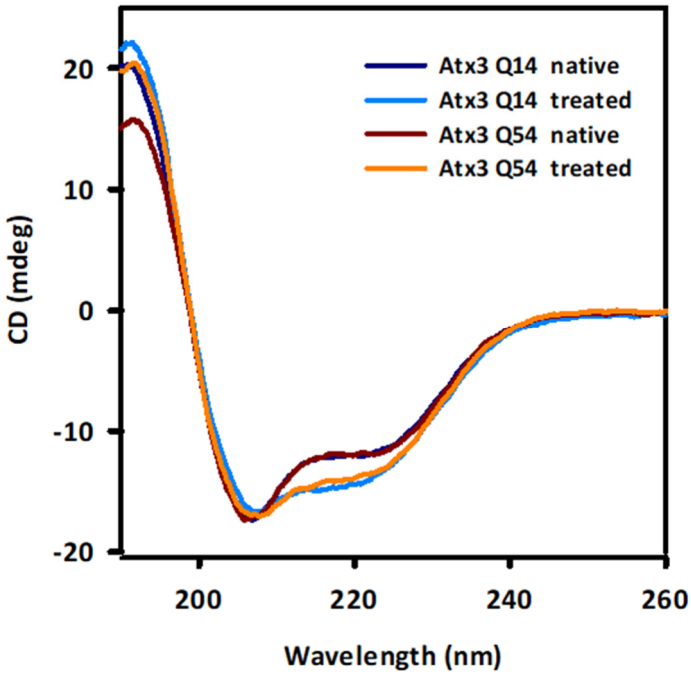

Figure 3.17: Comparison of far-UV CD spectra of 18μM of Atx3-Q14 before (dark blue line) and after (light blue line) incubation at 50°C for 20 hours and 18μM of Atx3-Q54 before (dark red line) and after (orange line) incubation at 50°C for 20 hours, in 20mM Na phosphate with 1mM TCEP, pH6.5. Far-UV CD spectra were recorded at 25°C in the range 260-190 nm, using a scan speed of 50 nm/min, a 1 nm bandwidth. Each spectrum is the result of the average of 5 accumulations.

The obtained data reflect that both Atx3-Q14 sample and Atx3-Q54 sample, in the tested conditions, undergo to profound changes in the structure, but these changes appear not to be dependent on polyQ length. Notably, the observed changes show similar modification to the no expanded Atx3-Q15 and Atx3 variants without polyQ tract (QHQ) observed by Ellisdon and colleagues[94]. Results reported till now have highlighted the monotonic growth of amyloid aggregates, this growth is paralleled by changes at secondary structure level leading to the formation of intermolecular β-sheets. In literature the growth of amyloid fibrils via a non-nucleated assembly mechanism involving the formation of intermolecular β-sheets was previously observed[204][205]. Many observations underline how the subtle balance between electrostatic and hydrophobic interactions affects the formation and stability of the organized hydrogen bond network constituting fibrils spine[206][207][208].

In order to evaluate how hydrophobic interactions are involved in the observed aggregation processes, the properties of the ANS dye were exploited. This was aimed both at elucidating the conformational changes in the solvent exposure of hydrophobic regions during aggregation and at exploring hydrophobic sites that may have different roles in the interaction with polyUb. Indeed, ANS fluorescence measurements are widely used to study the conformational changes

during aggregation process highlighting the role of hydrophobic regions of proteins if present. As discussed in Chapter 2, ANS is an extrinsic dye frequently used for protein folding and aggregation studies, that presents a fluorescent signal strongly dependent on the polarity of its environment[151]. Generally, a blue shift of fluorescence emission maxima and the increase of fluorescence intensity is observed when ANS binds the hydrophobic patches of proteins. Figure 3.18 shows ANS fluorescence spectra of freshly prepared Atx3-Q14 and Atx3-Q54, recorded in 20mM sodium phosphate buffer with 1mM TCEP, pH 6.5, before incubation at 50°C.

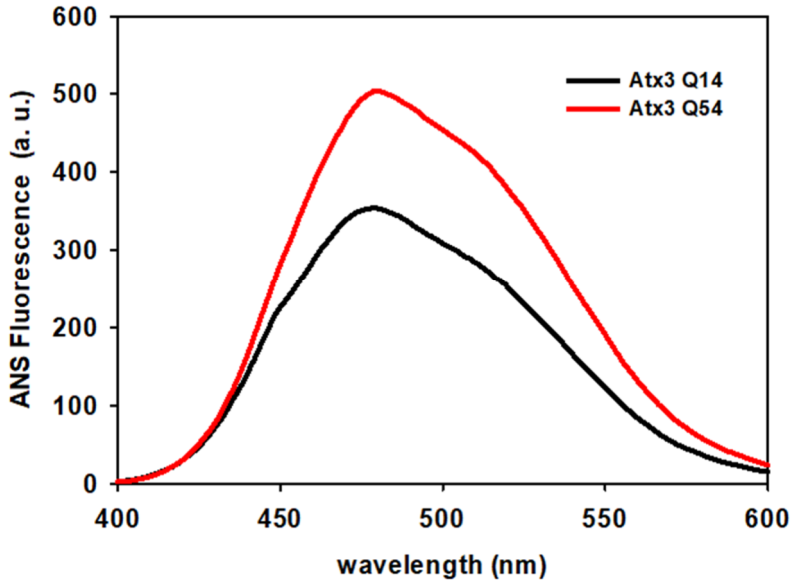

Figure 3.18: ANS fluorescence spectra of 18µM Atx3-Q14 (blue line) and 18µM Atx3-Q54 (red line) with 20 µM ANS in 20mM Na phosphate buffer with 1mM TCEP, pH 6.5. The spectra were recorded at 25°C. excitation wavelength was λ_{exc} =380nm; detection range: 400-600 nm.

As it is evident, Atx3-Q54 samples are characterised by higher fluorescence intensity signal, indicating that the expanded Atx3 variant has larger affinity to ANS with respect to Atx3-Q14. This possibly is because hydrophobic part of Atx3 are more exposed in presence of longer polyQ tract.

Figure 3.19 reports the analysis of ANS fluorescence measurements of both Atx3-Q14 and Atx3-Q54 in 20mM sodium phosphate buffer with 1mM TCEP, pH6.5, incubated at 50°C for 6 hours. Steady state fluorescence emission of ANS was acquired as a function of time every 6 minutes in the range 375-700 nm using excitation wavelength λ_{exc} =380nm. Panel a) reports the time evolution of ANS fluorescence intensity measured as the area of emission peak between 394 nm e 692 nm. Panel b) reports the average peak position.

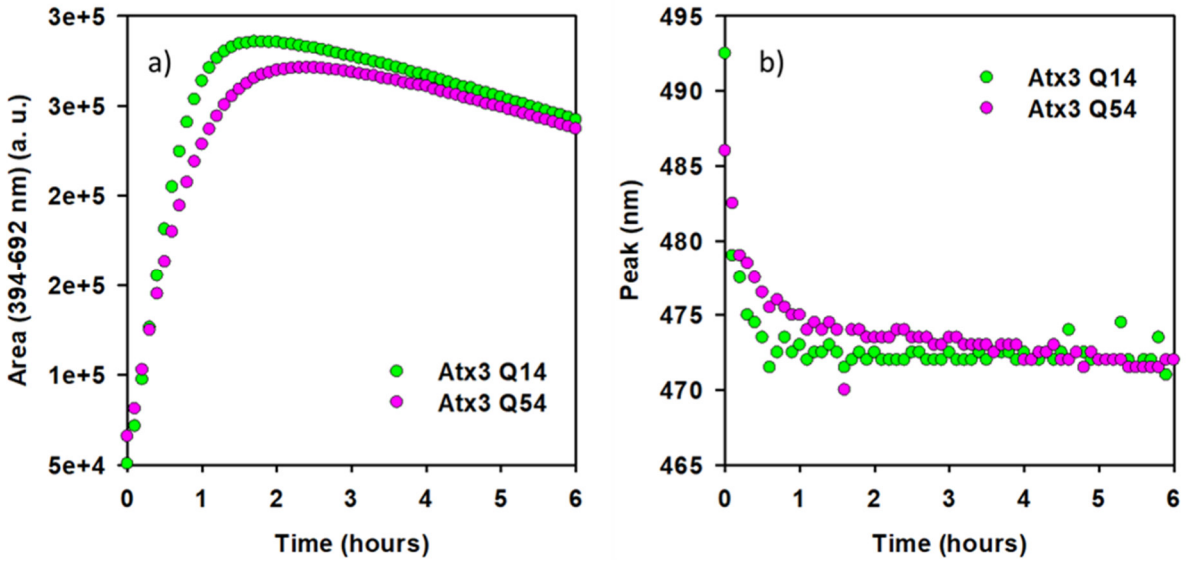

Figure 3.19: a) ANS fluorescence intensity measured as the area of emission peak between 394nm and 692nm as function of time **b)** Average position of the ANS fluorescence peak measured as a function of time, of 18μM Atx3-Q14 (green dots) and 18 μM Atx3-Q54 (pink dots) with 20 μM ANS, in 20mM Na phosphate buffer with 1mM TCEP, pH 6.5 incubated at 50°C for 6 hours. Excitation wavelength was λ_{exc} =380nm; detection range: 375-700 nm.

Data show that ANS intensity increases for both Atx3-Q14 and Atx3-Q54 for about 2 hours, indicating the formation of new hydrophobic sites in the same time range observed in previous analysis using ThT. ANS intensity shows a similar trend for both samples, increasing to a maximum and then slightly decreasing. In Atx3-Q14 sample the maximum value is reached in a shorter time. The peak position also indicates the formation of new hydrophobic binding sites for ANS and suggest a slower process for Atx3-Q54 variant. Small differences are highlighted which are not detected by ThT fluorescence measurements. These effects can be considered as negligible for their effect in supramolecular assembly, but need further investigations for example on samples with larger polyQ expansion.

In order to better establish the conditions for further analysis, and to understand the differences between our observations and nucleation-dependent pathway reported in literature, aggregation analysis of Atx3-Q14 and Atx3-Q54 was performed using different conditions, and in particular changing electrostatic conditions which strongly influence the amyloid formation.

It is known that protein aggregation is influenced by local environment, as solution pH, ionic strength and protein concentration[26][209][210]. Salt have large effect on the structure and properties of proteins, by varying the ionic strength is possible to modify the protein native state properties, conformation, and inter- and intra-molecular interactions.

Low concentration of salt is reported to stabilize protein structures through non-specific electrostatic interactions, while high concentration salt may hinder their stability and solubility[211]. This effect is caused by favourable interactions between salt ions and charges on protein surfaces. Atx3 in the analysed conditions is positively charged as its isoelectric point is 4.67, as consequence the addition of salt has the effect of shielding the exposed ionic charges. This allows to modify electrostatics interactions to investigate possibly different effect related to different in the polyQ tract length. Moreover, this allows getting closer to experimental conditions of reference studies in the literature, many of which were performed in buffers containing NaCl at physiological concentrations (about 150mM) [94][196][197][212].

Figure 3.20 reports ThT fluorescence emission intensities measured at 480nm as a function of time of both Atx3-Q14 and Atx3-Q54 in 20mM sodium phosphate buffer, with 1mM TCEP, pH6.5, in solution with 150mM NaCl during thermal incubation at 50°C. Measures in the absence of NaCl in the same experimental conditions are reported for comparison.

As observed in Fig. 3.20, for both Atx3-Q14 and Atx3-Q54, in the presence of salt a monotonic growth of ThT intensity is observed to a lower plateau value with respect to one reached by the same samples in the absence of salt. Moreover, it is evident that the plateau is reached with a faster rate. In fact, the plateau was reached in less than 30 minutes. However, no significant differences were observed comparing Atx3-Q14 and Atx3-Q54 in absence of salt and in presence of 150mM NaCl.

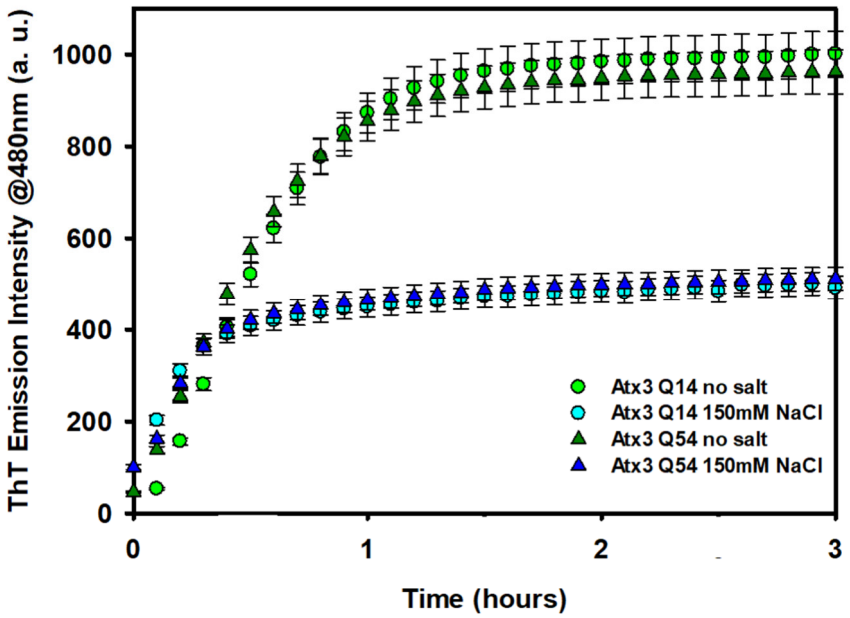

Figure 3.20: Time evolution of ThT fluorescence intensity measured at 480 nm of 18 μM Atx3-Q14 and 18 μM AtxQ54 with 26 μM ThT, in 20mM Na phosphate buffer 1mM TCEP, pH6.5, incubated at 50°C for 3 hours, Atx3-Q14 without salt (light green dots) and with 150mM NaCl(cyan dots); Atx3-Q54 without salt (dark green triangle) and with 150mM NaCl (blue triangles).

The observed reduction of ThT intensity cannot be directly attributed to a lower number of amyloid structures in solution, because of the exquisite sensitivity of fluorescence signals measured in the presence and in the absence of salt. This difference could be attributable to different environments experienced by the dye, due to difference in the ThT binding sites which may lead to different dye quantum yield, and/or to differences in the refraction index of the sample which may lead to alteration in measured signal.

In order to verify that also in these conditions it is possible to observe a growth of inter-molecular β-sheet Far-UV CD spectra recorded at 220 nm for both Atx3 variants while incubating samples at 50°C for 3 hours in absence and in presence of 150mM NaCl. Figure 3.21 reports the ΔFar-UV CD as a function of time and highlights that variations in CD signals at 220nm present analogous behavior for the two samples and both in the absence and presence of salt, being the last ones slightly faster.

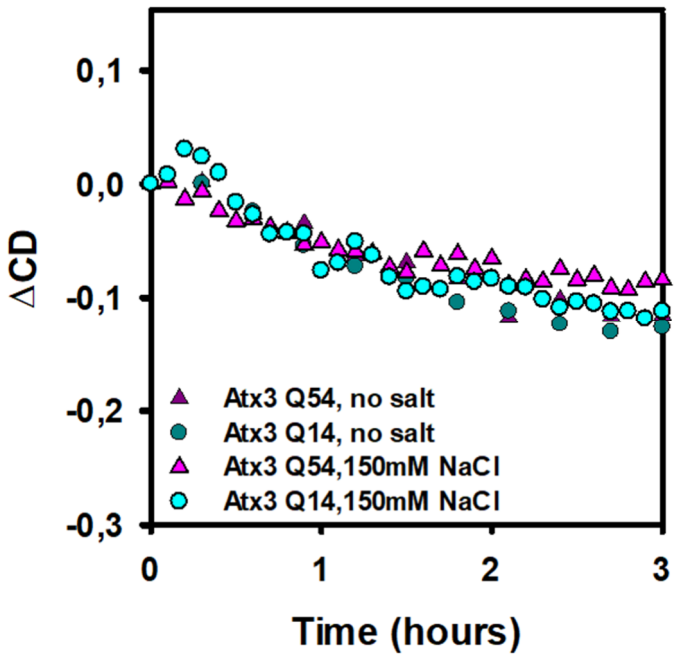

Figure 3.21: Time evolution of ΔFar-UV CD spectra measured at 220 nm of 18 μM Atx3-Q14 and 18 μM Atx3-Q54 incubated at 50°C for 3 hours, in 20mM sodium phosphate, 1mM TCEP, pH 6.5 in absence and in presence of 150mM NaCl. Atx3-Q54 without salt (dark pink tringles) and with 150mM NaCl (light pink triangles) and Atx3-Q14 without salt (dark cyan circles) and Atx3-Q14 with 150mM NaCl (cyan circles).

Notwithstanding the low signal to noise, these data confirm that the aggregation process is slightly accelerated when in solution is present salt, probably caused by minor electrostatic repulsion. This effect does not seem to depend on the length of polyQ because in both Atx3-Q14 and Atx3-Q54 proteins the same behaviour was observed, again the structural changes are possibly ascribable to Jos domain.

These data suggest that the electrostatic interactions, modulate the supramolecular assembly, however since the pI of Atx3-Q14 and Atx3-Q54 is 4.67 this effect may be poorly evident. For a quick exploration was performed a higher pH moving away from the pI. Indeed, changing pH conditions, it is possible to perturb the net charge of a protein and its conformational properties and to modulate electrostatic interactions during the aggregation pathway during aggregation[213]. Figure 3.22 shows ThT fluorescence emission at 480nm as a function of time of Atx3-Q14 and Atx3-Q54 while incubating samples at 50°C for 10 hours, at pH 7.4. In the same figure, results obtained at pH 7.4 are compared with the one obtained at pH 6.5, previously reported in Fig.3.16.

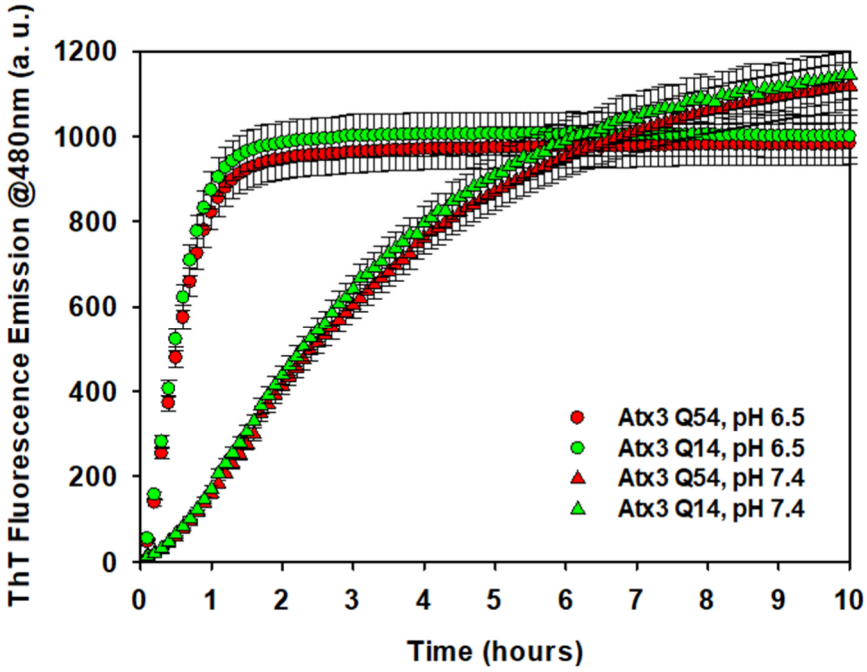

Figure 3.22: Time evolution of ThT fluorescence emission at 480 nm of 18 μM Atx3-Q14 and 18 μM Atx3-Q54 in 20mM Na phosphate with 1mM TCEP, incubated at 50°C for 10 hours with 26 μM ThT. Atx3-Q14 at pH 6.5 (green dots) and at pH 7.4(green triangles) and Atx3-Q54 at pH 6.5 (red dots) and at pH 7.4(red triangles).

As expected, at pH 7.4, away from the pI of Atx3, the aggregation process is slowed down and an increase in the formation of ThT positive aggregates was observed. The data are in line with the results reported by Chow and co-workers that analysed three Atx3 variant (Atx3-Q15, Atx3-Q28 and Atx3-Q50) aggregation using a wide range of pH (1.9-8) by means of several spectroscopic methods, as ThT, ANS and Far-UV CD measurements. Indeed, Chow and co-workers observed that polyQ tract did not affect the aggregation process of all the three Atx3 variants[197].

At pH 7.4 a reduction of aggregation rate is observed for both samples, the supramolecular assembly show a different shape allowing the observation of a concave profile in the initial stage. Importantly, also in these conditions no differences are observed between the two variants confirming consistent results over a wide range of experimental conditions. Ionic strength and pH conditions were explored and, as expected, they affected aggregation following general law regulating amyloid like growth at low concentrations[210].

Importantly, this highlighted that Atx3-Q14 and Atx3-Q54 do not show significative difference in their aggregation behaviour and this suggests that in the tested conditions a possible contribution of polyQ length on the aggregation process was not observed. Further investigation using an Atx3 variant with larger expansion in polyQ tract are certainly needed, and for this reason an Atx3 variant with more than 70Q has been already produced in the industrial partner labs.

3.3 In-cell co-expression of Ataxin-3 and tri-Ubiquitin chains

In this section results obtained in cellular environment are reported, aimed at analysing the behaviour of analysed Atx3 variants and possible interaction with triUb chains.

Hallmark of SCA3 pathology is the presence of nuclear inclusions in the cell of patients, that not only contain Atx3 aggregated but also polyubiquitinated proteins[69][215]. Several works investigated on expression of Atx3 variants in cell system and in mouse model[216][217]. Interestingly, it has been observed that Atx3 with longer polyQ tract, was more prone to form nuclear aggregates in cells, while the non-expanded Atx3 protein could also form smaller aggregates that remain in cytoplasm[218].

In order to study also the Atx3 variants behaviour in cell model, Atx3-Q14 and Atx3-Q55 were over-expressed in Human Embryonic Kidney (HEK293) cells to evaluate differences on cell cytotoxicity, and on the ability to form cell aggregates determined by the expansion of the polyQ tract. Moreover, to also test in cell the possible interaction between Atx3 and polyUb chains, a linear triUb DNA construct was generated. Western blot analysis and immunofluorescence assay were used to verify the expression of the exogenous proteins in cell system and to monitor the localization and the possible interaction between Atx3 and triUb in cellular environment.

Atx3-Q14 and Atx3-Q55 proteins were engineered to generate suitable DNAs constructs that could be expressed in cells. In order to recognize exogenous Atx3-Q14 and Atx3-Q55 from endogenous proteins, both DNAs constructs were modified by adding a Myc tag in their N-terminal region, and then they were cloned into vector for mammalian expression, as described in Chapter 2. The expression of the exogenous proteins was verified transfecting human cell line HEK293. As a control of the transfection method it was used a DNA construct expressing a fluorescent green protein (GFP), easily detected by fluorescence microscopy analysis. After 48 hours of transfection, the total protein extracts from transfected cells were evaluated by western blot analysis. This was possible thanks to the Myc tag that was recognized by specific antibodies, permitting to distinguish the exogenous proteins from endogenous proteins expressed at basal levels in cells. An antibody against Atx3 protein was also used, able to recognize both Atx3-Q14 and Atx3-Q55 by binding the region between Jos domain and polyQ tract.

As first experimental approach, Atx3 constructs were generated for an inducible expression system in human cells, using the inducible vector pTet-ONE. This vector permits to control high level expression of gene of interest, thanks to a control of a promoter, regulated by the presence of Doxycycline (Dox) in the cultured medium. This system was suitable to regulate the over-expression of exogenous proteins at different times. This approach was unsuccessful

because did not allow a good level of expression of exogenous proteins in cell. pCI-Neo no-inducible vector was then used, which is able to over-express proteins continuously in human cells. Figure 3.23 reports the western blot analysis of cell lysates from HEK293 cells transfected with Atx3 variants cloned in pTet-ONE vector, and those obtained using the pCI-Neo vector. After 48 hours transfection, cells were lysate and the total proteins extract was analysed by western blot. For western blot analysis an antibody against Atx3 was used. An antibody against Tom 20 protein was used as a control of analysis.

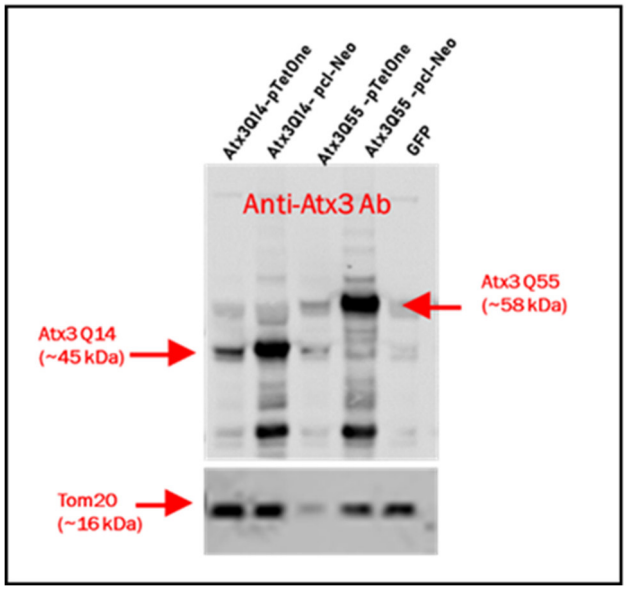

Figure 3.23: Western blot analysis, using Anti-Atx3 clone 1H9 antibody, of cell lysate from HEK293 cells transfected with Atx3-Q14 (lane 1)and Atx3-Q55(lane 3) in pTet-ONE vector, and with Atx3-Q14 (lane 2)and Atx3-Q55(lane 4) in pCI-Neo vector; Anti-Atx3 GFP plasmid was used as a control of transfection(lane 5); Anti-Tom20 antibody were used as a control.

As shown in Fig. 3.23, comparing the two expression strategies, the use of the pCI-Neo vector clearly increases the level expression of exogenous proteins. Considering the good results obtained using pCI-Neo vector, the vector was used also to generate a construct for expression of triUb protein in human cells. Although Atx3 shows high affinity of binding for K48-linked polyUb chains, it was not possible generate in cell recombinat K48-linked triUb. A linear M1-linked triUb was then generated with HA tag to distinguish exogenous construct from proteins in cells, and in order to visualize simultaneously Atx3 constructs and linear M1-linked triUb.
In order to investigate on the interaction between Atx3 isoforms and M1-linked triUb chains in cell model, HEK293 were co-transfected with a combination of Myc-tagged Atx3-Q14 and linear HA-tagged M1-linked triUb, or with a combination of Myc-tagged Atx3-Q55 and linear HA-tagged_M1-linked triUb, as described in chapter 2.

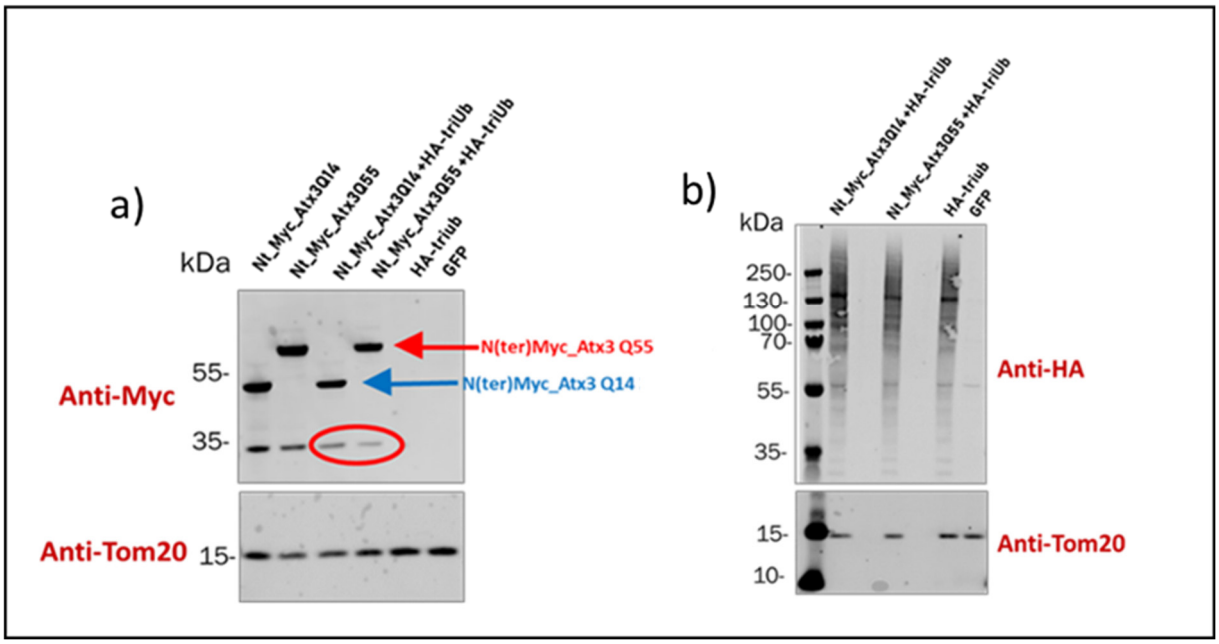

Figure 3.24: a) Western Blot analysis using Anti-Myc antibody, of cell lysate form HEK293 cells transfected with both Atx3-Q14 (lane 1)and Atx3-Q55 (lane 2)constructs alone, and western blot analysis of cell lysate form HEK293 cells co-transfected with both Atx3-Q14 (lane 3)and Atx3-Q55 (lane 4) with HA-M1-linked triUb; **b)** Western Blot analysis using Anti-HA antibody of cell lysate form HEK293 cells co-transfected with Atx3-Q14 (lane 1)and Atx3-Q55(lane 3) with HA-M1-linked triUb and HA-M1-linked triUb alone(lane 5). GFP plasmid was used as a control of transfection; Anti-Tom20 antibody were used as a control of the method.

Figure 3.24 shows the western blot analysis of cell lysates from HEK293 cells transfected for 48 hours with: i. Myc-tagged Atx3-Q14 alone; ii. Myc-tagged Atx3-Q14 co-expressed with linear HA-tagged M1-linked triUb; iii. Myc-tagged Atx3-Q55 alone; iv. Myc-tagged Atx3-Q55 co-expressed with linear HA-tagged M1-linked triUb. In panel a) detection of both Atx3-Q14 and Atx3-Q55 constructs was revealed by using anti-Myc antibody while in panel b) anti-HA antibody was used in order to recognize exogenous triUb. As in western blot analysis reported in Fig. 3.23 antibody against Tom 20 protein was used as control. The results showed in panel a) highlight the presence of a band around 35 KDa in all samples. This probably corresponds to Atx3 fragments containing the N-terminal region with Myc tag. Interestingly, when Atx3 is co-expressed with linear M1-linked triUb, the intensity of the band at about 35 KDa is lower (see bands highlighted with red circle in Fig. 3.24a). These observations strongly suggest that triUb is able to obscure the catalytic site in Atx3 reducing its auto-cleavage propensity[99]. The reported results also allow to infer that a direct interaction exists in cell between Atx3 and M1-linked triUb.

In order to evaluate the behaviour of the over-expressed linear M1-linked triUb in the cell, western blot analysis was performed using anti-HA antibody for both, cells transfected with

only triUb and cells co-transfected using triUb and Atx3-Q14 and Atx3-Q55 (Fig.3.24b). Data do not show differences that could be related to the interaction between Atx3 and triUb. This is possible because linear M1-linked triUb is able in cell system to interact with several proteins, therefore it is difficult to assess a specific interaction with the only Atx3 variants.

We also investigated by immunofluorescence assay the efficiency of transfection in HEK293 for both Atx3-Q14 and Atx3-Q55. HEK293 cells were transfected for 48 hours using Atx3-Q14 and Atx3-Q55 constructs and cells were stained using Anti-Myc and Anti-Atx3 antibodies, and DAPI for nuclei detection (Fig.3.25). As shown in figure both, Atx3-Q14 and Atx3-Q55 were mostly expressed in the cytoplasm, and partially in perinuclear region. Not significant differences were observed comparing the two Atx3 variants. Cell toxicity was not observed after 48 hours transfection over expressing both Atx3-Q14 and Atx3-Q55. In the presented experiments it is not possible to distinguish the formation of aggregates or local accumulation of proteins.

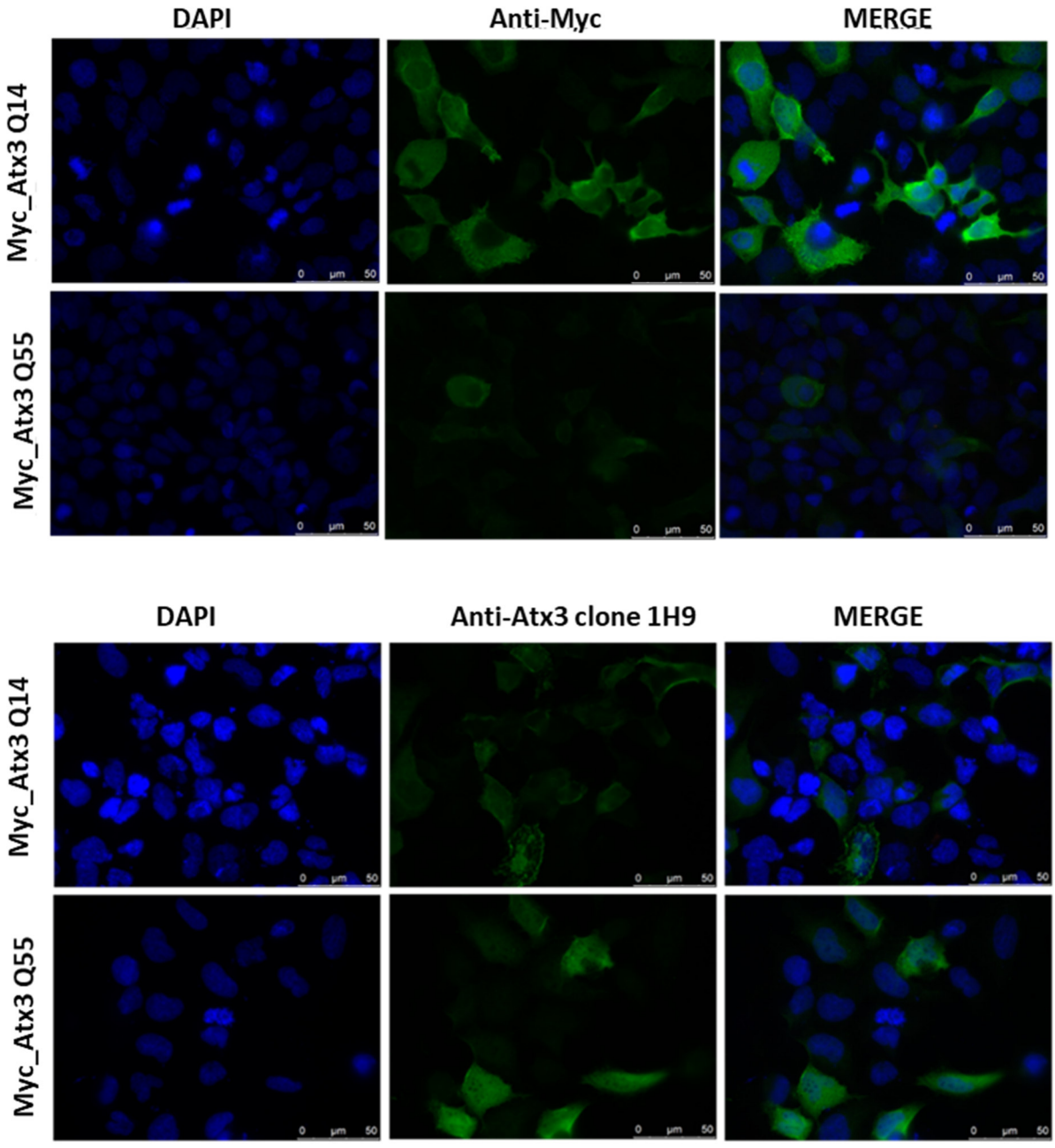

Figure 3.25: Immunofluorescence assay of HEK293 transfected using both Myc-tagged_Atx3-Q14 and Myc-tagged_Atx3-Q55 in pCI-Neo vector. The cells were fixed and immunostained with DAPI (blue), Anti-Myc and anti-Atx3 clone 1H9 (primary antibody) and AlexaFluor-488 (secondary antibody) (green).

Immunofluorescence assay were also performed for HEK293 cells after co-transfection of Atx3-Q14 and linear M1-linked triUb, and after co-transfection of Atx3-Q55 and linear M1-linked triUb (Fig. 3.26). On the basis of western blot analysis, these measurements add information on the localization of triUb in cell in order to evaluate a possible interaction between Atx3 and triUb. The analysis revealed that exogenous triUb protein is present in the cytoplasm and co-localize with both Atx3 constructs. Although not significant evidence of interaction was

observed using this method, the presence of both proteins in the same cell region suggest the possibility of interaction between Atx3 and triUb.

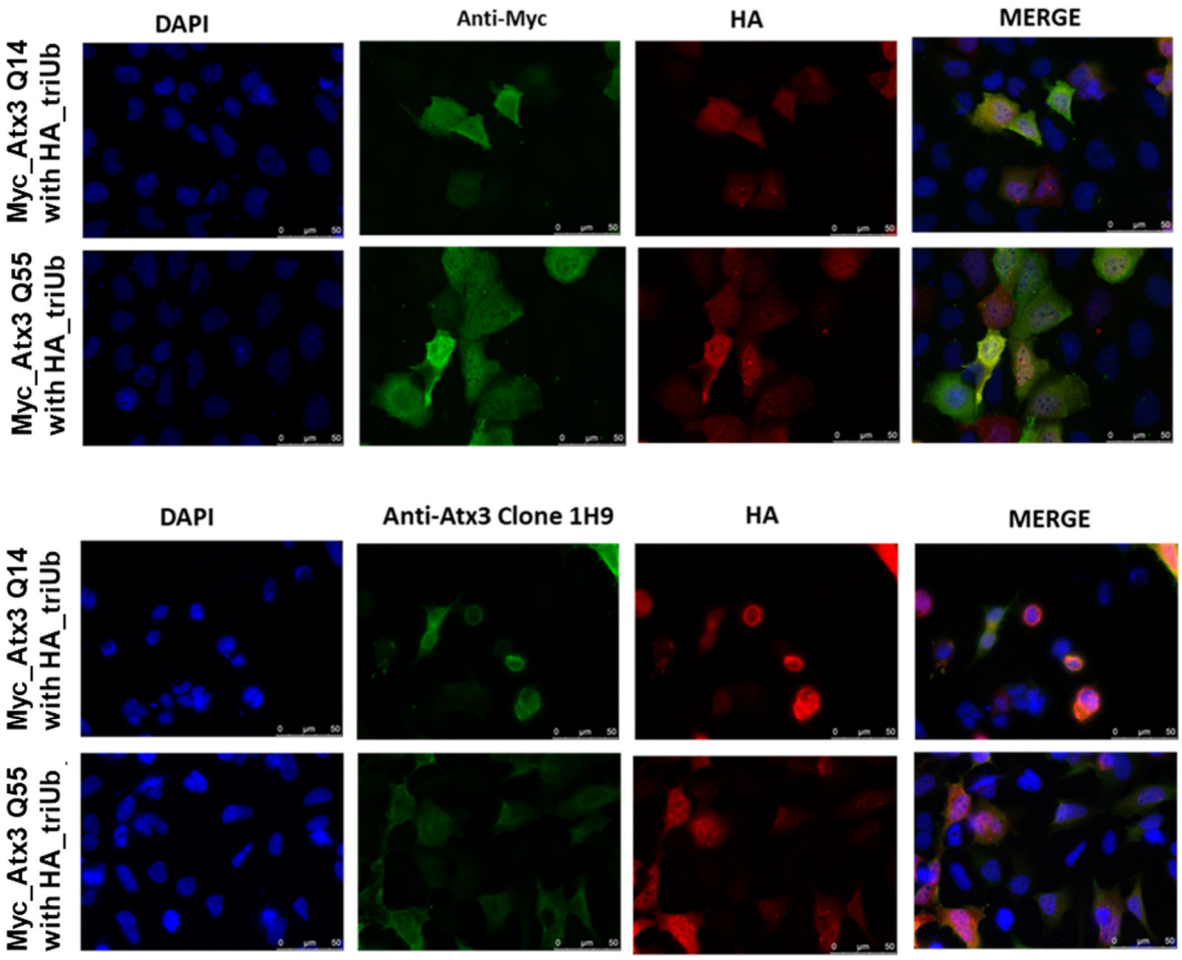

Figure 3.26: Immunofluorescence assay of HEK293 co-transfected with both Myc-tagged_Atx3-Q14 and Myc-tagged_Atx3-Q55 and linear HA-tagged_M1-linked triUb. The cells were fixed and stained with DAPI (blue), Anti-Myc and anti-Atx3 (primary antibody), AlexaFluor-488 (secondary antibody) (green) AlexaFluor-800 (secondary antibody) (red).

In this section, investigation on co-expression of Atx3 variants and linear M1-linked triUb in human cell model has been reported. Both, Atx3-Q14 and Atx3-Q55, and triUb were expressed in human cells. All proteins localize to the cytoplasm, and not cellular toxicity was observed after transfection, revealing that the constructs are suitable for in cell analysis.

Aggregates formation was not detected in cells and results suggest a possible interaction between Atx3 and linear M1-linked triUb. Presented results are in line with observations *in-vitro* reported in chapter 3, where no significant differences were observed between the two Atx3-Q14 and Atx3-Q54 variants. Furthermore, it was observed that Atx3 isoforms and linear M1-linked triUb co-localize in cells, suggesting that is not possible to exclude an interaction. Even

if, the natural partner of Atx3 is K48-linked triUb, the findings observed using linear M1-linked triUb provide information for further investigations.

3.4 Effect of K48-linked tri-Ubiquitin chains on Josephin domain aggregation process

Above reported studies both in solution and in cells, evidence that selected model Atx3 variants present the same behaviour that does not depend on the polyQ tract but on the globular domain Jos. According to results reported in the literature, Jos appears to be responsible for modulating the aggregation process of the full-length protein especially in the initial stages of the process. On the basis of this hypothesis, it was therefore decided to use Jos alone to evaluate *in-vitro* the possible protective role of polyUb on the Atx3 aggregation process. In vitro it was possible to use K48-linked triUb, that is recognized as target in the protein degradation process mediated by the proteasome in which Atx3 is also involved. In particular, K48-linked triUb were prepared by enzymatic reaction, and the effect of the interaction of these chains on the aggregation kinetics of Jos was investigated *in-vitro*. Several works have reported the aggregation analysis of the isolated Jos, confirming that Jos is able to aggregate under physiological conditions[49][96][102][203]. Nicastro and co-workers, hypothesized that the physiological function of Atx3 could protect against aggregation, and coherently with this hypothesis they found that interaction between Jos and mUb had the effect of slowing down Jos aggregation without reaching complete suppression. The aggregation pathway was modified in a way that final products were small amorphous aggregates[82]. Inspired by these encouraging data, an investigation on the effects of K48-linked triUb on Jos aggregation process was carried out in this thesis work. As the aim was to evaluate the effect of interaction between K48-linked triUb and Atx3 full-length, an optimization of an efficient protocol to study the interaction between K48-linked triUb and Atx3 full-length proteins was also conducted.

In this section, pilot measurements aimed at assessing the effect of the interaction between Jos and K48-linked triUb on the aggregation process are reported.

Figure 3.27 shows the Rayleigh Scattering intensity measured at 440 nm (a), together with ThT fluorescence emission at 480 nm as a function of time (b) for Jos alone, and in complex with K48-linked triUb, in a 1:1 molar ratio. Experiments were performed in 20mM sodium phosphate buffer with 1mM TCEP, pH6.5, incubating at 50°C for 8 hours. Rayleigh scattering intensity measured for Jos sample grows faster and reach higher values with respect to Jos in complex with triUb. Same trend is shown by ThT fluorescence, indicating that Jos samples forms aggregates with the same trend as the one observed for both Atx3 variants. This further

confirming previously described hypothesis that observed Atx3 aggregation processes were modulated by Jos. The plateau value for Jos domain is reached in about 2 hours. Jos in complex with K48 linked triUb, shows a slower kinetic leading to a lower plateau value.

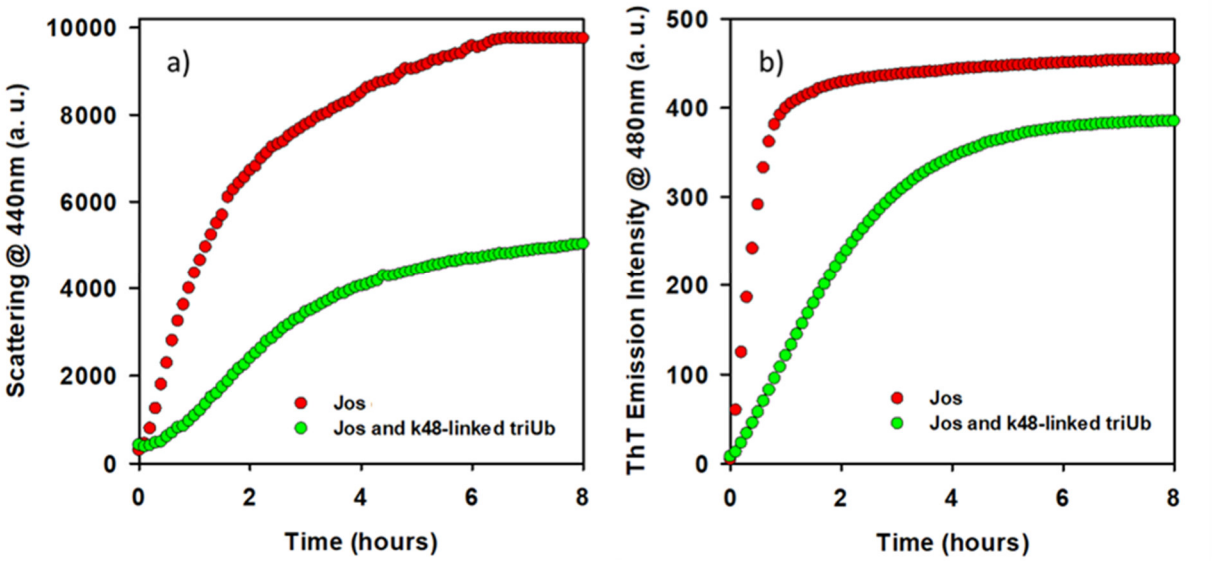

Figure 3.27: a) Comparison of Rayleigh scattering at 440nm as a function of time and **b)** ThT fluorescence emission at 480 nm as a function of time of 22 μM Jos (red dots) and 22μM Jos with k48-linked triUb chains (1:1 molar ratio) (green dots) with 26μM ThT, in 20mM Na phosphate buffer with 1mM TCEP, pH 6.5 incubated at 50°C for 8h.

Results suggest that, in line with project hypothesis, the interaction with K48-linked triUb chains interfere with the aggregation pathway of Atx3. These encouraging data open the way to further studies in this direction. The experimental work was devoted in setting up *in-vitro* and *in-cell* experimental platform to analyse if and how the physiological function of Atx3 had an effect on aggregation processes in the light of using it to define new therapeutic strategy to slow down or inhibit Atx3 aggregation process in SCA3 patients. Further studies will be possible on the interactions between polyUb chains of different lengths with Atx3 highlighting the effect on protein stability aggregation propensity and mechanisms. Analogous studies are in progress with Atx3 with more than Q70 variant.

4 Conclusions

This thesis was aimed at analysing the molecular mechanisms involved in the aberrant and pathogenic aggregation of Atx3 and the possible protective role of polyUb chains on this process. This in the hypothesis that the interaction of Atx3 with its physiological partners may stabilise the native state reducing aberrant supramolecular assembly[103]. At this purpose, a clear understanding of molecular details of the interaction interfaces it is fundamental to gain information about the inducing stabilizing effects, and can provide useful clues for the design of synthetic peptide which can be efficiently used as drugs to treat the SCA3 pathology. Experiments were performed in vitro and in cells in order to assess conditions and pivotal target mechanisms to analyse effects of polyUb chains on Atx3 variants selected as model of polyQ non-expanded and expanded proteins. A multiplexed experimental approach was developed based on protein engineering, which allows the preparation of high pure samples with suitable mutations, and biophysical methods.

The first part of this work was focused on the analysis of conformational properties and aggregation of Ub as a model of polyUb chain. This has the double purpose of defining the methodological approach for the study of aggregation processes and, at the same time, of analysing the conformational stability and structural changes of Ub in the experimental conditions chosen to investigate the possible protective role of polyUb on the Atx3 aggregation process.

A combined use of UV-visible absorption spectroscopy, fluorescence spectroscopy, circular dichroism, and FTIR techniques was applied to analyse the effects of stress on Ub. In particular, it was found that, at high temperature or under agitation, Ub may form oligomeric aggregates with not amyloid features, following a process that does not involve significant changes at secondary structure level. In parallel, changes induced by UV stress were observed on Ub during its aggregation process highlighting light induced modifications, which occurs in experimental conditions commonly used to analyse conformational changes of proteins by means of intrinsic fluorescence signal. Importantly, UV-irradiation was found to lead to critical changes in emission profile of Ub, and in particular to the formation of a new band in the range 350–550 nm, which was assigned to oxidation products of tyrosine residues[133]. Results also clearly indicated that the observed UV induced tyrosine oxidation occurs in proteins which lack in their sequence of tryptophan residues. The same spectral modifications were also observed for both Insulin and Aβ(1-40)-amyloid samples grown under UV exposure, demonstrating that the signal attributed to tyrosine oxidation substantially overlaps (both in terms of spectral range and lifetime distribution) with the one attributed to intrinsic amyloid fluorescence.

These findings clearly represent a caveat about the specificity of the blue fluorescence peak measured for amyloids, especially when grown in conditions in which tyrosine residues may be oxidized.

In the second part of the study, the experimental analysis of Atx3 aggregation processes both in cell and in vitro was performed to define the Atx3 aggregation mechanisms, and to investigate on interactions to be used for the analysis of polyUb effect on Atx3 aggregation process.

The study of Atx3 aggregation processes in vitro was performed using the experimental platform optimised for the study of Ub. Particular care was dedicated in avoiding/minimising UV-light exposure during the aggregation analysis steps. It is important to highlight that both Atx3-Q14 and Atx3-Q54 variants used for in vitro studies were engineering with the point mutation C14A, responsible for inactivation of the catalytic activity of Atx3 towards polyUb chains, and for the auto-proteolytic property of Atx3. This choice was aimed at reducing the complexity of the aggregation process under observation avoiding the formation of polyQ fragments generated by self-cleavage that could promote heterogeneous nucleation mechanisms. This also allowed to highlight the role of polyQ flanking domains in the regulation of Atx3 function and aggregation[102][197].

The results showed that both non-expanded Atx3-Q14 and expanded Atx3-Q54 variants follow, under selected experimental conditions, the same aggregation process. Notwithstanding the large difference in length of the polyQ tract, the two variants were found to form small amyloid like oligomers without involving nucleation mechanisms widely reported in other similar studies[94][95][196][197]. The observed monotonic growth of supramolecular assembly by means of light scattering and ThT fluorescence was paralleled by the progressive increase of intermolecular β-sheets highlighted by circular dichroism measurements. Different physic-chemical conditions were tested, which highlighted protein-solvent interactions, and in particular electrostatic interactions as dominant in regulating the fibrils formation. The results are in line with recent literature which puts in evidence general laws underlying aggregation mechanisms of globular proteins, suggesting that in the presented experimental conditions the folded Jos plays a dominant role in Atx3. The comparison of experimental results with literature, suggests that isolating Atx3 aggregation mechanisms leaded by Jos are due both to the experimental conditions, and to the selected Atx3 mutants with reduced self-cleavage propensity.

Experiments in human cells were performed at the Basic & Clinical Neuroscience Department of King's College of London, under the supervision of Prof. A. Pastore. The cell studies, as well as the in vitro studies, were focused at defining a suitable platform, and at revealing key interactions and suitable observables to analyse the effects of selected inhibitors on Atx3 toxicity in cellular environment. In particular, pilot experiments on the interaction between the two

Atx3 variants and polyUb were performed in HEK293 cells using recombinant linear M1-linked triUb as model. Over-expression of both solely Atx3-Q14 and solely Atx3-Q55 was also induced in HEK293 cells to evaluate differences between the two variants in terms of cytotoxicity and ability to form aggregates in cellular environment. In line with in vitro studies, results indicated that both Atx3 variants mainly localize in the cytoplasm, and do not form nuclear inclusions considered main hallmarks of cellular toxicity.

A dedicated protocol to investigate the interaction between Atx3 and polyUb chains was also set up in cells system. Experiment were performed co-expressing Atx3 with recombinant linear M1-linked triUb in HEK293 cells. Promising results were obtained which revealed that both Atx3 and triUb co-localize in the cell cytoplasm, and that the auto-proteolytic propensity of Atx3 is clearly reduced in presence of co-expressed triUb. This evidence suggests an interaction between the two proteins, and a binding at the catalytic site of Atx3 responsible also for its auto-proteolytic activity. Although in the tested conditions aberrant aggregation of expanded Atx3 was not highlighted, the co-expression results give evidences of a possible interaction and pave the way to the setup analogous studies using Atx3 variants with longer polyQ expansion.

Moreover, in cell studies revealed that Atx3 fragments are also physiologically generated, and that the size of these fragments is comparable to the size of the solely Jos. These results suggest that Jos, main actor of Atx3 catalytic function and key player in the early stage of Atx3 aggregation process, is a valuable target to investigated the effect of possible modulators of aberrant aggregation.

For this reason, Jos was the first target of polyUb interactions studies. This allowed to look at first only at simpler mechanisms occurring in the first step of Atx3 aggregation, which specifically involve Jos. In this way, other mechanisms related to the polyQ trait are excluded.

In vitro pilot experiments were performed using K48-linked triUb chains, prepared by enzymatic reaction, and recombinant Jos, containing the same C14A point mutation used for the full length Atx3 variants. Experimental studies performed in analogous conditions as the one used for Atx3 variants, revealed that the aggregation of Jos in presence of K48-linked triUb chains is clearly inhibited. Indeed, both the aggregation rate and the amount of final amyloid aggregates products resulted reduced, as indicated by combined scattering and ThT measurements.

It is important to note that all the presented results highlight the role in the aberrant Atx3 aggregation of fragments generated by auto-proteolytic activity of Atx3. In fact, under conditions in which this activity was inhibited or reduced, by temperature effect or because the presence of the point mutation C14A, no significant differences were observed between the two Atx3 variants.

The presented results confirm the hypothesis that functional interaction may increase target protein stability and may reduce aberrant aggregation, encouraging studies on Atx3 variants which include the polyQ tract. These studies are in progress and will benefit of the large amount of evidences and protocols background produced till now.

Bibliography

[1] J. Z. Zaretsky and D. H. Wreschner, “Protein Multifunctionality : Principles and Mechanisms,” pp. 99–136, 2008.

[2] H. S. Chan and K. A. Dill, “Protein folding in the landscape perspective: Chevron plots and non- rrhenius kinetics,” *Proteins Struct. Funct. Genet.*, vol. 30, no. 1, pp. 2–33, 1998.

[3] C. M. Dobson, “Protein folding and misfolding,” *Nature*, vol. 426, no. December, pp. 884–90, 2003.

[4] S. W. Englander and L. Mayne, “The nature of protein folding pathways,” *Proc. Natl. Acad. Sci. U. S. A.*, vol. 111, no. 45, pp. 15873–15880, 2014.

[5] K. Chan, H. and Dill, “Protein folding in the landscape perspective: chevron plots and non-Arrhenius kinetics.,” *Proteins*, vol. 30, pp. 2–33, 1998.

[6] J. Adamcik and R. Mezzenga, “Amyloid Polymorphism in the Protein Folding and Aggregation Energy Landscape,” *Angew. Chemie - Int. Ed.*, vol. 57, no. 28, pp. 8370–8382, 2018.

[7] T. R. Jahn and S. E. Radford, “Folding versus aggregation: Polypeptide conformations on competing pathways,” *Arch. Biochem. Biophys.*, vol. 469, no. 1, pp. 100–117, 2008.

[8] M. Morell *et al.*, “Inclusion bodies: Specificity in their aggregation process and amyloid-like structure,” *Biochim. Biophys. Acta - Mol. Cell Res.*, vol. 1783, no. 10, pp. 1815–1825, 2008.

[9] P. Salahuddin, M. T. Fatima, A. S. Abdelhameed, S. Nusrat, and R. H. Khan, “Structure of amyloid oligomers and their mechanisms of toxicities: Targeting amyloid oligomers using novel therapeutic approaches,” *Eur. J. Med. Chem.*, vol. 114, pp. 41–58, 2016.

[10] A. J. Baldwin *et al.*, “Metastability of native proteins and the phenomenon of amyloid formation,” *J. Am. Chem. Soc.*, vol. 133, no. 36, pp. 14160–14163, 2011.

[11] S. Keten and M. J. Buehler, “Geometric confinement governs the rupture strength of h-bond assemblies at a critical length scale,” *Nano Lett.*, vol. 8, no. 2, pp. 743–748, 2008.

[12] J. L. Jiménez, E. J. Nettleton, M. Bouchard, C. V. Robinson, C. M. Dobson, and H. R. Saibil, “The protofilament structure of insulin amyloid fibrils,” *Proc. Natl. Acad. Sci. U. S. A.*, vol. 99, no. 14, pp. 9196–9201, 2002.

[13] M. P. Jackson and E. W. Hewitt, “Why are functional amyloids non-toxic in humans?,” *Biomolecules*, vol. 7, no. 4, pp. 1–13, 2017.

[14] K. L. Zapadka, F. J. Becher, A. L. Gomes dos Santos, and S. E. Jackson, “Factors affecting the physical stability (aggregation) of peptide therapeutics,” *Interface Focus*, vol. 7, no. 6, 2017.

[15] V. Vetri and V. Foderà, “The route to protein aggregate superstructures: Particulates and amyloid-like spherulites,” *FEBS Lett.*, vol. 589, no. 19, pp. 2448–2463, 2015.

[16] K. ichi Yamaguchi, H. Naiki, and Y. Goto, “Mechanism by Which the Amyloid-like Fibrils of a β2-Microglobulin Fragment Are Induced by Fluorine-substituted Alcohols,” *J. Mol. Biol.*, vol. 363, no. 1, pp. 279–288, 2006.

[17] J. E. Gillam and C. E. Macphee, “Modelling amyloid fibril formation kinetics: Mechanisms of nucleation and growth,” *J. Phys. Condens. Matter*, vol. 25, no. 37, 2013.

[18] F. Ferrone, “Analysis of protein aggregation kinetics,” *Methods Enzymol.*, vol. 309, no. 1, pp. 256–274, 1999.

[19] P. Arosio, T. P. J. Knowles, and S. Linse, “On the lag phase in amyloid fibril formation,” *Phys. Chem. Chem. Phys.*, vol. 17, no. 12, pp. 7606–7618, 2015.

[20] V. Foderà, S. Cataldo, F. Librizzi, B. Pignataro, P. Spiccia, and M. Leone, “Self-organization pathways and spatial heterogeneity in insulin amyloid fibril formation,” *J. Phys. Chem. B*, vol. 113, no. 31, pp. 10830–10837, 2009.

[21] A. Lomakin, D. B. Teplow, D. A. Kirschner, and G. B. Benedeki, “Kinetic theory of fibrillogenesis of amyloid β-protein,” *Proc. Natl. Acad. Sci. U. S. A.*, vol. 94, no. 15, pp. 7942–7947, 1997.

[22] T. R. Serio *et al.*, “Nucleated conformational conversion and the replication of conformational information by a prion determinant,” *Science (80-.).*, vol. 289, no. 5483, pp. 1317–1321, 2000.

[23] V. N. Uversky and A. L. Fink, “Conformational constraints for amyloid fibrillation: The importance of being unfolded,” *Biochim. Biophys. Acta - Proteins Proteomics*, vol. 1698, no. 2, pp. 131–153, 2004.

[24] M. M. Pallitto and R. M. Murphy, “A mathematical model of the kinetics of β-amyloid fibril growth from the denatured state,” *Biophys. J.*, vol. 81, no. 3, pp. 1805–1822, 2001.

[25] W. S. Gosal, I. J. Morten, E. W. Hewitt, D. A. Smith, N. H. Thomson, and S. E. Radford, “Competing pathways determine fibril morphology in the self-assembly of β2-microglobulin into amyloid,” *J. Mol. Biol.*, vol. 351, no. 4, pp. 850–864, 2005.

[26] V. Vetri *et al.*, “Amyloid fibrils formation and amorphous aggregation in concanavalin A,” *Biophys. Chem.*, vol. 125, no. 1, pp. 184–190, 2007.

[27] V. Vetri *et al.*, “Bovine Serum Albumin protofibril-like aggregates formation: Solo but not simple mechanism,” *Arch. Biochem. Biophys.*, vol. 508, no. 1, pp. 13–24, 2011.

[28] V. N. Uversky and A. V. Finkelstein, “Life in phases: Intra-and inter-molecular phase transitions in protein solutions,” *Biomolecules*, vol. 9, no. 12, 2019.

[29] C. A. Ross, “Huntington’s disease: New paths to pathogenesis,” *Cell*, vol. 118, no. 1, pp.

4–7, 2004.

[30] C. G. Chung, H. Lee, and S. B. Lee, “Mechanisms of protein toxicity in neurodegenerative diseases,” *Cell. Mol. Life Sci.*, vol. 75, no. 17, pp. 3159–3180, 2018.

[31] D. E. and M. Jucker, “The amyloid state of proteins in human diseases,” *Cell.*, vol. 148, no. 6, pp. 1188–1203, 2012.

[32] M. Stefani and C. M. Dobson, “Protein aggregation and aggregate toxicity: New insights into protein folding, misfolding diseases and biological evolution,” *J. Mol. Med.*, vol. 81, no. 11, pp. 678–699, 2003.

[33] A. Burns and S. Iliffe, “Alzheimer’s disease,” *BMJ*, vol. 338, no. 7692, pp. 467–471, 2009.

[34] S. Sveinbjornsdottir, “The clinical symptoms of Parkinson’s disease,” *J. Neurochem.*, vol. 139, pp. 318–324, 2016.

[35] T. W. Todd and J. Lim, “Aggregation formation in the polyglutamine diseases: Protection at a cost?,” *Mol. Cells*, vol. 36, no. 3, pp. 185–194, 2013.

[36] M. Stefani, “Protein misfolding and aggregation: New examples in medicine and biology of the dark side of the protein world,” *Biochim. Biophys. Acta - Mol. Basis Dis.*, vol. 1739, no. 1, pp. 5–25, 2004.

[37] M. Stefani, “Biochemical and biophysical features of both oligomer/fibril and cell membrane in amyloid cytotoxicity,” *FEBS J.*, vol. 277, no. 22, pp. 4602–4613, 2010.

[38] J. E. Straub and D. Thirumalai, “Membrane-protein interactions are key to understanding amyloid formation,” *J. Phys. Chem. Lett.*, vol. 5, no. 3, pp. 633–635, 2014.

[39] J. R. Gatchel and H. Y. Zoghbi, “Diseases of unstable repeat expansion: mechanisms and common principles,” *Nat. Rev. Genet.*, vol. 6, no. 10, pp. 743–755, 2005.

[40] A. L. Robertson and S. P. Bottomley, “Towards the Treatment of Polyglutamine Diseases: The Modulatory Role of Protein Context,” *Curr. Med. Chem.*, vol. 17, no. 27, pp. 3058–3068, 2010.

[41] T. Yushchenko, E. Deuerling, and K. Hauser, “Insights into the Aggregation Mechanism of PolyQ Proteins with Different Glutamine Repeat Lengths,” *Biophys. J.*, vol. 114, no. 8, pp. 1847–1857, 2018.

[42] C. A. Ross, M. A. Poirier, E. E. Wanker, and M. Amzel, “Polyglutamine fibrillogenesis: The pathway unfolds,” *Proc. Natl. Acad. Sci. U. S. A.*, vol. 100, no. 1, pp. 1–3, 2003.

[43] T. Schmitz-Hübsch *et al.*, “Spinocerebellar ataxia types 1, 2, 3, and 6: Disease severity and nonataxia symptoms,” *Neurology*, vol. 71, no. 13, pp. 982–989, 2008.

[44] A. L. Darling and V. N. Uversky, “Intrinsic disorder in proteins with pathogenic repeat expansions,” *Molecules*, vol. 22, no. 12, pp. 8–13, 2017.

[45] H. C. Fan *et al.*, “Polyglutamine (PolyQ) diseases: Genetics to treatments,” *Cell Transplant.*, vol. 23, no. 4–5, pp. 441–458, 2014.

[46] J. Miller *et al.*, “Identifying polyglutamine protein species in situ that best predict neurodegeneration,” *Nat. Chem. Biol.*, vol. 7, no. 12, pp. 925–934, 2012.

[47] S. Chen, F. A. Ferrone, and R. Wetzel, “Huntington’s disease age-of-onset linked to polyglutamine aggregation nucleation,” *PNAS*, vol. 99, pp. 11884–11889, 2002.

[48] R. H. Walters and R. M. Murphy, “Aggregation kinetics of interrupted polyglutamine peptides,” *J. Mol. Biol.*, vol. 412, no. 3, pp. 505–519, 2011.

[49] H. M. Saunders and S. P. Bottomley, “Multi-domain misfolding: Understanding the aggregation pathway of polyglutamine proteins,” *Protein Eng. Des. Sel.*, vol. 22, no. 8, pp. 447–451, 2009.

[50] G. Nicastro, R. P. Menon, L. Masino, P. P. Knowles, N. Q. McDonald, and A. Pastore, “The solution structure of the Josephin domain of ataxin-3: Structural determinants for molecular recognition,” *Proc. Natl. Acad. Sci. U. S. A.*, vol. 102, no. 30, pp. 10493–10498, 2005.

[51] L. Masino, G. Nicastro, A. De Simone, L. Calder, J. Molloy, and A. Pastore, “The Josephin domain determines the morphological and mechanical properties of ataxin-3 fibrils,” *Biophys. J.*, vol. 100, no. 8, pp. 2033–2042, Apr. 2011.

[52] R. R. Kopito, “Aggresomes, inclusion bodies and protein aggregation,” *Trends Cell Biol.*, vol. 10, no. 12, pp. 524–530, 2000.

[53] J. Shao and M. I. Diamond, “Polyglutamine diseases: Emerging concepts in pathogenesis and therapy,” *Hum. Mol. Genet.*, vol. 16, no. R2, pp. 115–123, 2007.

[54] A. Haacke, F. U. Hartl, and P. Breuer, “Calpain inhibition is sufficient to suppress aggregation of polyglutamine-expanded ataxin-3,” *J. Biol. Chem.*, vol. 282, no. 26, pp. 18851–18856, 2007.

[55] N. A. Marian DiFiglia, Ellen Sapp, Kathryn O. Chase, Stephen W. Davies, Gillian P. Bates, J. P. Vonsattel, “Aggregation of Huntingtin in Neuronal Intranuclear Inclusions and Dystrophic Neurites in Brain,” *Science (80-.).*, vol. 277, no. 5334, pp. 1990–1993, 1997.

[56] O. Schmidt, T., Landwehrmeyer, G.B., Schmitt, I., Trottier, Y., Auburger, G., Laccone, F., Klockgether, T., Völpel, M., Epplen, J.T., Schöls, L. and Riess, “An Isoform of Ataxin-3 Accumulates in the Nucleus of Neuronal Cells in Affected Brain Regions of SCA3 Patients,” *Brain Pathol.*, vol. 8, pp. 669–679, 1998.

[57] T. Takeuchi and Y. Nagai, “Protein misfolding and aggregation as a therapeutic target for polyglutamine diseases,” *Brain Sci.*, vol. 7, no. 10, 2017.

[58] C. A. Matos, S. de Macedo-Ribeiro, and A. L. Carvalho, “Polyglutamine diseases: The special case of ataxin-3 and Machado-Joseph disease,” *Progress in Neurobiology*, vol. 95, no. 1. pp. 26–48, 15-Sep-2011.

[59] Y. Kawaguchi *et al.*, “CAG expansions in a novel gene for Machado-Joseph disease at chromosome 14q32.1,” *Nat. Genet.*, vol. 8, no. 3, pp. 221–228, 1994.

[60] H. L. Paulson *et al.*, “of Expanded Polyglutamine Protein in Spinocerebellar Ataxia Type 3,” *Cell*, vol. 19, pp. 333–344, 1997.

[61] H. Paulson, “Machado-Joseph Disease/Spinocerebellar Ataxia Type 3,” *Handb Clin Neurol*, vol. 103, pp. 437–449, 2012.

[62] P. Coutinho and C. Andrade, “Autosomal dominant system degeneration in Portuguese families of the Azores Islands,” *Neurology*, vol. 28, no. July, pp. 703–709, 1978.

[63] C. P. Lima L, “Clinical criteria for diagnosis of Machado-Joseph disease: report of a non-Azorena Portuguese family.,” *Neurology*, vol. 30, no. 3, pp. 319–22, 1980.

[64] H. L. Paulson, “Dominantly inherited ataxias: Lessons learned from Machado-Joseph disease/spinocerebellar ataxia type 3,” *Semin. Neurol.*, vol. 27, no. 2, pp. 133–142, 2007.

[65] O. Riess, U. Rüb, A. Pastore, P. Bauer, and L. Schöls, “SCA3: neurological features, pathogenesis and animal models.,” *Cerebellum*, vol. 7, no. 2, pp. 125–137, 2008.

[66] R. N. Rosenberg, “Machado-Joseph disease: An autosomal dominant motor system degeneration,” *Mov. Disord.*, vol. 7, no. 3, pp. 193–203, 1992.

[67] C. S. Lu *et al.*, “The parkinsonian phenotype of spinocerebellar ataxia type 3 in a Taiwanese family,” *Park. Relat. Disord.*, vol. 10, no. 6, pp. 369–373, 2004.

[68] R. S. Landau WM, Schmidt RE, McGlennen RC, “Hereditary Spastic Paraplegia and Hereditary Ataxia: Part 2: A Family Demonstrating Various Phenotypic Manifestations With the SCA3 Genotype,” *Arch Neurol.*, vol. 57, no. 7, pp. 733–739, 2000.

[69] A. Dürr *et al.*, “Spinocerebellar ataxia 3 and Machado-Joseph disease: Clinical, molecular, and neuropathological features,” *Ann. Neurol.*, vol. 39, no. 4, pp. 490–499, 1996.

[70] T. Matilla, A. McCall, S. H. Subramony, and H. Y. Zoghbi, “Molecular and clinical correlations in spinocerebellar ataxia type 3 and Machado-Joseph disease,” *Ann. Neurol.*, vol. 38, no. 1, pp. 68–72, 1995.

[71] Y. W. A *et al.*, “Six cases of SCA3/MJD patients that mimic hereditary spastic paraplegia in clinic,” *J. Neurol. Sci.*, vol. 285, pp. 121–124, 2009.

[72] L. R. Moore *et al.*, “Evaluation of Antisense Oligonucleotides Targeting ATXN3 in SCA3 Mouse Models,” *Mol. Ther. - Nucleic Acids*, vol. 7, no. June, pp. 200–210, 2017.

[73] J. Hu *et al.*, “Allele-selective inhibition of ataxin-3 (ATX3) expression by antisense

oligomers and duplex RNAs," *Biol. Chem.*, vol. 392, no. 4, pp. 315–325, 2011.

[74] N. Fujikake, Y. Nagai, H. A. Popiel, Y. Okamoto, M. Yamaguchi, and T. Toda, "Heat shock transcription factor 1-activating compounds suppress polyglutamine-induced neurodegeneration through induction of multiple molecular chaperones," *J. Biol. Chem.*, vol. 283, no. 38, pp. 26188–26197, 2008.

[75] M. Thomas, J. M. Harrell, Y. Morishima, H. M. Peng, W. B. Pratt, and A. P. Lieberman, "Pharmacologic and genetic inhibition of hsp90-dependent trafficking reduces aggregation and promotes degradation of the expanded glutamine androgen receptor without stress protein induction," *Hum. Mol. Genet.*, vol. 15, no. 11, pp. 1876–1883, 2006.

[76] F. M. Menzies *et al.*, "Calpain inhibition mediates autophagy-dependent protection against polyglutamine toxicity," *Cell Death Differ.*, vol. 22, no. 3, pp. 433–444, 2015.

[77] and J. H. W. Yunfu Lin, Leroy Hubert Jr., "Transcription Destabilizes Triplet Repeats," *Mol Carcinog*, vol. 48, no. 4, pp. 350–361, 2009.

[78] L. Masino *et al.*, "Domain architecture of the polyglutamine protein ataxin-3: A globular domain followed by a flexible tail," *FEBS Lett.*, vol. 549, no. 1–3, pp. 21–25, 2003.

[79] P. M. A. Antony *et al.*, "Identification and functional dissection of localization signals within ataxin-3," *Neurobiol. Dis.*, vol. 36, no. 2, pp. 280–292, 2009.

[80] B. Burnett, F. Li, and R. N. Pittman, "The polyglutamine neurodegenerative protein ataxin-3 binds polyubiquitylated proteins and has ubiquitin protease activity," *Hum. Mol. Genet.*, vol. 12, no. 23, pp. 3195–3205, 2003.

[81] M. Albrecht, M. Golatta, U. Wüllner, and T. Lengauer, "Structural and functional analysis of ataxin-2 and ataxin-3," *Eur. J. Biochem.*, vol. 271, no. 15, pp. 3155–3170, 2004.

[82] G. Nicastro *et al.*, "Josephin domain of ataxin-3 contains two distinct ubiquitin-binding sites," *Biopolym. - Pept. Sci. Sect.*, vol. 91, no. 12, pp. 1203–1214, 2009.

[83] S. V. Todi, B. J. Winborn, K. M. Scaglione, J. R. Blount, S. M. Travis, and H. L. Paulson, "Ubiquitination directly enhances activity of the deubiquitinating enzyme ataxin-3," *EMBO J.*, vol. 28, no. 4, pp. 372–382, 2009.

[84] I. Schmitt *et al.*, "Inactivation of the mouse Atxn3 (ataxin-3) gene increases protein ubiquitination," *Biochem. Biophys. Res. Commun.*, vol. 362, no. 3, pp. 734–739, 2007.

[85] P. X. K. Matthew Scaglione, Eszter Zavodszky, Sokol V. Todi, Srikanth Patury, J. Edgardo Rodríguez-Lebrón, Svetlana Fischer1, John Konen, Ana Djarmati, and and H. L. P. Peng, Jason E. Gestwicki, "Ube2w and ataxin-3 coordinately regulate the ubiquitin ligase CHIP," *Mol Cell.*, vol. 43, no. 4, pp. 599–612, 2011.

[86] Q. Wang, A. Li, and Y. Ye, “Regulation of retrotranslocation by p97-associated deubiquitinating enzyme ataxin-3,” *J. Cell Biol.*, vol. 174, no. 7, pp. 963–971, 2006.

[87] E. W. Doss-Pepe, E. S. Stenroos, W. G. Johnson, and K. Madura, “Ataxin-3 Interactions with Rad23 and Valosin-Containing Protein and Its Associations with Ubiquitin Chains and the Proteasome Are Consistent with a Role in Ubiquitin-Mediated Proteolysis,” *Mol. Cell. Biol.*, vol. 23, no. 18, pp. 6469–6483, 2003.

[88] X. Zhong and R. N. Pittman, “Ataxin-3 binds VCP/p97 and regulates retrotranslocation of ERAD substrates,” *Hum. Mol. Genet.*, vol. 15, no. 16, pp. 2409–2420, 2006.

[89] T. M. Durcan *et al.*, “The machado-joseph disease-associated mutant form of ataxin-3 regulates parkin ubiquitination and stability,” *Hum. Mol. Genet.*, vol. 20, no. 1, pp. 141–154, 2011.

[90] B. J. Winborn *et al.*, “The deubiquitinating enzyme ataxin-3, a polyglutamine disease protein, edits Lys63 linkages in mixed linkage ubiquitin chains,” *J. Biol. Chem.*, vol. 283, no. 39, pp. 26436–26443, 2008.

[91] D. Komander and M. Rape, “The Ubiquitin Code,” *Annu. Rev. Biochem.*, vol. 81, no. 1, pp. 203–229, 2012.

[92] F. Li, T. Macfarlan, R. N. Pittman, and D. Chakravarti, “Ataxin-3 is a histone-binding protein with two independent transcriptional corepressor activities,” *J. Biol. Chem.*, vol. 277, no. 47, pp. 45004–45012, 2002.

[93] B. O. Evert *et al.*, “Ataxin-3 represses transcription via chromatin binding, interaction with histone deacetylase 3, and histone deacetylation,” *J. Neurosci.*, vol. 26, no. 44, pp. 11474–11486, 2006.

[94] A. M. Ellisdon, B. Thomas, and S. P. Bottomley, “The two-stage pathway of ataxin-3 fibrillogenesis involves a polyglutamine-independent step,” *J. Biol. Chem.*, vol. 281, no. 25, pp. 16888–16896, 2006.

[95] A. M. Ellisdon, M. C. Pearce, and S. P. Bottomley, “Mechanisms of Ataxin-3 Misfolding and Fibril Formation: Kinetic Analysis of a Disease-associated Polyglutamine Protein,” *J. Mol. Biol.*, vol. 368, no. 2, pp. 595–605, Apr. 2007.

[96] L. Masino, G. Nicastro, A. De Simone, L. Calder, J. Molloy, and A. Pastore, “The Josephin domain determines the morphological and mechanical properties of ataxin-3 fibrils,” *Biophys. J.*, vol. 100, no. 8, pp. 2033–2042, 2011.

[97] F. Pellistri *et al.*, “Different ataxin-3 amyloid aggregates induce intracellular Ca2+ deregulation by different mechanisms in cerebellar granule cells,” *Biochim. Biophys. Acta - Mol. Cell Res.*, vol. 1833, no. 12, pp. 3155–3165, Dec. 2013.

[98] L. Masino, G. Kelly, K. Leonard, Y. Trottier, and A. Pastore, “Solution structure of

polyglutamine tracts in GST-polyglutamine fusion proteins," *FEBS Lett.*, vol. 513, no. 2–3, pp. 267–272, 2002.

[99] P. L. Mauri *et al.*, "Ataxin-3 is subject to autolytic cleavage," *FEBS J.*, vol. 273, no. 18, pp. 4277–4286, 2006.

[100] G. Invernizzi, M. Lambrughi, M. E. Regonesi, P. Tortora, and E. Papaleo, "The conformational ensemble of the disordered and aggregation-protective 182-291 region of ataxin-3," *Biochim. Biophys. Acta - Gen. Subj.*, vol. 1830, no. 11, pp. 5236–5247, 2013.

[101] M. L. Duennwald, S. Jagadish, P. J. Muchowski, and S. Lindquist, "Flanking sequences profoundly after polyglutamine toxicity in yeast," *Proc. Natl. Acad. Sci. U. S. A.*, vol. 103, no. 29, pp. 11045–11050, 2006.

[102] C. A. Scarff, B. Almeida, J. Fraga, S. Macedo-Ribeiro, S. E. Radford, and A. E. Ashcroft, "Examination of ataxin-3 (atx-3) aggregation by structural mass spectrometry techniques: A rationale for expedited aggregation upon polyglutamine (polyQ) expansion," *Mol. Cell. Proteomics*, vol. 14, no. 5, pp. 1241–1253, May 2015.

[103] L. Masino, G. Nicastro, L. Calder, M. Vendruscolo, and A. Pastore, "Functional interactions as a survival strategy against abnormal aggregation," *FASEB J.*, vol. 25, no. 1, pp. 45–54, Jan. 2011.

[104] S. S. Srandall K. Saik, David H. Gelfand, G. T. H. Stephen J. Scharf, Russell Higuchi, And H. A. E. Kary B. Mullis, "Primer-Directed Enzymatic Amplification of DNA with a Thermostable DNA Polymerase," *Science (80-.).*, vol. 979, pp. 487–491, 1988.

[105] F. W. Studier, "Use of bacteriophage T7 lysozyme to improve an inducible T7 expression system," *J. Mol. Biol.*, vol. 219, no. 1, pp. 37–44, 1991.

[106] T. W. Overton, "Recombinant protein production in bacterial hosts," *Drug Discov. Today*, vol. 19, no. 5, pp. 590–601, 2014.

[107] T. Sambrook, J., Fritsch, E.F. & Maniatis, *Molecular Cloning: A laboratory manual*. 1989.

[108] A. Bertero, S. Brown, and L. Vallier, *Methods of Cloning*. Elsevier Inc., 2017.

[109] C. Aslanidis, P. J. De Jong, and G. Schmitz, "Minimal length requirement of the single-stranded tails for ligation-independent cloning (LIC) of PCR products," *Genome Res.*, vol. 4, no. 3, pp. 172–177, 1994.

[110] M. Y. Zhou and C. E. Gomez-Sanchez, "Universal TA cloning.," *Curr. Issues Mol. Biol.*, vol. 2, no. 1, pp. 1–7, 2000.

[111] A. Fontes, "Cloning Technologies," in *Methods Mol Biol.*, vol. 997, pp. 253–61, 2013.

[112] Paul T. Wingfield, "Overview of the Purification of Recombinant Proteins," *Curr Protoc*

Protein Sci, vol. 80, pp. 6.1.1–6.1.35, 2015.

[113] R. Chen, "Bacterial expression systems for recombinant protein production: E. coli and beyond," *Biotechnol. Adv.*, vol. 30, no. 5, pp. 1102–1107, 2012.

[114] S. Zerbs, S. Giuliani, and F. Collart, *Small-scale expression of proteins in E. coli*, 1st ed., vol. 536. Elsevier Inc., 2014.

[115] F. W. Studier and B. A. Moffatt, "Use of bacteriophage T7 RNA polymerase to direct selective high-level expression of cloned genes," *J. Mol. Biol.*, vol. 189, no. 1, pp. 113–130, 1986.

[116] V. Gaberc-Porekar and V. Menart, "Perspectives of immobilized-metal affinity chromatography," *J. Biochem. Biophys. Methods*, vol. 49, no. 1–3, pp. 335–360, Oct. 2001.

[117] M. L. and T. Danieli, "Purification of Proteins Fused to Maltose-Binding Protein.," in *Protein Chromatography*, pp. 281–293,2010.

[118] P. G. Blommel and B. G. Fox, "A combined approach to improving large-scale production of tobacco etch virus protease," *Protein Expr. Purif.*, vol. 55, no. 1, pp. 53–68, 2007.

[119] J. Wu and M. Filutowicz, "Hexahistidine (His6)-tag dependent protein dimerization: A cautionary tale," *Acta Biochimica Polonica*, vol. 46, no. 3. pp. 591–599, 1999.

[120] P. Perron-Savard, G. De Crescenzo, and H. Le Moual, "Dimerization and DNA binding of the Salmonella enterica PhoP response regulator are phosphorylation independent," *Microbiology*, vol. 151, no. 12, pp. 3979–3987, 2005.

[121] W. T. Chan, C. S. Verma, D. P. Lane, and S. K. E. Gan, "A comparison and optimization of methods and factors affecting the transformation of Escherichia coli," *Biosci. Rep.*, vol. 33, no. 6, 2013.

[122] G. L. Rosano and E. A. Ceccarelli, "Recombinant protein expression in Escherichia coli: Advances and challenges," *Front. Microbiol.*, vol. 5, no. APR, pp. 1–17, 2014.

[123] H. G. Mori, S., & Barth, *Size exclusion chromatography*. Springer Science & Business Media, 2013.

[124] M. Noronha, J. C. Lima, M. Bastos, H. Santos, and A. L. Maçanita, "Unfolding of ubiquitin studied by picosecond time-resolved fluorescence of the tyrosine residue.," *Biophys. J.*, vol. 87, no. 4, pp. 2609–2620, 2004.

[125] W. J. Cook, L. C. Jeffrey, M. Carson, Z. Chen, and C. M. Pickart, "Structure of a diubiquitin conjugate and a model for interaction with ubiquitin conjugating enzyme (E2)," *J. Biol. Chem.*, vol. 267, no. 23, pp. 16467–16471, 1992.

[126] S. Faggiano, C. Alfano, and A. Pastore, "The missing links to link ubiquitin: Methods

for the enzymatic production of polyubiquitin chains," *Anal. Biochem.*, vol. 492, pp. 82–90, 2016.

[127] A. H. and A. Ciechanover, "The ubiquitin system," *Annu. Rev. Biochem.*, vol. 67, pp. 425–79, 1998.

[128] M. D'Amico, M. G. Di Carlo, M. Groenning, V. Militello, V. Vetri, and M. Leone, "Thioflavin T promotes Aβ(1-40) amyloid fibrils formation," *J. Phys. Chem. Lett.*, vol. 3, no. 12, pp. 1596–1601, 2012.

[129] M. Manno, E. F. Craparo, V. Martorana, D. Bulone, and P. L. San Biagio, "Kinetics of insulin aggregation: Disentanglement of amyloid fibrillation from large-size cluster formation," *Biophys. J.*, vol. 90, no. 12, pp. 4585–4591, 2006.

[130] M. G. Di Carlo *et al.*, "Thioflavin T templates amyloid β(1-40) conformation and aggregation pathway," *Biophys. Chem.*, vol. 206, pp. 1–11, 2015.

[131] E. R. Stadtman and R. L. Levine, "Free radical-mediated oxidation of free amino acids and amino acid residues in proteins," *Amino Acids*, vol. 25, no. 3–4, pp. 207–218, 2003.

[132] C. Giulivi and K. J. A. Davies, "Mechanism of the Formation and Proteolytic Release of H2O 2-induced Dityrosine and Tyrosine Oxidation Products in Hemoglobin and Red Blood Cells," *J. Biol. Chem.*, vol. 276, no. 26, pp. 24129–24136, 2001.

[133] A. Fricano, F. Librizzi, E. Rao, C. Alfano, and V. Vetri, "Blue autofluorescence in protein aggregates 'lighted on' by UV induced oxidation," *Biochim. Biophys. Acta - Proteins Proteomics*, vol. 1867, no. 11, pp. 1–35, 2019.

[134] L. Nielsen *et al.*, "Effect of environmental factors on the kinetics of insulin fibril formation: Elucidation of the molecular mechanism," *Biochemistry*, vol. 40, no. 20, pp. 6036–6046, 2001.

[135] K. F. DuBay, A. P. Pawar, F. Chiti, J. Zurdo, C. M. Dobson, and M. Vendruscolo, "Prediction of the absolute aggregation rates of amyloidogenic polypeptide chains," *J. Mol. Biol.*, vol. 341, no. 5, pp. 1317–1326, 2004.

[136] V. Villegas, J. Zurdo, V. V. Filimonov, F. X. Avilés, C. M. Dobson, and L. Serrano, "Protein engineering as a strategy to avoid formation of amyloid fibrils," *Protein Sci.*, vol. 9, no. 9, pp. 1700–1708, 2000.

[137] F. Schmid, "Biological Macromolecules: UV-visible Spectrophotometry," *eLS, (Ed.).*, 2001.

[138] G. Oster, "Light Scattering From Polymerizing And Coagulating Systems," pp. 291–299, 1947.

[139] P. Doty and J. T. Edsall, "Light Scattering in Protein Solutions," *Adv. Protein Chem.*, vol. 6, no. C, pp. 35–121, 1951.

[140] J. S. Pedersen, D. Dikov, J. L. Flink, H. A. Hjuler, G. Christiansen, and D. E. Otzen, "The changing face of glucagon fibrillation: Structural polymorphism and conformational imprinting," *J. Mol. Biol.*, vol. 355, no. 3, pp. 501–523, 2006.

[141] J. R. Lakowicz and B. R. Masters, "Principles of Fluorescence Spectroscopy, Third Edition," *J. Biomed. Opt.*, vol. 13, no. 2, p. 029901, 2008.

[142] V. Vetri, M. Leone, L. A. Morozova-Roche, B. Vestergaard, and V. Foderà, "Unlocked Concanavalin A Forms Amyloid-like Fibrils from Coagulation of Long-lived 'Crinkled' Intermediates," *PLoS One*, vol. 8, no. 7, 2013.

[143] H. Le Vine, "Quantification of beta-Sheet Amyloid Fibril Structures with Thioflavin T," *Methods Enzymol.*, vol. 309, pp. 274–284, 1999.

[144] E. S. Voropai *et al.*, "Spectral Properties Of Thioflavin T And Its Complexes With Amyloid Fibrils," *JJournal Appl. Spectrosc.*, vol. 70, no. 6, pp. 868–874, 2003.

[145] M. B. and S. Koide, "Molecular Mechanism of Thioflavin-T Binding to Amyloid Fibrils," vol. 1804, no. 7, pp. 1405–1412, 2011.

[146] V. Foderà *et al.*, "Thioflavin T hydroxylation at basic pH and its effect on amyloid fibril detection," *J. Phys. Chem. B*, vol. 112, no. 47, pp. 15174–15181, 2008.

[147] O. B. Ptitsyn, "How does protein synthesis give rise to the 3D-structure?," *FEBS Lett.*, vol. 285, no. 2, pp. 176–181, 1991.

[148] M. Engelhard and P. A. Evans, "Kinetics of interaction of partially folded proteins with a hydrophobic dye: Evidence that molten globule character is maximal in early folding intermediates," *Protein Sci.*, vol. 4, no. 8, pp. 1553–1562, 1995.

[149] M. Lindgren, K. Sörgjerd, and P. Hammarström, "Detection and characterization of aggregates, prefibrillar amyloidogenic oligomers, and protofibrils using fluorescence spectroscopy," *Biophys. J.*, vol. 88, no. 6, pp. 4200–4212, 2005.

[150] G. V. Semisotnov, N. A. Rodionova, O. I. Razgulyaev, V. N. Uversky, A. F. Gripas', and R. I. Gilmanshin, "Study of the 'molten globule' intermediate state in protein folding by a hydrophobic fluorescent probe," *Biopolymers*, vol. 31, no. 1, pp. 119–128, 1991.

[151] A. Hawe, M. Sutter, and W. Jiskoot, "Extrinsic fluorescent dyes as tools for protein characterization," *Pharm. Res.*, vol. 25, no. 7, pp. 1487–1499, 2008.

[152] S. Kelly and N. Price, "The Use of Circular Dichroism in the Investigation of Protein Structure and Function," *Curr. Protein Pept. Sci.*, vol. 1, no. 4, pp. 349–384, 2005.

[153] S. M. Kelly, T. J. Jess, and N. C. Price, "How to study proteins by circular dichroism," *Biochim. Biophys. Acta - Proteins Proteomics*, vol. 1751, no. 2, pp. 119–139, 2005.

[154] P. Juszczyk, A. S. Kołodziejczyk, and Z. Grzonka, "Circular dichroism and aggregation studies of amyloid β (11-28) fragment and its variants," *Acta Biochim. Pol.*, vol. 52, no.

2, pp. 425–431, 2005.

[155] G. Holzwarth and P. Doty, “The Ultraviolet Circular Dichroism of Polypeptides,” *J. Am. Chem. Soc.*, vol. 87, no. 2, pp. 218–228, 1965.

[156] J. T. Venyaminov, S. Y., Baikalov, I. A., Shen, Z. M., Wu, C. S. C., & Yang, “Circular Dichroic Analysis of Denatured Proteins: Inclusion of Denatured Proteins in the Reference Set.,” *Anal. Biochem.*, vol. 214, no. 1, pp. 17–24, 1993.

[157] D. Corrêa and C. Ramos, “The use of circular dichroism spectroscopy to study protein folding, form and function,” *African J Biochem Res*, vol. 3, no. 5, pp. 164–173, 2009.

[158] J. R. Lakowicz, *Principles of Fluorescence Spectroscopy,* 2008.

[159] M. A. Digman, V. R. Caiolfa, M. Zamai, and E. Gratton, “The phasor approach to fluorescence lifetime imaging analysis,” *Biophys. J.*, vol. 94, no. 2, pp. 14–16, 2008.

[160] C. Stringari, A. Cinquin, O. Cinquin, M. A. Digman, P. J. Donovan, and E. Gratton, “Phasor approach to fluorescence lifetime microscopy distinguishes different metabolic states of germ cells in a live tissue,” *Proc. Natl. Acad. Sci.*, vol. 108, no. 33, pp. 13582–13587, 2011.

[161] D. G. Gibson, L. Young, R. Y. Chuang, J. C. Venter, C. A. Hutchison, and H. O. Smith, “Enzymatic assembly of DNA molecules up to several hundred kilobases,” *Nat. Methods*, vol. 6, no. 5, pp. 343–345, 2009.

[162] T. K. Kim and J. H. Eberwine, “Mammalian cell transfection: The present and the future,” *Anal. Bioanal. Chem.*, vol. 397, no. 8, pp. 3173–3178, 2010.

[163] W. J. M. Carolyn A. Dennis-Sykes, William J. Miller, “A quantitative Western Blot method for protein measurement,” *J. Biol. Stand.*, vol. 13, no. 4, p. Pages 309-314, 1985.

[164] B. Russell, H., Sampson, J. S., Schmid, G. P., Wilkinson, H. W., & Plikaytis, “Enzyme-Linked Immunosorbent Assay and Indirect Immunofluorescence Assay for Lyme Disease.,” *J. Infect. Dis.*, vol. 149, no. 3, pp. 65–470, 1984.

[165] Y. Chai, S. S. Berke, R. E. Cohen, and H. L. Paulson, “Poly-ubiquitin Binding by the Polyglutamine Disease Protein Ataxin-3 Links Its Normal Function to Protein Surveillance Pathways,” *J. Biol. Chem.*, vol. 279, no. 5, pp. 3605–3611, 2004.

[166] W. K. D. W. Turcu Francisca E. Reyes, Ventii Karen H., “Nicotine-induced Upregulation of Nicotinic Receptors: Underlying Mechanisms,” *Biochem Pharmacol*, vol. 78, no. 7, pp. 756–765, 2009.

[167] M. Correia, M. T. Neves-Petersen, P. B. Jeppesen, S. Gregersen, and S. B. Petersen, “UV-Light Exposure of Insulin: Pharmaceutical Implications upon Covalent Insulin Dityrosine Dimerization and Disulphide Bond Photolysis,” *PLoS One*, vol. 7, no. 12, 2012.

[168] J. Pansieri *et al.*, “Ultraviolet–visible–near-infrared optical properties of amyloid fibrils shed light on amyloidogenesis,” *Nat. Photonics*, vol. 13, no. 7, pp. 473–479, 2019.

[169] Z. Gazova, Z. Bednarikova, A. Bartos, J. Klaschka, and Z. Kristofikova, “Surface tension and intrinsic amyloid fluorescence of serum and cerebrospinal fluid samples in Alzheimeŕs disease,” *Biomark. Med.*, vol. 13, no. 4, pp. 267–277, 2019.

[170] J. M. Antosiewicz and D. Shugar, “UV–Vis spectroscopy of tyrosine side-groups in studies of protein structure. Part 2: selected applications,” *Biophys. Rev.*, vol. 8, no. 2, pp. 163–177, 2016.

[171] G. B. and A. M. Dancewicz, “Radiation-induced dimerization of tyrosine and glycyltyrosine in aqueous solutions,” *Int. J . Radiat. Biol .,* vol. 39, no. 2, pp. 163–174, 1981.

[172] C. M. Pickart, M. T. Haldeman, E. M. Kasperek, and Z. Chen, “Iodination of tyrosine 59 of ubiquitin selectively blocks ubiquitin’s acceptor activity in diubiquitin synthesis catalyzed by E225K,” *J. Biol. Chem.*, vol. 267, no. 20, pp. 14418–14423, 1992.

[173] L. A. Munishkina and A. L. Fink, “Fluorescence as a method to reveal structures and membrane-interactions of amyloidogenic proteins,” vol. 1768, pp. 1862–1885, 2007.

[174] F. Librizzi, R. Carrotta, D. Spigolon, D. Bulone, and P. L. San Biagio, “α-Casein inhibits insulin amyloid formation by preventing the onset of secondary nucleation processes,” *J. Phys. Chem. Lett.*, vol. 5, no. 17, pp. 3043–3048, 2014.

[175] M. Noronha *et al.*, “Thermal unfolding kinetics of ubiquitin in the microsecond-to-second time range probed by Tyr-59 fluorescence,” *J. Phys. Chem. B*, vol. 114, no. 30, pp. 9912–9919, 2010.

[176] C. Giulivi, N. J. Traaseth, and K. J. A. Davies, “Tyrosine oxidation products: Analysis and biological relevance,” *Amino Acids*, vol. 25, no. 3–4, pp. 227–232, 2003.

[177] S. S. Lehrer and G. D. Fasman, “Ultraviolet Irradiation Effects in Poly-L-tyrosine and Model Compounds. Identification of Bityrosine as a Photoproduct,” *Biochemistry*, vol. 6, no. 3, pp. 757–767, 1967.

[178] G. J. Smith and T. G. Haskell, “The fluorescent oxidation products of dihydroxyphenylalanine and its esters,” *J. Photochem. Photobiol. B Biol.*, vol. 55, no. 2–3, pp. 103–108, 2000.

[179] D. M. Rayner, D. T. Krajcarski, and A. G. Szabo, “Excited state acid–base equilibrium of tyrosine,” *Can. J. Chem.*, vol. 56, no. 9, pp. 1238–1245, 1978.

[180] J. W. Heineckes, W. Li, H. L. Daehnke, and J. A. Goldstein, “Dityrosine, a Specific Marker of Oxidation,” vol. 202, 1993.

[181] A. Van Maarschalkerweerd *et al.*, “Formation of covalent di-tyrosine dimers in

recombinant α-synuclein," *Intrinsically Disord. Proteins*, vol. 3, no. 1, 2015.

[182] B. Ibarra-Molero, V. V. Loladze, G. I. Makhatadze, and J. M. Sanchez-Ruiz, "Thermal versus guanidine-induced unfolding of ubiquitin. An analysis in terms of the contributions from charge-charge interactions to protein stability," *Biochemistry*, vol. 38, no. 25, pp. 8138–8149, 1999.

[183] M. Groenning, "Binding mode of Thioflavin T and other molecular probes in the context of amyloid fibrils-current status," *J. Chem. Biol.*, vol. 3, no. 1, pp. 1–18, 2010.

[184] F. T. S. Chan, G. S. Kaminski Schierle, J. R. Kumita, C. W. Bertoncini, C. M. Dobson, and C. F. Kaminski, "Protein amyloids develop an intrinsic fluorescence signature during aggregation," *Analyst*, vol. 138, no. 7, pp. 2156–2162, 2013.

[185] D. A. Malencik and S. R. Anderson, "Dityrosine as a product of oxidative stress and fluorescent probe," *Amino Acids*, vol. 25, no. 3–4, pp. 233–247, 2003.

[186] P. H. Lakner, M. G. Monaghan, Y. Möller, and M. A. Olayioye, "Applying phasor approach analysis of multiphoton FLIM measurements to probe the metabolic activity of three- dimensional in vitro cell culture models," *Nat. Publ. Gr.*, no. February, pp. 1–11, 2017.

[187] Z. Cai, B. Zhao, and A. Ratka, "Oxidative stress and β-amyloid protein in Alzheimer's disease," *NeuroMolecular Medicine*, vol. 13, no. 4. pp. 223–250, 2011.

[188] D. R. a. Park, K.a, Gross, M.b, Lee, D.-H.c, Holvoet, P.d, Himes, J.H.a, Shikany, J.M.e, Jacobs Jr., "Oxidative Stress and Insulin Resistance The Coronary Artery Risk Development in Young Adults study," no. April, pp. 3–8, 2009.

[189] S. Vilasi *et al.*, "Biological and biophysics aspects of metformin - induced effects : cortex mitochondrial dysfunction and promotion of toxic amyloid pre - fibrillar aggregates," vol. 8, no. 8, pp. 1718–1734, 2016.

[190] P. Picone *et al.*, "Biochimica et Biophysica Acta Metformin increases APP expression and processing via oxidative stress , mitochondrial dysfunction and NF- κ B activation : Use of insulin to attenuate metformin ' s effect," *BBA - Mol. Cell Res.*, vol. 1853, no. 5, pp. 1046–1059, 2015.

[191] A. B. T. Ghisaidoobe and S. J. Chung, "Intrinsic tryptophan fluorescence in the detection and analysis of proteins: A focus on förster resonance energy transfer techniques," *Int. J. Mol. Sci.*, vol. 15, no. 12, pp. 22518–22538, 2014.

[192] J. R. T. and L. C. S. Youssra K Al-Hilaly, Thomas L Williams, Maris Stewart-Parker, Lenzie Ford, Eldhose Skaria, Michael Cole, William Grant Bucher, Kyle L Morris, Alaa Abdul Sad1, "A central role for dityrosine crosslinking of Amyloid-β in Alzheimer's disease," *Acta Neuropathol. Commun.*, vol. 1, p. 83, 2013.

[193] B. H. Thal DR, Rüb U, Orantes M, "Phases of A beta-deposition in the human brain and its relevance for the development of AD.," *Neurology*, vol. 58, no. 12, pp. 1791–800., 2002.

[194] M. do C. Costa and H. L. Paulson, "Toward understanding Machado-Joseph disease," *Prog. Neurobiol.*, vol. 97, no. 2, pp. 239–257, 2012.

[195] C. A. Scarff, A. Sicorello, R. J. L. Tomé, S. Macedo-Ribeiro, A. E. Ashcroft, and S. E. Radford, "A tale of a tail: Structural insights into the conformational properties of the polyglutamine protein ataxin-3," *Int. J. Mass Spectrom.*, vol. 345–347, pp. 63–70, 2013.

[196] A. E. Bevivino and P. J. Loll, "An expanded glutamine repeat destabilizes native ataxin-3 structure and mediates formation of parallel β-fibrils," *Proc. Natl. Acad. Sci. U. S. A.*, vol. 98, no. 21, pp. 11955–11960, 2001.

[197] M. K. M. Chow, A. M. Ellisdon, L. D. Cabrita, and S. P. Bottomley, "Polyglutamine expansion in ataxin-3 does not affect protein stability: Implications for misfolding and disease," *J. Biol. Chem.*, vol. 279, no. 46, pp. 47643–47651, 2004.

[198] G. M. Harris, K. Dodelzon, L. Gong, P. Gonzalez-Alegre, and H. L. Paulson, "Splice isoforms of the polyglutamine disease protein ataxin-3 exhibit similar enzymatic yet different aggregation properties," *PLoS One*, vol. 5, no. 10, 2010.

[199] J. Goto *et al.*, "Machado-Joseph disease gene products carrying different carboxyl termini," *Neurosci. Res.*, vol. 28, no. 4, pp. 373–377, 1997.

[200] and V. T. Meenakshi Verma, Abhishek Vats, "Toxic species in amyloid disorders: Oligomers or mature fibrils," *Ann Indian Acad Neurol.*, vol. 18, no. 2, pp. 138–145, 2015.

[201] C. A. Scarff, B. Almeida, J. Fraga, S. Macedo-Ribeiro, S. E. Radford, and A. E. Ashcroft, "Examination of ataxin-3 (atx-3) aggregation by structural mass spectrometry techniques: A rationale for expedited aggregation upon polyglutamine (polyQ) expansion," *Mol. Cell. Proteomics*, vol. 14, no. 5, pp. 1241–1253, 2015.

[202] Z. Ignatova and L. M. Gierasch, "Extended Polyglutamine Tracts Cause Aggregation and Structural Perturbation of an Adjacent β Barrel Protein " vol. 281, no. 18, pp. 12959–12967, 2006.

[203] L. Masino, G. Nicastro, R. P. Menon, F. D. Piaz, L. Calder, and A. Pastore, "Characterization of the structure and the amyloidogenic properties of the Josephin domain of the polyglutamine-containing protein ataxin-3," *J. Mol. Biol.*, vol. 344, no. 4, pp. 1021–1035, 2004.

[204] G. Sancataldo, V. Vetri, V. Foderà, G. Di Cara, V. Militello, and M. Leone, "Oxidation enhances human serum albumin thermal stability and changes the routes of amyloid fibril formation," *PLoS One*, vol. 9, no. 1, 2014.

[205] J. M. Jung, G. Savin, M. Pouzot, C. Schmitt, and R. Mezzenga, "Structure of heat-induced β-lactoglobulin aggregates and their complexes with sodium-dodecyl sulfate," *Biomacromolecules*, vol. 9, no. 9, pp. 2477–2486, 2008.

[206] S. Jordens, J. Adamcik, I. Amar-Yuli, and R. Mezzenga, "Disassembly and reassembly of amyloid fibrils in water-ethanol mixtures," *Biomacromolecules*, vol. 12, no. 1, pp. 187–193, 2011.

[207] N. Nespovitaya, J. Gath, K. Barylyuk, C. Seuring, B. H. Meier, and R. Riek, "Dynamic Assembly and Disassembly of Functional β-Endorphin Amyloid Fibrils," *J. Am. Chem. Soc.*, vol. 138, no. 3, pp. 846–856, 2016.

[208] S. L. Shammas *et al.*, "Perturbation of the stability of amyloid fibrils through alteration of electrostatic interactions," *Biophys. J.*, vol. 100, no. 11, pp. 2783–2791, 2011.

[209] E. Y. Chi, S. Krishnan, T. W. Randolph, and J. F. Carpenter, "Physical stability of proteins in aqueous solution: Mechanism and driving forces in nonnative protein aggregation," *Pharm. Res.*, vol. 20, no. 9, pp. 1325–1336, 2003.

[210] V. Foderà, A. Zaccone, M. Lattuada, and A. M. Donald, "Electrostatics controls the formation of amyloid superstructures in protein aggregation," *Phys. Rev. Lett.*, vol. 111, no. 10, pp. 1–5, 2013.

[211] S. Lindman, W. F. Xue, O. Szczepankiewicz, M. C. Bauer, H. Nilsson, and S. Linse, "Salting the charged surface: pH and salt dependence of protein G B1 stability," *Biophys. J.*, vol. 90, no. 8, pp. 2911–2921, 2006.

[212] F. Pellistri *et al.*, "Different ataxin-3 amyloid aggregates induce intracellular Ca2+ deregulation by different mechanisms in cerebellar granule cells," *Biochim. Biophys. Acta - Mol. Cell Res.*, vol. 1833, no. 12, pp. 3155–3165, 2013.

[213] S. Yun, B. Urbanc, L. Cruz, G. Bitan, D. B. Teplow, and H. E. Stanley, "Role of electrostatic interactions in amyloid β-protein (Aβ) oligomer formation: A discrete molecular dynamics study," *Biophys. J.*, vol. 92, no. 11, pp. 4064–4077, 2007.

[214] K. Nozaki, O. Onodera, H. Takano, and S. Tsuji, "Amino acid sequences flanking polyglutamine stretches influence their potential for aggregate formation," *Neuroreport*, vol. 12, no. 15, pp. 3357–3364, 2001.

[215] H. Y. Zoghbi and H. T. Orr, "Polyglutamine diseases: Protein cleavage and aggregation," *Curr. Opin. Neurobiol.*, vol. 9, no. 5, pp. 566–570, 1999.

[216] H. P. Nguyen, J. Hübener, J. J. Weber, S. Grueninger, O. Riess, and A. Weiss, "Cerebellar Soluble Mutant Ataxin-3 Level Decreases during Disease Progression in Spinocerebellar Ataxia Type 3 Mice," *PLoS One*, vol. 8, no. 4, 2013.

[217] B. Ramani *et al.*, "Comparison of spinocerebellar ataxia type 3 mouse models identifies

early gain-of-function, cell-autonomous transcriptional changes in oligodendrocytes," *Hum. Mol. Genet.*, vol. 26, no. 17, pp. 3362–3374, 2017.

[218] P. Breuer, A. Haacke, B. O. Evert, and U. Wüllner, "Nuclear aggregation of polyglutamine-expanded ataxin-3: fragments escape the cytoplasmic quality control," *J. Biol. Chem.*, vol. 285, no. 9, pp. 6532–6537, 2010.

ANNEX I

His6-TEV-Jos1-182 C14A

```
catcaccatcaccatcacgagaatctttattttcagggcgccatggagtccatcttccac
H  H  H  H  H  H  E  N  L  Y  F  Q  G  A  M  E  S  I  F  H
gagagacaagaaggctcacttgctgctcaacattgcctgaataacttattgcaaggagaa
E  R  Q  E  G  S  L  A  A  Q  H  C  L  N  N  L  L  Q  G  E
tattttagccctgtggaattatcctcaattgcacatcagctggatgaggaggagaggatg
Y  F  S  P  V  E  L  S  S  I  A  H  Q  L  D  E  E  E  R  M
agaatggcagaaggaggagttactagtgaagattatcgcacgtttttacagcagccttct
R  M  A  E  G  G  V  T  S  E  D  Y  R  T  F  L  Q  Q  P  S
ggaaatatggatgacgtggtttttctctattcaggttataagcaatgccttgagagtt
G  N  M  D  D  S  G  F  F  S  I  Q  V  I  S  N  A  L  R  V
tggggtttagaactaatcctgttcaacagtccagagtatcagaggctcaggatcgatcct
W  G  L  E  L  I  L  F  N  S  P  E  Y  Q  R  L  R  I  D  P
ataaatgaaagatcatttatatgcaattataaggaacactggtttacagttagaagatta
I  N  E  R  S  F  I  C  N  Y  K  E  H  W  F  T  V  R  R  L
ggaagacagtggtttacttgaattctctcttgacgggtccagaattaatatcagataca
G  R  Q  W  F  N  L  N  S  L  L  T  G  P  E  L  I  S  D  T
tatcttgcacttttcttggctcaattacaacaggaaggttattctatatttgtcgttagg
Y  L  A  L  F  L  A  Q  L  Q  Q  E  G  Y  S  I  F  V  V  R
ggtgatctgccagattgcgaagctgaccaactcctgcagatgattaggtag
G  D  L  P  D  C  E  A  D  Q  L  L  Q  M  I  R
```

Jos1-182 C14A sequence

```
      10         20         30         40         50         60
MESIFHERQE GSLAAQHCLN NLLQGEYFSP VELSSIAHQL DEEERMRMAE GGVTSEDYRT

      70         80         90        100        110        120
FLQQPSGNMD DSGFFSIQVI SNALRVWGLE LILFNSPEYQ RLRIDPINER SFICNYKEHW

     130        140        150        160        170        180
FTVRRLGRQW FNLNSLLTGP ELISDTYLAL FLAQLQQEGY SIFVVRGDLP DCEADQLLQM

IR
```

	HisTag -TEV-Jos1-182 C14A	Jos1-182 C14A
Number of amino acids	196	182
Molecular weight	22889.68	21143.84
Theoretical pI	4.95	4.67
Amino acid composition	Ala (A) 9 4.6% Arg (R) 13 6.6% Asn (N) 10 5.1% Asp (D) 9 4.6% Cys (C) 3 1.5% Gln (Q) 15 7.7% Glu (E) 18 9.2% Gly (G) 12 6.1% His (H) 10 5.1% Ile (I) 11 5.6% Leu (L) 25 12.8% Lys (K) 1 0.5% Met (M) 5 2.6% Phe (F) 12 6.1% Pro (P) 6 3.1% Ser (S) 15 7.7% Thr (T) 5 2.6% Trp (W) 3 1.5% Tyr (Y) 7 3.6% Val (V) 7 3.6% Pyl (O) 0 0.0% Sec (U) 0 0.0%	Ala (A) 8 4.4% Arg (R) 13 7.1% Asn (N) 9 4.9% Asp (D) 9 4.9% Cys (C) 3 1.6% Gln (Q) 14 7.7% Glu (E) 17 9.3% Gly (G) 11 6.0% His (H) 4 2.2% Ile (I) 11 6.0% Leu (L) 24 13.2% Lys (K) 1 0.5% Met (M) 5 2.7% Phe (F) 11 6.0% Pro (P) 6 3.3% Ser (S) 15 8.2% Thr (T) 5 2.7% Trp (W) 3 1.6% Tyr (Y) 6 3.3% Val (V) 7 3.8% Pyl (O) 0 0.0% Sec (U) 0 0.0%
Total number of negatively charged (Asp + Glu)	27	26
Total number of positively charged (Arg + Lys)	14	14
Ext. coefficient at 280 nm (assuming all pairs of Cys residues form cysteines)	27055	25565
Abs 0.1% (=1 g/l) (assuming all pairs of Cys residues form cysteines)	1.182	1.209
Ext. coefficient at 280 nm (assuming all Cys residues are reduced)	26930	25440
Abs 0.1% (=1 g/l) (assuming all Cys residues are reduced)	1.177	1.203

MBP-His6-TEV-FL Atx3 C14A Q14 3UIMs Isoform V212 G310

```
atgaaaatcgaagaaggtaaactggtaatctggattaacggcgataaaggctataacggt
M  K  I  E  E  G  K  L  V  I  W  I  N  G  D  K  G  Y  N  G
ctcgctgaagtcggtaagaaattcgagaaagataccggaattaaagtcaccgttgagcat
L  A  E  V  G  K  K  F  E  K  D  T  G  I  K  V  T  V  E  H
ccggataaactggaagagaaattcccacaggttgcggcaactggcgatggccctgacatt
P  D  K  L  E  E  K  F  P  Q  V  A  A  T  G  D  G  P  D  I
atcttctgggcacacgaccgctttggtggctacgctcaatctggcctgttggctgaaatc
I  F  W  A  H  D  R  F  G  G  Y  A  Q  S  G  L  L  A  E  I
accccggacaaagcgttccaggacaagctgtatccgtttacctgggatgccgtacgttac
T  P  D  K  A  F  Q  D  K  L  Y  P  F  T  W  D  A  V  R  Y
aacggcaagctgattgcttacccgatcgctgttgaagcgttatcgctgatttataacaaa
N  G  K  L  I  A  Y  P  I  A  V  E  A  L  S  L  I  Y  N  K
gatctgctgccgaacccgccaaaaacctgggaagagatcccggcgctggataaagaactg
D  L  L  P  N  P  P  K  T  W  E  E  I  P  A  L  D  K  E  L
aaagcgaaaggtaagagcgcgctgatgttcaacctgcaagaaccgtacttcacctggccg
K  A  K  G  K  S  A  L  M  F  N  L  Q  E  P  Y  F  T  W  P
ctgattgctgctgacgggggttatgcgttcaagtatgaaaacggcaagtacgacattaaa
L  I  A  A  D  G  G  Y  A  F  K  Y  E  N  G  K  Y  D  I  K
gacgtgggcgtggataacgctggcgcgaaagcgggtctgaccttcctggttgacctgatt
D  V  G  V  D  N  A  G  A  K  A  G  L  T  F  L  V  D  L  I
aaaaacaaacacatgaatgcagacaccgattactccatcgcagaagctgcctttaataaa
K  N  K  H  M  N  A  D  T  D  Y  S  I  A  E  A  A  F  N  K
ggcgaaacagcgatgaccatcaacggcccgtgggcatggtccaacatcgacaccagcaaa
G  E  T  A  M  T  I  N  G  P  W  A  W  S  N  I  D  T  S  K
gtgaattatggtgtaacggtactgccgaccttcaagggtcaaccatccaaaccgttcgtt
V  N  Y  G  V  T  V  L  P  T  F  K  G  Q  P  S  K  P  F  V
ggcgtgctgagcgcaggtattaacgccgccagtccgaacaaagagctggcaaaagagttc
G  V  L  S  A  G  I  N  A  A  S  P  N  K  E  L  A  K  E  F
ctcgaaaactatctgctgactgatgaaggtctggaagcggttaataaagacaaaccgctg
L  E  N  Y  L  L  T  D  E  G  L  E  A  V  N  K  D  K  P  L
ggtgccgtagcgctgaagtcttacgaggaagagttggtgaaagatccgcgtattgccgcc
G  A  V  A  L  K  S  Y  E  E  E  L  V  K  D  P  R  I  A  A
actatggaaaacgcccagaaaggtgaaatcatgccgaacatcccgcagatgtccgctttc
T  M  E  N  A  Q  K  G  E  I  M  P  N  I  P  Q  M  S  A  F
tggtatgccgtgcgtactgcggtgatcaacgccgccagcggtcgtcagactgtcgatgaa
W  Y  A  V  R  T  A  V  I  N  A  A  S  G  R  Q  T  V  D  E
gccctgaaagacgcgcagactaattcgagctcgaacaacaacaacaataacaataacaac
A  L  K  D  A  Q  T  N  S  S  S  N  N  N  N  N  N  N  N  N
aacctcgggatcgagggaaggatttcacatcaccatcatcaccacgaaaacctgtacttt
N  L  G  I  E  G  R  I  S  H  H  H  H  H  H  E  N  L  Y  F
cagggcatggagtccatcttccacgagaaacaagaaggctcacttgctgctcaacattgc
Q  G  M  E  S  I  F  H  E  K  Q  E  G  S  L  A  A  Q  H  C
ctgaataacttattgcaaggagaatattttagccctgtggaattatcctcaattgcacat
L  N  N  L  L  Q  G  E  Y  F  S  P  V  E  L  S  S  I  A  H
cagctggatgaggaggagaggatgagaatggcagaaggaggagttactagtgaagattat
Q  L  D  E  E  E  R  M  R  M  A  E  G  G  V  T  S  E  D  Y
cgcacgtttttacagcagccttctggaaatatggatgacagtggtttttttctctattcag
R  T  F  L  Q  Q  P  S  G  N  M  D  D  S  G  F  F  S  I  Q
gttataagcaatgccttgaaagtttggggtttagaactaatcctgttcaacagtccagag
V  I  S  N  A  L  K  V  W  G  L  E  L  I  L  F  N  S  P  E
tatcagaggctcaggatcgatcctataaatgaaagatcatttatatgcaattataaggaa
Y  Q  R  L  R  I  D  P  I  N  E  R  S  F  I  C  N  Y  K  E
cactggtttacagttagaaaattaggaaaacagtggtttaacttgaattctctcttgacg
H  W  F  T  V  R  K  L  G  K  Q  W  F  N  L  N  S  L  L  T
ggtccagaattaatatcagatacatatcttgcacttttcttggctcaattacaacaggaa
G  P  E  L  I  S  D  T  Y  L  A  L  F  L  A  Q  L  Q  Q  E
ggttattctatatttgtcgttaagggtgatctgccagattgcgaagctgaccaactccta
G  Y  S  I  F  V  V  K  G  D  L  P  D  C  E  A  D  Q  L  L
cagatgattagggtccaacagatgcatcgaccaaaacttattggagaagaattagcacaa
Q  M  I  R  V  Q  Q  M  H  R  P  K  L  I  G  E  E  L  A  Q
ctaaaagagcaaagagtccataaaacagacctggaacgagtgttagaagcaaatgatggc
```

```
L  K  E  Q  R  V  H  K  T  D  L  E  R  V  L  E  A  N  D  G
tcaggaatgttagacgaagatgaggaggatttgcagagggctctggcactaagtcgccaa
S  G  M  L  D  E  D  E  E  D  L  Q  R  A  L  A  L  S  R  Q
gaaattgacatggaagatgaggaagcagatctccgcagggctattcagctaagtatgcaa
E  I  D  M  E  D  E  E  A  D  L  R  R  A  I  Q  L  S  M  Q
ggtagttccagaaacatatctcaagatatgacacagacatcaggtacaaatcttacttca
G  S  S  R  N  I  S  Q  D  M  T  Q  T  S  G  T  N  L  T  S
gaagagcttcggaagagacgagaagcctactttgaaaaacagcagcaaaagcagcaacag
E  E  L  R  K  R  R  E  A  Y  F  E  K  Q  Q  Q  K  Q  Q  Q
cagcagcagcagcagcagcaggggacctatcaggacagagttcacatccatgtgaaagg
Q  Q  Q  Q  Q  Q  Q  G  D  L  S  G  Q  S  S  H  P  C  E  R
ccagccaccagttcaggagcacttgggagtgatctaggtgatgctatgagtgaagaagca
P  A  T  S  S  G  A  L  G  S  D  L  G  D  A  M  S  E  E  D
atgcttcaggcagctgtgaccatgtctttagaaactgtcagaaatgatttgaaaacagaa
M  L  Q  A  A  V  T  M  S  L  E  T  V  R  N  D  L  K  T  E
ggaaaaaaataa
G  K  K  -
```

Atx3 C14A Q14 3UIMs Isoform V212;G310 after TEV cleavage

```
     10          20          30          40          50          60
GMESIFHEKQ  EGSLCAQHCL  NNLLQGEYFS  PVELSSIAHQ  LDEEERMRMA  EGGVTSEDYR

         70          80          90         100         110         120
TFLQQPSGNM  DDSGFFSIQV  ISNALKVWGL  ELILFNSPEY  QRLRIDPINE  RSFICNYKEH

        130         140         150         160         170         180
WFTVRKLGKQ  WFNLNSLLTG  PELISDTYLA  LFLAQLQQEG  YSIFVVKGDL  PDCEADQLLQ

        190         200         210         220         230         240
MIRVQQMHRP  KLIGEELAQL  KEQRVHKTDL  ERVLEANDGS  GMLDEDEEDL  QRALALSRQE

        250         260         270         280         290         300
IDMEDEEADL  RRAIQLSMQG  SSRNISQDMT  QTSGTNLTSE  ELRKRREAYF  EKQQQKQQQQ

        310         320         330         340         350         360
QQQQQQGDLS  GQSSHPCERP  ATSSGALGSD  LGDAMSEEDM  LQAAVTMSLE  TVRNDLKTEG

KK
```

	MBP-HisTag -TEV- Atx3 C14A Q14 3UIMs	**Atx3 C14A Q14 3UIMs**
Number of amino acids	763	362
Molecular weight	85617.06	41307.09
Theoretical pI	4.95	4.69
Amino acid composition	Ala (A) 62 8.1% Arg (R) 27 3.5% Asn (N) 46 6.0% Asp (D) 47 6.2% Cys (C) 5 0.7% Gln (Q) 49 6.4% Glu (E) 67 8.8% Gly (G) 54 7.1% His (H) 16 2.1% Ile (I) 39 5.1% Leu (L) 75 9.8% Lys (K) 51 6.7% Met (M) 20 2.6% Phe (F) 28 3.7% Pro (P) 30 3.9% Ser (S) 47 6.2% Thr (T) 33 4.3% Trp (W) 11 1.4% Tyr (Y) 23 3.0% Val (V) 33 4.3% Pyl (O) 0 0.0% Sec (U) 0 0.0%	Ala (A) 19 5.2% Arg (R) 21 5.8% Asn (N) 13 3.6% Asp (D) 23 6.4% Cys (C) 5 1.4% Gln (Q) 39 10.8% Glu (E) 38 10.5% Gly (G) 23 6.4% His (H) 7 1.9% Ile (I) 15 4.1% Leu (L) 43 11.9% Lys (K) 15 4.1% Met (M) 13 3.6% Phe (F) 12 3.3% Pro (P) 9 2.5% Ser (S) 31 8.6% Thr (T) 14 3.9% Trp (W) 3 0.8% Tyr (Y) 7 1.9% Val (V) 12 3.3% Pyl (O) 0 0.0% Sec (U) 0 0.0%
Total number of negatively charged (Asp + Glu)	114	61
Total number of positively charged (Arg + Lys)	78	36
Ext. coefficient at 280 nm (assuming all pairs of Cys residues form cysteines)	95020	27180
Abs 0.1% (=1 g/l) (assuming all pairs of Cys residues form cysteines)	1.110	0.658
Ext. coefficient at 280 nm (assuming all Cys residues are reduced)	94770	26930
Abs 0.1% (=1 g/l) (assuming all Cys residues are reduced)	1.107	0.652

MBP-His6-TEV-FL Atx3 C14A Q54 3UIMs Isoform V212 G310

```
atgaaaatcgaagaaggtaaactggtaatctggattaacggcgataaaggctataacggt
M  K  I  E  E  G  K  L  V  I  W  I  N  G  D  K  G  Y  N  G
ctcgctgaagtcggtaagaaattcgagaaagataccggaattaaagtcaccgttgagcat
L  A  E  V  G  K  K  F  E  K  D  T  G  I  K  V  T  V  E  H
ccggataaactggaagagaaattcccacaggttgcggcaactggcgatggccctgacatt
P  D  K  L  E  E  K  F  P  Q  V  A  A  T  G  D  G  P  D  I
atcttctgggcacacgaccgctttggtggctacgctcaatctggcctgttggctgaaatc
I  F  W  A  H  D  R  F  G  G  Y  A  Q  S  G  L  L  A  E  I
accccggacaaagcgttccaggacaagctgtatccgtttacctgggatgccgtacgttac
T  P  D  K  A  F  Q  D  K  L  Y  P  F  T  W  D  A  V  R  Y
aacggcaagctgattgcttacccgatcgctgttgaagcgttatcgctgatttataacaaa
N  G  K  L  I  A  Y  P  I  A  V  E  A  L  S  L  I  Y  N  K
gatctgctgccgaacccgccaaaaacctgggaagagatcccggcgctggataaagaactg
D  L  L  P  N  P  P  K  T  W  E  E  I  P  A  L  D  K  E  L
aaagcgaaaggtaagagcgcgctgatgttcaacctgcaagaaccgtacttcacctggccg
K  A  K  G  K  S  A  L  M  F  N  L  Q  E  P  Y  F  T  W  P
ctgattgctgctgacgggggttatgcgttcaagtatgaaaacggcaagtacgacattaaa
L  I  A  A  D  G  G  Y  A  F  K  Y  E  N  G  K  Y  D  I  K
gacgtgggcgtggataacgctggcgcgaaagcgggtctgaccttcctggttgacctgatt
D  V  G  V  D  N  A  G  A  K  A  G  L  T  F  L  V  D  L  I
aaaaacaaacacatgaatgcagacaccgattactccatcgcagaagctgcctttaataaa
K  N  K  H  M  N  A  D  T  D  Y  S  I  A  E  A  A  F  N  K
ggcgaaacagcgatgaccatcaacggcccgtgggcatggtccaacatcgacaccagcaaa
G  E  T  A  M  T  I  N  G  P  W  A  W  S  N  I  D  T  S  K
gtgaattatggtgtaacggtactgccgaccttcaagggtcaaccatccaaaccgttcgtt
V  N  Y  G  V  T  V  L  P  T  F  K  G  Q  P  S  K  P  F  V
ggcgtgctgagcgcaggtattaacgccgccagtccgaacaaagagctggcaaaagagttc
G  V  L  S  A  G  I  N  A  A  S  P  N  K  E  L  A  K  E  F
ctcgaaaactatctgctgactgatgaaggtctggaagcggttaataaagacaaaccgctg
L  E  N  Y  L  L  T  D  E  G  L  E  A  V  N  K  D  K  P  L
ggtgccgtagcgctgaagtcttacgaggaagagttggtgaaagatccgcgtattgccgcc
G  A  V  A  L  K  S  Y  E  E  E  L  V  K  D  P  R  I  A  A
actatggaaaacgcccagaaaggtgaaatcatgccgaacatcccgcagatgtccgctttc
T  M  E  N  A  Q  K  G  E  I  M  P  N  I  P  Q  M  S  A  F
tggtatgccgtgcgtactgcggtgatcaacgccgccagcggtcgtcagactgtcgatgaa
W  Y  A  V  R  T  A  V  I  N  A  A  S  G  R  Q  T  V  D  E
gccctgaaagacgcgcagactaattcgagctcgaacaacaacaacaataacaataacaac
A  L  K  D  A  Q  T  N  S  S  S  N  N  N  N  N  N  N  N  N
aacctcgggatcgagggaaggatttcacatcaccatcatcaccacgaaaacctgtacttt
N  L  G  I  E  G  R  I  S  H  H  H  H  H  H  E  N  L  Y  F
cagggcatggagtccatcttccacgagaaacaagaaggctcacttgctgctcaacattgc
Q  G  M  E  S  I  F  H  E  K  Q  E  G  S  L  A  A  Q  H  C
ctgaataacttattgcaaggagaatattttagccctgtggaattatcctcaattgcacat
L  N  N  L  L  Q  G  E  Y  F  S  P  V  E  L  S  S  I  A  H
cagctggatgaggaggagaggatgagaatggcagaaggaggagttactagtgaagattat
Q  L  D  E  E  E  R  M  R  M  A  E  G  G  V  T  S  E  D  Y
cgcacgtttttacagcagccttctggaaatatggatgacagtggtttttttctctattcag
R  T  F  L  Q  Q  P  S  G  N  M  D  D  S  G  F  F  S  I  Q
gttataagcaatgccttgaaagtttggggtttagaactaatcctgttcaacagtccagag
V  I  S  N  A  L  K  V  W  G  L  E  L  I  L  F  N  S  P  E
tatcagaggctcaggatcgatcctataaatgaaagatcatttatatgcaattataaggaa
Y  Q  R  L  R  I  D  P  I  N  E  R  S  F  I  C  N  Y  K  E
cactggtttacagttagaaaattaggaaaacagtggtttaacttgaattctctcttgacg
H  W  F  T  V  R  K  L  G  K  Q  W  F  N  L  N  S  L  L  T
ggtccagaattaatatcagatacatatcttgcacttttcttggctcaattacaacaggaa
G  P  E  L  I  S  D  T  Y  L  A  L  F  L  A  Q  L  Q  Q  E
ggttattctatatttgtcgttaagggtgatctgccagattgcgaagctgaccaactccta
G  Y  S  I  F  V  V  K  G  D  L  P  D  C  E  A  D  Q  L  L
cagatgattagggtccaacagatgcatcgaccaaaacttattggagaagaattagcacaa
Q  M  I  R  V  Q  Q  M  H  R  P  K  L  I  G  E  E  L  A  Q
ctaaaagagcaaagagtccataaaacagacctggaacgagtgttagaagcaaatgatggc
```

```
L  K  E  Q  R  V  H  K  T  D  L  E  R  V  L  E  A  N  D  G
tcaggaatgttagacgaagatgaggaggatttgcagagggctctggcactaagtcgccaa
S  G  M  L  D  E  D  E  E  D  L  Q  R  A  L  A  L  S  R  Q
gaaattgacatggaagatgaggaagcagatctccgcagggctattcagctaagtatgcaa
E  I  D  M  E  D  E  E  A  D  L  R  R  A  I  Q  L  S  M  Q
ggtagttccagaaacatatctcaagatatgacacagacatcaggtacaaatcttacttca
G  S  S  R  N  I  S  Q  D  M  T  Q  T  S  G  T  N  L  T  S
gaagagcttcggaagagacgagaagcctactttgaaaaacagcagcaaaagcagcaacag
E  E  L  R  K  R  R  E  A  Y  F  E  K  Q  Q  Q  K  Q  Q  Q
cagcagcagcagcagcagcagcagcagcagcagcagcagcagcagcagcagcagcagcag
Q  Q  Q  Q  Q  Q  Q  Q  Q  Q  Q  Q  Q  Q  Q  Q  Q  Q  Q  Q
cagcagcagcagcagcagcagcagcagcagcagcagcagcagcagcagcagcagcagcag
Q  Q  Q  Q  Q  Q  Q  Q  Q  Q  Q  Q  Q  Q  Q  Q  Q  Q  Q  Q
cagcagcagcagcagcagggggacctatcaggacagagttcacatccatgtgaaagg
Q  Q  Q  Q  Q  Q  Q  G  D  L  S  G  Q  S  S  H  P  C  E  R
ccagccaccagttcaggagcacttgggagtgatctaggtgatgctatgagtgaagaagac
P  A  T  S  S  G  A  L  G  S  D  L  G  D  A  M  S  E  E  D
atgcttcaggcagctgtgaccatgtctttagaaactgtcagaaatgatttgaaaacagaa
M  L  Q  A  A  V  T  M  S  L  E  T  V  R  N  D  L  K  T  E
ggaaaaaaataa
G  K  K  -
```

Atx3 C14A Q54 3UIMs after TEV cleavage

```
      10         20         30         40         50         60
GMESIFHEKQ EGSLAAQHCL NNLLQGEYFS PVELSSIAHQ LDEEERMRMA EGGVTSEDYR

        70         80         90        100        110        120
TFLQQPSGNM DDSGFFSIQV ISNALKVWGL ELILFNSPEY QRLRIDPINE RSFICNYKEH

       130        140        150        160        170        180
WFTVRKLGKQ WFNLNSLLTG PELISDTYLA LFLAQLQQEG YSIFVVKGDL PDCEADQLLQ

       190        200        210        220        230        240
MIRVQQMHRP KLIGEELAQL KEQRVHKTDL ERVLEANDGS GMLDEDEEDL QRALALSRQE

       250        260        270        280        290        300
IDMEDEEADL RRAIQLSMQG SSRNISQDMT QTSGTNLTSE ELRKRREAYF EKQQQKQQQQ

       310        320        330        340        350        360
QQQQQQQQQQ QQQQQQQQQQ QQQQQQQQQQ QQQQQQQQQQ QQQQQQGDLS GQSSHPCERP

       370        380        390        400
ATSSGALGSD LGDAMSEEDM LQAAVTMSLE TVRNDLKTEG KK
```

	MBP-HisTag -TEV- Atx3 C14A Q54 3UIMs	Atx3 C14A Q54 3UIMs
Number of amino acids	803	402
Molecular weight	90710.23	46400.26
Theoretical pI	4.95	4.69
Amino acid composition	Ala (A) 63 7.8% Arg (R) 27 3.4% Asn (N) 46 5.7% Asp (D) 47 5.9% Cys (C) 4 0.5% Gln (Q) 89 11.1% Glu (E) 67 8.3% Gly (G) 54 6.7% His (H) 16 2.0% Ile (I) 39 4.9% Leu (L) 75 9.3% Lys (K) 51 6.4% Met (M) 20 2.5% Phe (F) 28 3.5% Pro (P) 30 3.7% Ser (S) 47 5.9% Thr (T) 33 4.1% Trp (W) 11 1.4% Tyr (Y) 23 2.9% Val (V) 33 4.1% Pyl (O) 0 0.0% Sec (U) 0 0.0%	Ala (A) 20 5.0% Arg (R) 21 5.2% Asn (N) 13 3.2% Asp (D) 23 5.7% Cys (C) 4 1.0% Gln (Q) 79 19.7% Glu (E) 38 9.5% Gly (G) 23 5.7% His (H) 7 1.7% Ile (I) 15 3.7% Leu (L) 43 10.7% Lys (K) 15 3.7% Met (M) 13 3.2% Phe (F) 12 3.0% Pro (P) 9 2.2% Ser (S) 31 7.7% Thr (T) 14 3.5% Trp (W) 3 0.7% Tyr (Y) 7 1.7% Val (V) 12 3.0% Pyl (O) 0 0.0% Sec (U) 0 0.0%
Total number of negatively charged (Asp + Glu)	114	61
Total number of positively charged (Arg + Lys)	78	36
Ext. coefficient at 280 nm (assuming all pairs of Cys residues form cysteines)	95020	27180
Abs 0.1% (=1 g/l) (assuming all pairs of Cys residues form cysteines)	1.048	0.586
Ext. coefficient at 280 nm (assuming all Cys residues are reduced)	94770	26930
Abs 0.1% (=1 g/l) (assuming all Cys residues are reduced)	1.045	0.580

ANNEX II

pCI-Neo Vector Multiple Cloning Region (from Promega):

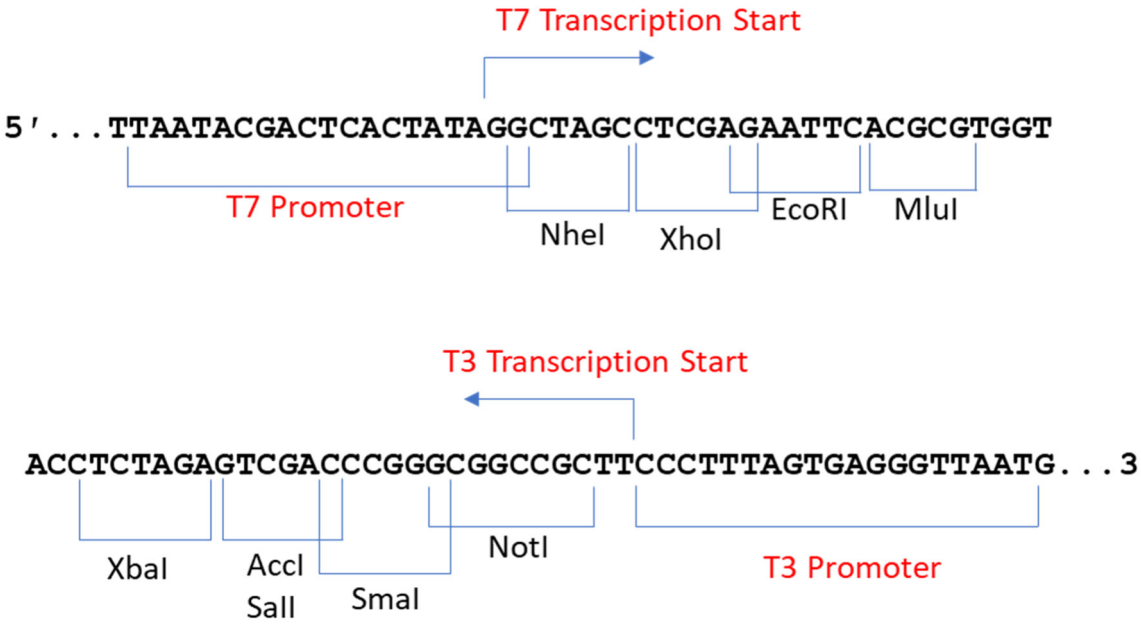

Figure T7 and T3 RNA polymerase promoters and multiple cloning region sequence of the pCI-Neo Vector. The sequence shown corresponds to RNA synthesized by T7 RNA polymerase and is complementary to RNA synthesized by T3 RNA polymerase. The strand shown is the same as the ssDNA produced by the vector.

pCI-Neo Vector Circle Map (from Promega):

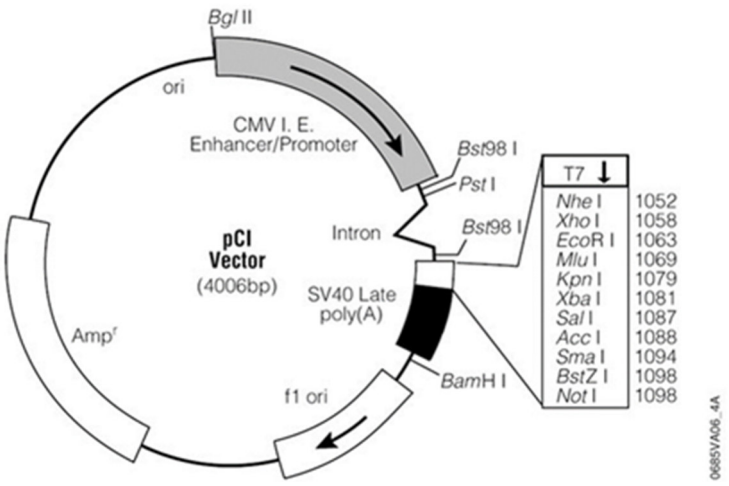

pCI-Neo Sequence Reference Points:

CMV immediate-early enhancer/promoter region 1–750

Chimeric intron 890–1022

T7-EEV sequencing primer binding region 1053–1074

T7 RNA polymerase promoter (–17 to +2) 1067–1085

Multiple cloning region 1085–1137

T3 RNA polymerase promoter (–17 to +3) 1140–1158

SV40 late polyadenylation signal 1167–1388

Phage f1 region 1483–1938

SV40 enhancer and early promoter 2000–2418

SV40 minimum origin of replication 2316–2381

Coding region of neomycin phosphotransferase 2463–3257

Synthetic polyadenylation signal 3321–3369

β-lactamase (Ampr) coding region 3780–4640

pTet-ONE vector Circle Map (from Clontech® Laboratories, Inc):

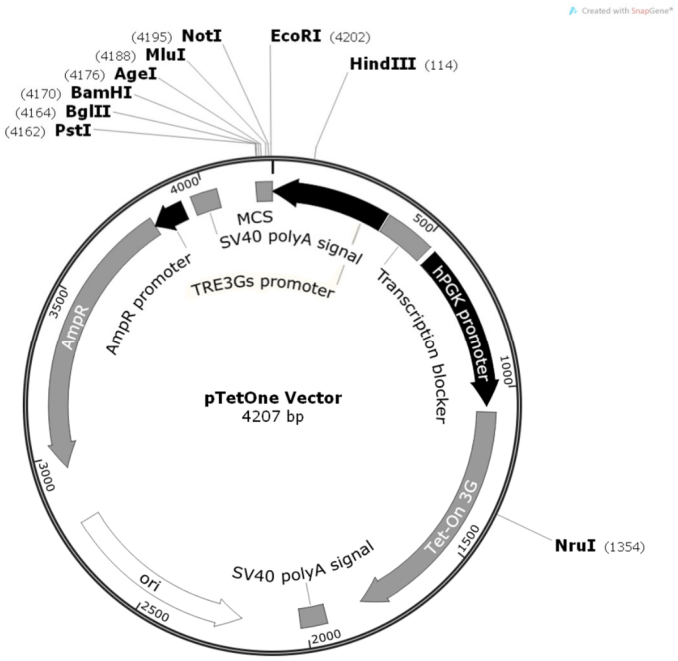

ACKNOWLEDGMENTS

I would like to express my gratitude to my tutors, Dr Caterina Alfano, from Ri.MED Foundation and Prof. Valeria Vetri from University of Palermo, whose patience and kindness, as well as their academic experiences have been invaluable to me. I also would like to express my gratitude to Prof. Annalisa Pastore, from King's College of London, for her good advices and great opportunity to enjoy her lab during my experience abroad, and especially for making me feel at home. I would like to thanks all my colleagues from King's College London Lab, for their support and their good advices, they have been precious to me academically as well as at personal level. In particular, I would thank Dr Tommaso Vannocci for his support and for his scientific contribution to this work and also for being a point of reference during my period in London. I also would thank my colleagues from Structural Biology and Biophysics Lab in Palermo for having accompanied me throughout this journey, for their patience and support. In particular a special thanks to Maria whose encouragements have supported me every step of the way. Last but not least my colleagues from the Biophysics Lab of the University of Palermo, for always helping me. Then I would like to give a special thanks to Chiara and Martina, they were not only colleagues but also two friends that I discovered during this experience. Finally, I could not write this thesis without the help, support and love of my family and in particular of my beloved husband who shared with me joys and sorrows of this journey.

La borsa di dottorato è stata cofinanziata con risorse del
Programma Operativo Nazionale Ricerca e Innovazione 2014-2020 (CCI 2014IT16M2OP005),
Fondo Sociale Europeo, Azione I.1 “Dottorati Innovativi con caratterizzazione Industriale”

UNIONE EUROPEA
Fondo Sociale Europeo